Tanja Consolati, BSc

Design of immobilized sYFP as intensity ratiometric biosensor for temporal and spatial resolution of pH gradients in solid-supported biocatalysts

MASTERARBEIT

zur Erlangung des akademischen Grades

Diplom-Ingenieurin

Masterstudium Biotechnologie

eingereicht an der

Technischen Universität Graz

Betreuer

Univ.-Prof. Dipl.-Ing. Dr. techn. Bernd Nidetzky

Institut für Biotechnologie und Bioprozesstechnik

Dr. Juan M. Bolivar
Institut für Biotechnologie und Bioprozesstechnik

Graz, September 2014

EIDESSTATTLICHE ERKLÄRUNG

AFFIDAVIT

Ich erkläre an Eides statt, dass ich die vorliegende Arbeit selbstständig verfasst, andere als die angegebenen Quellen/Hilfsmittel nicht benutzt, und die den benutzten Quellen wörtlich und inhaltlich entnommenen Stellen als solche kenntlich gemacht habe. Das in TUGRAZonline hochgeladene Textdokument ist mit der vorliegenden Masterarbeit identisch.

I declare that I have authored this thesis independently, that I have not used other than the declared sources/resources, and that I have explicitly indicated all material which has been quoted either literally or by content from the sources used. The text document uploaded to TUGRAZonline is identical to the present master‘s thesis.

Datum / Date

Unterschrift / Signature

Für meine Eltern

DANKSAGUNG

Prof. Bernd Nidetzky, Juan M. Bolivar und Torsten Mayr danke für eure Unterstützung und euer Vertrauen in mich während der letzten drei Jahre. Ich danke euch für jede Kritik und jede Diskussion die diese gemeinsame Arbeit so vorangebracht hat.

Prof. José M. Guisán muchas gracias por recibirme en tu laboratorio. Sé que no era facil siempre conmigo, pero gracias a ti he crecido y he aprendido mucho scientificamente y personalmente.

Prof. Aurelio Hidalgo y Prof. José Berenguer gracias por la estancia cortida en vuestro laboratorio. El trabajo con vosotros me ha dado mucha motivacion seguir en ciencia y me ha ayudado saber que quiero hacer en el futuro.

Fernando Lopez-Gallego, Javier Rocha-Martín y Oscar Romero gracias por los millones de ideas que han hecho este proyecto possible y gracias por vuesto ayuda y apoyo con todos los experimentos durante la estancia.

Omi, Opi, Mama und Papa danke für euer Verständnis wenn ich euch mal wieder links liegen lassen musste, danke dass ihr versucht mich zu akzeptieren wie ich bin und mir die Freiheit gebt meine Träume zu leben.

Vielen Dank auch an alle Menschen die ich um mich herum sammeln durfte und die ein kleines Stück meines Weges mit mir gegangen sind. Oscar, Juanma, Cristina, Andrea, Jutta, Chris, Sanel, Martin, Simon, Reinmar, Berni, Josef, Sabine, Mareike, Jihey, Wolfi, Kalli, Kathi, Nadine, Conny, Antonio, Marco, Marzia, Caio, Óscar und Tobi.

ABSTRACT

pH is a key process parameter in enzyme catalysis. When immobilized enzymes are used, pH inside the particle might deviate from the one in liquid solution. A static pH gradient might be originated by partition effects and since catalysis takes place inside the enzyme carrier in addition a dynamic pH gradient may arise due to generation or consumption of protons. Influence of local pH onto activity, selectivity and stability of solid-supported enzymes remains a critical parameter masked when using conventional analytical enzyme characterization tools. Recent studies made a significant progress in the characterization of heterogeneous biocatalysts based on the real-time quantification of the internal microenvironment by co-attachment of a pH dependent luminescence molecule. Different luminescence based sensing platforms are available, however, suitability for analysis of immobilized biocatalysts is limited and together with the lack of general labeling strategies for enzyme carriers and the sensitivity of many enzymes against chemical pH indicators a broad application is impeded.

In this master thesis a new biosensor for the internal quantification of pH in homogeneous and heterogeneous catalysis is presented. The naturally pH dependent optical properties of superfolder yellow fluorescent protein (sYFP) were exploited as self-referencing pH indicator. Internal pH responsive materials have been developed based on the controlled homogeneous incorporation of sYFP into different widely used enzyme carriers (Sepabeads®, mesoporous silica and agarose BCL) following two general strategies (oriented immobilization via a His-Tag and a multi-point covalent attachment). Compatibility with enzyme immobilization was achieved by the use of well-established techniques of carrier surface activation and exemplary studied with covalently attached penicillin G acylase.

The establishment of ratiometric intensity measurements using CLSM has shown the suitability of the immobilized sYFP to resolve pH in the range of 8.5-6.0 with a dynamic response adequate for the hydrolytic reactions rate used: 30 mM/min to 0.3 mM/min. A maximum pH gradient of 1.8 units has been observed related to the diffusional control of immobilized enzyme performance. Modulation of the internal pH-gradient by modification of catalyst loading and buffering capacity of reaction medium has been studied. The internal visualization of pH based on solid-supported sYFP offers a general applicable valuable opportunity for biocatalyst development and bioprocess intensification.

KURZFASSUNG

pH ist ein wichtiger Prozessparameter in der Enzymkatalyse. Wenn immobilisierte Enzyme verwendet werden, könnte sich der pH Wert im Partikel von dem in Lösung unterscheiden. Ein statischer pH Gradient könnte durch Partitionseffekte entstehen und da die Katalyse im Enzymträger stattfindet, könnte zusätzlich aufgrund der Erzeugung oder des Verbrauchs von Protonen ein dynamischer pH-Gradient auftreten. Der Einfluss vom lokalen pH-Wert auf die Aktivität, Selektivität und Stabilität von immobilisierten Enzymen bleibt ein kritischer Parameter, maskiert wenn herkömmliche analytische Methoden zur Enzymcharakterisierung verwendet werden. Jüngste Studien haben einen signifikanten Fortschritt bei der Charakterisierung von heterogenen Biokatalysatoren gemacht, basierend auf der Echtzeitquantifizierung der internen Mikroumwelt durch ein coimmobilisiertes pH-abhängiges Lumineszenz Molekül. Verschiedene Lumineszenz basierende Sensorplattformen stehen zur Verfügung, dennoch ist die Eignung für die Analyse von immobilisierten Biokatalysatoren begrenzt und eine breite Anwendung durch den allgemeinen Mangel an Strategien für das Labeling von Enzymträgern und der Empfindlichkeit vieler Enzyme gegen chemische pH-Indikatoren erschwert.

In dieser Masterarbeit wird ein neuer Biosensor für die interne Quantifizierung von pH-Werten in homogener und heterogener Katalyse vorgestellt. Die natürlich pH-abhängigen optischen Eigenschaften von superfolder yellow fluorescent protein (sYFP) wurden als selbst-referenzierender pH-Indikator genutzt. Intern pH-abhänige Materialien wurden entwickelt, basierend auf der kontrollierten homogenen Immobilisierung von sYFP in verschiedene häufig genutzte Enzymträger (Sepabeads®, mesoporöses Siliziumdioxid und Agarose BCL) indem zwei generelle Strategien verfolgt wurden (orientierte Immobilisierung via His-Tag und multi-point-kovalente Bindung). Die Kompatibilität mit der Enzymimmobilisierung wurde durch die Verwendung von etablierten Oberflächenaktivierungstechniken erreicht und beispielhaft mit kovalent immobilisierter Penicillin G Acylase studiert.

Die Etablierung von ratiometrischen Intensitätsmessungen mit CLSM zeigte die Eignung des immobilisierten sYFPs pH-Werte in der Größenordnung von 8.5-6.0 aufzulösen, mit einer Dynamik angemessen für die benutzte hydrolytische Reaktionsrate: 30 mM/min bis 0,3 mM/min. Ein maximaler pH Gradient von 1.8 Einheiten konnte beobachtet werden, bezogen auf die von Diffusion kontrollierten Leistung immobilisierter Enzyme. Modulierung des internen pH-Gradienten durch Modifizierung der Katalysatorbeladung und Pufferkapazität des Reaktionsmediums sind studiert worden. Die interne Visualisierung von pH-Werten basierend auf immobilisiertem sYFP bietet eine generell anwendbare wertvolle Möglichkeit für die Entwicklung von Biokatalysatoren und zur Bioprozess-Intensivierung.

TABLE OF CONTENTS

1 INTRODUCTION

Immobilized biocatalysts constitute the prevalent form of enzymes applied in currently performed industrial scale biotransformations [1–3]. This preference of immobilized over free enzymes is mainly due to their easy implementation into continuous bioprocesses through integrated re-use of the catalyst [2–4]. Stabilization associated to properly designed immobilization strategies is another advantage that usually leads to a significant increase of catalyst productivity. The development of active, selective and cost-efficient immobilized biocatalysts is a common goal [5–7]. A multitude of materials with different geometrical features and different immobilization techniques are available. The selection of most suitable combination is a complex task depending on many factors [8–12]. Still common procedures are largely empirical and imply to test many alternative formulations from where the best for a specific purpose is selected [2, 5, 7, 11]. This originates mainly from a limited understanding and prediction capability of two overlapping phenomena that are occurring in solid-bound enzymes. First the surface-enzyme interaction that determines the activity of the enzyme after attachment [13, 14] and second the existence of mass transfer resistances and partition effects between liquid bulk and solid carrier that leads to a different catalytic environment inside the carrier matrix compared to the liquid phase [5, 15]. A boundary layer surrounding the enzyme carrier might slow down transfer of reagents from the bulk to the external catalytic surface or vice versa. In case of porous carriers additionally internal diffusion into the pore might generate gradients of substrates and products negatively affecting reaction velocity and yield [5, 16].

One key operational variable that has a crucial role is pH. Internal pH might suffer a significant deviation from values observed in liquid phase. These deviations come from two situations. When the carrier contains a charged surface or if a proton consuming or proton forming enzyme-catalyzed reaction is involved. Support-generated static proton gradients originate from partition between charged groups on solute molecules with stationary charges on the carrier causing a pH shift inside the particle compared to the bulk solution [5, 15]. Reaction generated proton gradients develop when the enzyme reaction involves the consumption or release of protons. This dynamic proton gradient leads to a shift of pH along the pore and again to conditions inside the carrier that might differ substantially from those set in the bulk liquid [5, 15, 17].

A pH gradient inside the particle relative to bulk pH could affect catalytic activity not only in terms of apparent kinetic properties of the enzyme (activity, selectivity, specificity) but also because of the influence of pH on protein stability [5, 15, 17]. Hydrolytic reactions, such as those catalyzed

by lipases, esterases and amidases, are among the most widely used biotransformations in industry [1] and if the enzyme is applied in immobilized form especially sensitive to be affected by mass transfer resistances [15, 17]. In reactions such as the hydrolysis of esters or amides, the formation of even small amounts of protons contributes significantly to pH shifts and hence to alteration of reactions rates. Therefore, development of those biocatalysts should contain a strong component of rational design of the immobilization approach based on internal proton concentration gradients and their local effect on enzyme catalytic properties as key parameter [15, 18].

Macroscopic behavior of biocatalysts results from a combination of both, kinetic and mass transport effects. The magnitude of the internal diffusional limitation is dependent on the fraction of active immobilized enzyme, where reaction velocity might be limited by the rate of diffusion inside the pores [4, 6, 15]. This phenomenon is determined by physical and geometrical properties of the carrier, physical properties of the solute and conditions of reaction mix [4, 15].

The key problem in practice is to determine the relative magnitude of each effect onto the overall performance [4]. Conventional macroscopic biocatalyst characterizations based on apparent parameters can provide hints about microscopic phenomena. However, a distinction between the two principal effects onto observed activity is not possible since bulk measurements cannot uncover the internal environment the enzyme is exposed to [18]. Direct measurements into enzyme carriers would enable to assess the relative importance of pH onto immobilized enzyme performance [18]. Evidence thus obtained would give essential guidelines for targeted optimization of both the immobilization chemistry and the carrier features.

Whereas the pH measurements at liquid phase is successfully carried out using well-established and robust electrochemical sensors, the application at the carrier microenvironment is disabled due to their large size. The use of opto-chemical sensing methods is a promising alternative based on the use of pH dependent luminescent dyes [19]. In the last decade a few studies have been published in which fluorescent based techniques have been applied for detection of pH in immobilized biocatalysts summarized in a recent review [18]. Strategies differ in fluorophores used, luminescence labeling methods and read-out instruments [20–31].

A first work was presented by Spiess et al., [25], who measured intraparticle pH for immobilized penicillin G acylase (PGA) and glutaryl acylase using a pH sensitive fluorescent dye, fluorescein isothiocyanate (FITC), directly coupled to the enzyme. Measurement is based on fluorescence intensity and can be performed in stirred-tank or fixed-bed reactors. A difference was observable between particles and bulk solution under the conditions used for measurement. Direct

fluorescence measurements are prone to interferences as drifts in the optoelectronic system, leaching and/or bleaching of the indicator, nonhomogeneous dye distribution, and turbidity of the sample. Hence, a quantification of proton concentrations is often hardly trustable if the fluorescence signal is not acquired in a referenced form, especially in case of a low signal to noise ratio [19, 32].

The same group tried to overcome this limitation by conducting a referenced intensity measurement with confocal laser scanning microscopy (CLSM) [27]. This measurement set-up does not only reference out many of the above mentioned distorting effects but also permits acquirement of spatial resolved data. Two fluorescent dyes, FITC as pH responsive indicator dye and tetramethylrhodamin isothiocyanat (TRITC) as pH-insensitive reference dye, were co-attached to PGA and enzyme was immobilized to different commercial enzyme carriers. PenG hydrolysis, as well as Amoxicillin and Cephalexin synthesis was studied at steady-state in a fixed-bed reactor. pH profiles over the particle radius at different scanning depths could be obtained. However, an unexplainable dependence of the pH calibration curve onto the scanning depth was reported.

Heinemann et al., [21] tried to further investigate the factors leading to this phenomenon in the measurement of macroscopic large particles. They entrapped the pH-sensitive indicator SNARF-4F 5-(and-6)-carboxylic acid into alginate beads and evaluated the dependence of the pH calibration curve on the scanning depth by a combination of CLSM and modeling of the experimentally obtained results. The employed fluorescence dye exhibits a pH-dependent dual-emission spectra permitting the authors to normalize the intensity signal by rationing two fluorescence intensities measured at different wavelengths. This set-up is less prone to signal perturbations originating from different photobleaching rates or variations in probe loading as in case of two fluorescent dyes. As main interferences wavelength-dependent light scattering and pH-dependent re-absorption of emitted light by the fluorophore was identified. The artifacts can be reduced by a reduction of dye concentration due to a decreased re-absorption probability, small beads and/or more transparent materials since less light will be lost by scattering. Since the main interference originates from light re-absorption, the authors state that the only possibility to completely overcome this signal perturbation would be the use of a dual-emission fluorescent dye exhibiting a Stokes shift large enough to ensure that absorption and emission spectra do not overlap.

Self-referenced measurements based on the determination of the fluorescence excited-state lifetime might be superior to intensity based techniques due to the simple fact that lifetime is not

affected by intensity or wavelength-dependent interferences. Fluorescence lifetime can be measured by the pulse (or time-domain) method and phase modulation (or frequency-domain) method [19, 32]. There are two studies investigating the usefulness of time-domain methods for intraparticle pH measurements, Spiess et al., [26] use a lifetime CLSM to quantify diffusion coefficients for propionic acid in labeled hydrogel beads and Kuwana et al., [23, 33] describe fluorescence lifetime spectroscopy as method for pH quantification in multiply scattering solutions containing an immobilized fluorescent dye.

Only one study actually measures pH in immobilized biocatalysts by the use of a frequency-domain method. Boniello et al., [31] applies dual lifetime referencing (DLR) for the measurement of internal pH in immobilized cephalosporin C amidase (CCA). FITC as pH indicator dye and a ruthenium complex (Rudpp) as reference were incorporated into the enzyme particle and an average pH was measured for the immobilizate suspended into a stirred tank reactor. The dependence of intraparticle pH on reaction conditions and carrier characteristics was investigated. A more detailed methodological overview about the use of DLR for biocatalyst characterization can be found in Boniello et al., [20].

The main disadvantage of fluorescence lifetime based methods is the fact that fluorescence pH indicator dyes exhibit very short lifetimes in the nanometer range which needs sophisticated optoelectronic equipments [19]. DLR is overcoming this drawback by the use of a reference dye depicting a lifetime in the micrometer range. This makes the use of a simple and inexpensive set-up possible, however, reference dye need to fit to specific requirements (decay time in the µs range, overlapping excitation and emission spectra, spectral properties unaffected by analyte) which make the search of a proper dye/reference dye couple by far not an easy task [20]. Moreover, this method currently is restricted to time resolved data of a suspension of immobilizate.

The opto-chemical sensing of pH into biocatalyst particles implies the preparation of internally responsive materials by incorporation of fluorescent dyes and the establishment of a suitable read-out methodology. All current pH sensing methods developed for the study of immobilized enzymes involve the attachment of a chemical fluorescent indicator molecule onto enzyme or carrier surface. The direct conjugation of enzyme and fluorophore present the disadvantages of potential alteration of enzyme function or lack of signal intensity. Direct incorporation on the carrier matrix would generate independency on the specific enzyme to be used but to perform the labeling compatible with enzyme immobilization is challenging [18]. Fluorophores are usually very hydrophobic chemical molecules and their controlled attachment onto a hydrophilic enzyme

carrier is not easy [19]. Attachment approach or simply their presence onto the carrier could lead to substantial enzyme inactivation. A general labeling procedure easily applicable to different materials is missing [18]. Another group of fluorescent molecules widely applied in biosciences might depict an interesting alternative; Fluorescent proteins (FP) and among those the well-known green fluorescent protein (avGFP) from the jellyfish *Aequorea victoria*. avGFP and engineered variants have been used as fluorescent reporters in a variety of applications due to their remarkable properties [34–37]. The FP can be cloned and expressed by conventional molecular biology techniques and fused to other proteins or (purification) tags without losing its optical properties. Furthermore, molecular engineering permits the modification of spectral and photophysical characteristics to suit specific requirements of the researcher [38]. Incorporation into an enzyme carrier can be controlled by conventional established protein immobilization procedures and inactivation of catalyst as a consequence of the presence of a fluorescent protein inside the porous structure is not expected.

Fluorescence originates from a chromophore, generated by spontaneous posttranslational cyclization of three consecutive amino acids (S65, Y66 and G67) in the center of the proteins β-barrel structure (see Scheme 1). Formation of the chromophore is a genetically encoded species independent process with no need for substrates or cofactors [39, 40]. Residues (Q69, Q94, R96, H148, T203, S205 and E222) placed around the chromophore function as proton donors and acceptors and are the ones defining the final spectral and photo-physical properties of each FP variant [41, 42].

Though wild-type protein is relatively insensitive to pH the two absorbance bands of a number of avGFP variants are interconvertible as a function of pH attributed to the ionization equilibrium of the chromophore [43, 44]. A detailed description of the physical and chemical characteristics of avGFP and mutants can be found elsewhere [45–47]. Briefly avGFP exists in one of two ground states, denoted A and B, which correspond to the neutral-protonated and anionic-deprotonated form of the chromophores Tyr^{66} phenolic group, respectively (see Scheme 1). State A absorb maximally at about 398 nm, state B exhibits a maximal absorption at about 475 nm [48, 49]. When pH increases state A progressively converts to state B. Emission takes place via a common pathway from the excited anionic chromophore. While the excited anionic B* state emits directly, the excited A* state is relaxing in two ways (i) direct emission from the A* state or (ii) via an excited-state proton transfer (ESPT) mechanism involving one or more intermediate metastable states. The weak emission from A* is usually overhelmed by the latter [41, 50, 51].

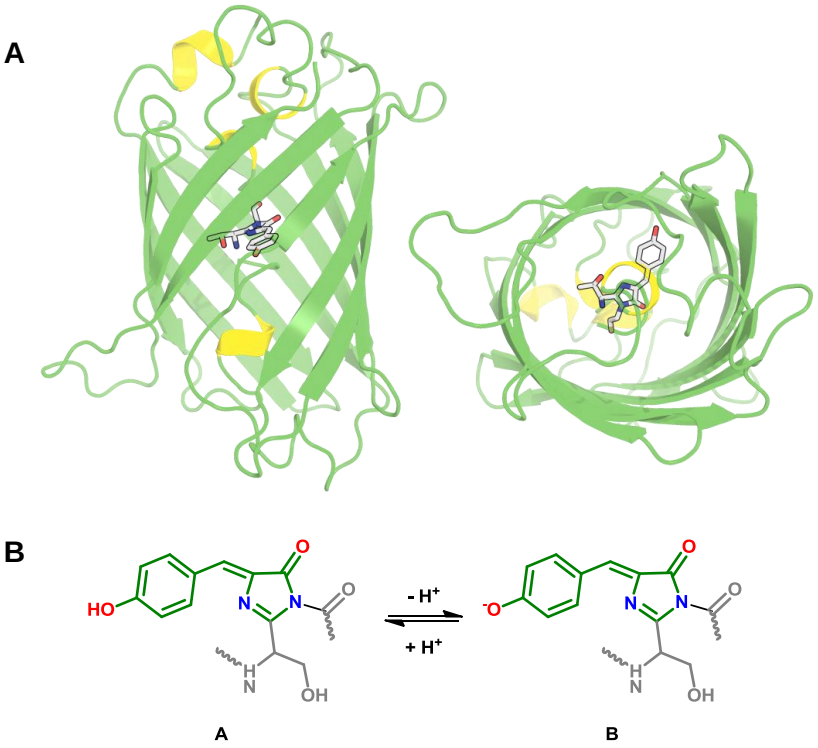

Scheme 1. Protein structure and protonation equilibrium of avGFP redrawn from [36]. (A) Three-dimensional structure of avGFP (PDB ID. 1EMA). The chromophore is shown in stick representation. (B) Protonated neutral (A state) and deprotonated anionic (B state) of avGFP chromophore.

The basis of pH sensing with FPs is the influence of pH onto equilibrium between A and B state [46]. For many avGFP variants photophysical behavior can be explained by ionization of Tyr^{66} phenolic group alone, however, for other mutants the spectral features are not described well with the simple scheme of phenol ionization. Bizarri et al [45, 46] therefore suggest a two-side model (shown in Scheme 2) based on the presence of a second ionizable group X in close proximity to the chromophore phenol. That implies four distinct ground states (denoted A', A, B' and B) corresponding to all four possible combinations of protonation states of X and the chromophore. Optical properties are affected when X is coupled to the chromophore thermodynamically. If uncoupled, X is thought to affect kinetics of proton exchange between solvent and chromophore but spectral features can be explained well by the simple model of phenol ionization. Two residues were identified in several avGFP mutants; in those were X is His^{148} chromophore is uncoupled, if X is Glu^{222} a strong anti-cooperative coupling (i.e. deprotonation of one forbids the deprotonation of the other) was found whenever Glu^{222} residue

was not forced into a single protonation state by a hydrogen-bonding action by another nearby reside such as Thr^{65} [45, 47].

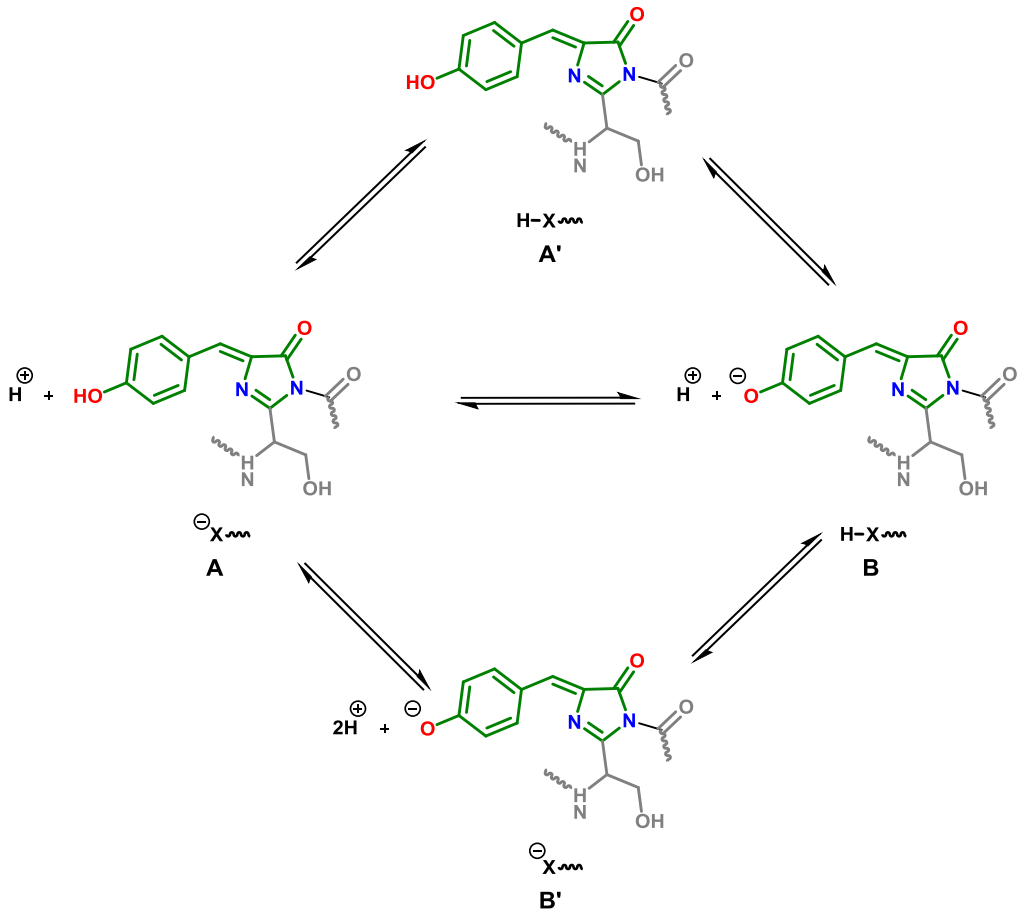

Scheme 2. Two-side model of pH dependent ground states in avGFP redrawn from [46]. X represents an ionizable group located close to the chromophore. When X and the chromophore are uncoupled only state A' and B are relevant and optical properties follow equilibrium shown in Scheme 1. If X is coupled with the chromophore, ionization of one impede the ionization of the other (anticooperative coupling) and the fully deprotonated state B' is populated at a pH beyond the stability range of avGFP. Optical response follows single ionization of protonated A' state to an apparent mixed form of the A and B states [45].

Both, coupled and uncoupled avGFP variants depict a pH dependency in their optical properties, that can be well described by the proposed two-side model [45, 46]. Hence, in principle all avGFP mutants possessing a Tyr^{66} residue are utilizable as pH indicators. However, many avGFP variants and among those also wtGFP depict a pH dependent response in a range far from where most of enzymatic reactions take place (response at pH<6 and from pH 10-12) [44].

Those are usually coupled variants characterized by a strong buffering capacity from Glu^{222} residue [46, 47].

In the last years an immense research was performed for the implementation of FPs as genetically encodable pH indicators for *in vivo* use, summarized in a recent review [52]. avGFP-based pH indicators are classified into (i) non-ratiometric and (ii) ratiometric pH sensors. Intensity-based non-ratiometric pH sensors are usually characterized by a poor emissivity of the neutral chromophore and due to a complicate calibration mostly applied to report pH changes rather than pH itself. Ratiometric pH-sensitive proteins depict dual excitation and/or emission spectra permitting intensity ratiometric measurements either in excitation or emission. This allows correcting the signal for optical interferences originated by the optical read-out system, photobleaching and inhomogeneities in indicator loading [32]. Moreover, the self-referencing nature of these FP-based indicators makes use of a second pH-independent (chemical) reference dye unnecessary.

So far only a few truly ratiometric protein-based pH indicators have been reported [52]. The variants developed by the group of Beltram [53, 54] depict excellent properties as pH ratiometric probe. E^1GFP and E^2GFP are both yellow fluorescent protein (YFP) variants, which are well known for their enhanced sensitivity to pH due to a less tight embedded phenolic end of the chromophore [55]. Based on the work performed on E^1GFP and E^2GFP, we tested superfolder yellow fluorescent protein (sYFP) developed by the group of Berenguer [56] for its suitability as self-referencing pH indicator in the application of internal pH sensing in immobilized biocatalysts. A methodology for the real-time pH quantification within immobilized biocatalysts based on intensity ratiometric measurements in CLSM will be presented. First, a strategy for the homogeneous incorporation of sYFP into different commercial enzyme carriers was developed. The suitable pH range and dynamic pH response of the heterogeneous sYFP sensors were studied for monitoring of pH decrease promoted by a homogeneous enzyme catalyzed acidification reaction. Penicillin G acylase was coimmobilized sYFP and internal pH was measured in real-time for different set of conditions. The application of the methodology has enabled the quantification of internal pH gradients in PGA immobilizates and it represents a valuable strategy applicable to other pH-dependent immobilized biocatalysts.

2 MATERIALS AND METHODS

2.1 MATERIALS

Penicillin G acylase (PGA) from *E. coli* and Penicillin G (PenG) were supplied by Antibióticos S.A. (León, Spain). His tagged sYFP was provided by Dr. Aurelio Hidalgo from *Centro de Biología Molecular "Severo Ochoa" (CBMSO, Madrid, Spain)*. Carboxylated Platinum(II)-5,10,15,20-tetrakis-(2,3,4,5,6-pentafluorphenyl)-porphyrin (PtTFPP) was synthetized in the Institute of Analytical Chemistry and Food Chemistry (TU Graz, Graz, Austria) according to the following protocol: 1 equivalent of PtTFPP was incubated with 3 equivalents of 3-thiopropionic acid and 25 equivalents of triethylamine in dimethylformamide at 50 °C for 16 h. Finally, the soluble carboxylated-PtTFPP (c-PtTFPP) was recovered and washed by successive steps of precipitation in acidic water and resuspension in basic water.

Agarose 6 BCL (Ag BCL) STANDARD (particle size 50-150 µm) or FINE (particle size 20-50 µm) was obtained from Agarose Bead Technologies (Madrid, Spain). TRISOPERL® controlled pore glass (CPG) beads (particle size 50−100 µm diameter, pore size 161.2 nm, pore volume 1520.91 mm^3/g and specific surface area 43.16 m^2/g) were obtained from VitraBio GmbH (Steinach, Germany). Sepabeads® EC-EP (Sepabeads) (standard grade; particle size 150-300 µm; pore size 10-20 nm) were provided by Resindion (Milan, Italy).

Serum bovine albumin (BSA), epichlorohydrine, sodium borohydrate ($NaBH_4$), 2-Nitro-5-phenylacetamidobenzoic acid (NiPAB), (3-glycidoxypropyl) trimethoxysilane (GPMES, 99.7%), N,N′-diisopropylcarbodiimide (DIC), N-hydroxysuccinimide (NHS), ethanolamine, imidazole, iminodiacetic acid (IDA) and phenyl acetic acid (PAA) were purchased from Sigma Aldrich (St Louis MO, USA).

All other reagents are of analytical grade and obtained elsewhere.

2.2 ASSAYS

Activity of soluble and immobilized PGA was determined spectrophotometrically using NIPAB as a substrate and by direct quantification of PenG hydrolysis.

NIPAB activity

Activity of soluble and immobilized PGA was determined by measuring the increase in absorbance at 405 nm upon hydrolysis of 0.15 mM NiPAB in 50 mM sodium phosphate buffer

(SPB) at 25°C and pH 7.50 (ε = 9090 $M^{-1}cm^{-1}$). Reaction was initiated by addition of 0.05-0.20 mL of enzyme solution or suspended immobilizate to a cuvette containing substrate solution. One activity unit (IU_{NiPAB}) is the amount of PGA that hydrolyzes 1 µmol of NiPAB per minute.

PenG activity

The hydrolytic activity of soluble and immobilized PGA was performed by titration of phenylacetic acid released upon hydrolysis of 10 mM PenG. Measurements were conducted using an automatic titrator (DL 50 Mettler Toledo) in a final volume of 25 mL SPB (0.1 M) at pH 7.50 and 25°C using 25 mM NaOH as titrant solution. One activity unit (IU_{PenG}) is the amount of PGA that hydrolyzes 1 µmol of PenG per minute.

Under the applied conditions of measurements the ratio of activity between the two assays is IU_{PenG}/IU_{NiPAB}= 1.8

Protein quantification

Protein concentration was determined using the method of Bradford [57] referenced against known concentrations of BSA.

2.3 ANALYSIS OF PenG HYDROLYSIS

pH time courses were used for the quantification of initial reaction rates based on the kinetic of PenG hydrolysis catalyzed by soluble PGA. The kinetic for hydrolysis of PenG is widely accepted [58] and has been recently validated for the variant of PGA used in this thesis [59–61]. Hydrolysis kinetic depicts substrate and double product inhibition from phenylacetic acid (PAA) and 6-aminopenicillanic acid (6-APA) in a competitive and noncompetitive manner respectively. Kinetic equation is shown in Equation 1.

$$V = \frac{V_{max} \cdot S}{K + S + \frac{S^2}{k_s} + \frac{K \cdot P_1}{k_1} + \frac{K \cdot P_2}{k_2} + \frac{S \cdot P_2}{k_2} + \frac{K \cdot P_1 \cdot P_2}{k_1 \cdot k_2}} \qquad (1)$$

Parameters used for Eq. 1 are shown in Table 1.

Table 1. Parameters used for the calculation of initial reaction rates in the hydrolysis of PenG by soluble PGA based on Eq. 1.

Component	Parameter	Value	Units
Enzyme	Vmax	0.3-30	mM/min
Penicilin G (S)	K	0.13	mM
Penicilin G (S)	K_s	821	mM
PAA (P1)	K_1	1.82	mM
6-APA (P2)	K_2	48	mM

For each mole of PenG consumed, one mole of acidic product PAA is produced. Considering the reported pK_a value of 4.31 for the carboxylic group of PAA, it is assumed that PAA generated in the enzymatic reaction will be completely dissociated at the pH range used in this study (5.50-9.00), therefore a substrate molar equivalent to a proton is formed in the reaction at rate V (mM/min). The pH change due to the release of protons is described by the Henderson-Hasselbalch equation:

$$pH = pK_a + log_{10}\left(\frac{[HPO_4^{2-}]_0 - [H^+]}{[H_2PO_4^-]_0 + [H^+]}\right) \qquad (2)$$

Concentration of phosphate monoanion and dianion at the start of the reaction were calculated from the initial pH using a pK_a of 7.20. $[H^+]$ is the proton concentration generated by PenG hydrolysis. To include the dependence between enzymatic activity and pH it is assumed that only V_{max} is significantly influenced by pH. The acidic limb of the pH curve is known from experiments to be described by the following equation:

$$V_{max} = \frac{V^*_{max}}{1 + 10^{pK-pH}} \qquad (3)$$

V_{max} is the maximum reaction rate at a certain pH, V^*_{max} is the maximum reaction rate at optimum pH. Reaction rates are dependent on the amount of enzyme suspended per unit of volume and were used for the fitting and calculation of volumetric activities in acidification experiments (V_{max}).

V_{max} was calculated in Berkeley-Madonna™ (http://www.berkeleymadonna.com/) by fitting the experimental pH time courses using the code provided in the appendix. Once V_{max} was calculated differential equation model was used for simulation of pH time courses under different experimental conditions (buffer concentrations and enzyme activities).

2.4 PREPARATION OF IMMOBILIZATION SUPPORTS

Epoxy activated Agarose 6 BCL (Ag-epoxy)

The activation of agarose with epoxy groups was performed as described previously [62]. 55.0 g of Agarose 6 BCL (Ag BCL) thoroughly washed with distilled water was suspended in a mixture of 80 mL Acetone and 220 mL of water containing 1.0 g $NaBH_4$ and 16.4 g NaOH. 55 mL epichlorohydrine was added drop-wise to the suspension under gentle stirring and activation was allowed to proceed for 16 h. Activated agarose gel was washed with an excess of distilled water and kept at 4°C until further use.

Number of epoxy groups introduced was quantified spectrophotometrically by back-titration with $NaHCO_3$/KI as described by Guisán [63]. Briefly, epoxy groups were hydrolyzed to glyceryl groups by incubating 1.0 g of support with 10 mL 500 mM H_2SO_4 for 2 h followed by oxidation to glyoxyl groups with 10 mL $NaIO_4$ (20 mM in water). Number of epoxy groups was calculated by the difference in consumption of periodate between hydrolyzed support and initial epoxy support. Remaining periodate was quantified by titration with potassium iodide as described previously [62].

Trisoperl® epoxy (CPG-epoxy)

The carrier was activated with epoxy groups according to a modified protocol derived from [64]. 1.0 g of wet support was activated in 30 mL of toluene containing 5% GPMES at reflux and 105°C for 3 h under gentle stirring. Activated support was washed extensively with acetone to remove toluene and residual functionalization reagent and further with distilled water. Support was dried and stored at 4°C until further use.

Glyoxyl agarose (Ag-glyoxyl)

Support was derived from Ag-epoxy by hydrolysis of epoxy groups to glyceryl groups and subsequent oxidation with $NaIO_4$ to glyoxyl groups as described above.

Metal chelate supports

Carriers were activated with iminodiacetic acid according to a modified protocol derived from [65]. 1.0 g of corresponding epoxy-support was suspended in 10 ml of 100 mM sodium bicarbonate buffer (SBB) containing 0.9 g of IDA. pH was adjusted to 11 by addition of solid NaOH and left to incubate at 25°C under gentle stirring. Ag-epoxy activation was performed for 2 h. For CPG-epoxy and Sepabeads (Sep-epoxy) activation was allowed to proceed overnight. IDA activated supports (Ag-IDA, CPG-IDA and Sep-IDA) were washed extensively with water. Residual epoxy groups were hydrolyzed to glyceryl groups as described above. To prepare the metal chelate supports, the IDA supports were incubated in distilled water containing 10 mg/mL $NiSO_4$ for 30 min. Residual metal was removed by washing the supports with distilled water and glyceryl-IDA-Ni^{2+}-chelate carriers (Ag-Ni, CPG-Ni and Sep-Ni) were kept at 4°C until further use.

Heterofunctional metal chelate glyoxyl agarose (Ag-Ni-glyoxyl)

Ag-IDA carrier was prepared as described previously. Residual epoxy groups were hydrolyzed to glyceryl groups and oxidized with $NaIO_4$ to glyoxyl groups as described before. Incubation with $NiSO_4$ was carried out as explained above.

2.5 sYFP PURIFICATION

Polyhistidine (poly-His) tagged sYFP was purified from *E. coli* crude extract by selective adsorption onto Ag-Ni. Purification was performed by offering 10 mL of protein solution in 50 mM SPB, pH 7.00 (maximal concentration used was 1.5 mg/mL) to 1.0 g of Ag-Ni. In order to prevent unspecific adsorption buffer was supplemented with 30 mM imidazole. Suspension was incubated overnight at 4°C. Carrier was washed extensively with buffer to remove unbound protein followed by desorption of sYFP with 1 M of imidazole. Imidazole was removed by dialysis from protein solution at 4°C overnight against 10 mM SPB, pH 7.50.

2.6 PGA PREPARATION

E. coli crude extract containing overexpressed PGA was dialyzed at 4°C overnight against 50 mM SPB, pH 7.50. Protein solution was concentrated 10x and desalted with 10 kDa MWCO Amicon Ultra centrifugal filters (Milipore, Germany) and 5 mM SPB, pH 7.00.

2.7 ENZYME IMMOBILIZATION

PGA (2-400 IU_{NiPAB}/g of carrier) and sYFP (8-10 mg/g of carrier) immobilization was conducted by addition of 1.0 g of the corresponding support to 10 mL of protein solution and suspension was incubated under gentle mixing and unless mentioned at room temperature. Progress of PGA immobilization was followed by withdrawing samples at different time points and measuring PGA activity in the supernatant and suspension using NiPAB as substrate. sYFP attachment was followed by determining residual protein in the supernatant. The amount of protein or activity immobilized was calculated from protein mass or activity balances. Immobilization yield is defined as the percentage ratio of bound to offered protein or activity.

PGA immobilization onto Ag-Ni-glyoxyl

Multipoint covalent attachment of PGA on Ag-Ni-glyoxyl was performed as described previously [66] in a mixture of 100 mM PAA in 25% (v/v) glycerol and 100 mM SBB, pH 10.05 at RT. Reduction of Schiff's bases was carried out by addition of solid sodium borohydride up to a final concentration of 1 mg/mL and suspension was allowed to incubate at 4°C for 30 minutes under gentle stirring. Support was filtered and washed extensively with distilled water in order to remove reduced Ni^{2+}. Additionally, attachment of PGA was performed with Ag-IDA-glyoxyl at 4°C or RT supplementing the immobilization mixture with different concentrations of NaCl as indicated for each experiment.

sYFP immobilization onto Ag-glyoxyl

sYFP immobilization was carried out at 4°C in 100 mM SBB at pH 10.05 supplemented with either 1 M ethanolamine, 1 M Tris buffer or without supplementation. Concentration of ethanolamine and Tris buffer was diluted step-wise during immobilization process to a final concentration of 31.25 mM by addition of the corresponding amount of SBB and left to incubate overnight.

sYFP immobilization on Carrier-Ni

Immobilization was conducted in 25 mM SPB, pH 8.00, containing 300 mM imidazole which further was diluted step-wise to a final concentration of 37.50 mM by addition of the corresponding amount of SPB and left to incubate overnight. The same immobilization was performed on Agarose FINE activated with IDA-Ni^{2+}-groups as described for Ag-Ni. Resulting immobilizate will be referred as control particles.

sYFP-PGA coimmobilization on Ag-Ni-glyoxyl

First, PGA immobilization was conducted as described above for Ag-Ni-glyoxyl, followed by an incubation of the immobilizate in 10 mM SPB, pH 7.00 containing 1 mg/mL $NiSO_4$ for 30 min. Unbound metal was removed by washing the support with distilled water. No difference in expressed activity measured with NiPAB as substrate was determinable for immobilized PGA before and after incubation in $NiSO_4$. Adsorption of sYFP was performed as described above for the metal chelate supports.

2.8 SDS-PAGE ANALYSIS

SDS-PAGE electrophoresis was performed as described previously [67] in a Mini-PROTEAN® Tetra Cell (BioRad) by using a 12% polyacrylamide gel. A solution of soluble or immobilized protein (1 mg/mL) was dissolved in SDS-loading buffer and boiled for 10 min. Supernatant was injected directly into the gel. Gel staining was conducted according to the Coomassie method [68]. Molecular weight markers were used from Pharmacia LMW kit (14.4–97.0 kDa).

2.9 PGA LABELING

PGA immobilized onto Ag-Ni-glyoxyl was labeled with a luminescent NHS-ester activated dye (PtTFPP-NHS); activation and coupling of the dye were performance according to a modified protocol derived from [69].

Dye activation

To 1 mL of a 1 mM c-PtTFPP solution in dioxane, 3.2 µL of DIC and 28.8 mg of NHS were added. Reaction was left under mild magnetic stirring and light protection for 2 h at RT. Solution was filtered and used the same day without further purification.

PGA labeling

Ni^{2+} was eluted from covalent attached PGA by incubation in 500 mM EDTA in water, pH 7.5. 100 mg of washed PGA immobilizate was resuspended in a solution of 0.85 mL 100 mM SPB, pH 7.50 and 150 mL of c-PtTFPP-NHS solution. If necessary pH was corrected to 7.50 and coupling reaction was allowed to proceed under light protection at RT for 3 h. Labeled PGA-biocatalyst was extensively washed with distiller water. In order to control if washing steps are sufficient to remove all unbound luminophore, control particles (Agarose BCL FINE) without attached PGA were prepared and treated as described for Ag-Ni-glyoxyl.

2.10 CONFOCAL LASER SCANNING MICROSCOPY (CLSM)

Ratiometric imaging was conducted with a Zeiss LSM 710 inverted confocal microscope (Carl Zeiss, Jena, Germany) using an EC Plan-Neofluar 10X/0.30 M27 objective and the 458 and 488 nm laser lines of the Argon laser. Images were acquired for excitation ratiometric method by exciting the sample at λ_{x1}=458 nm and λ_{x2}=488 nm while collecting emission at λ_e=500-600 nm applying a sequential scanning mode. In emission ratiometric setting images were collected simultaneously during excitation at λ_x=458 nm and emission was monitored in two windows at λ_{e1}=475-515 nm and λ_{e2}=515-600 nm. For each ratiometric couple of images (excitation or emission), care was taken to operate at the same photomultiplier voltage.
Digital image processing (background subtraction, median filter) and quantitative evaluation was performed using Fiji imageJ processing package software [70] version ImageJ 1.49d (http://fiji.sc/Fiji). For assembly of pH maps images processed in Fiji were exported to Matlab R2009b (version 7.9.0.529, The MathWorks Inc.). Images were calculated according to the script shown in the appendix.

Protein distribution analysis

Distribution of PGA and sYFP was visualized by CLSM. PGA immobilizates labeled as described above were resuspended in 50 mM SPB, pH 7.50 in a ratio of 1:100 (w/v) and 10 µL of this suspension were added to an 8-well glass bottom µ-Slide (Ibidi, Munich, Germany) for analysis. Confocal images were acquired by excitation of c-PtTFPP at λ_x=405 nm and collecting emission at λ_e=550-740 nm. sYFP immobilizates were resuspended in 10 mM SPB, pH 7.00 and analyzed as described for PGA exciting at λ_x=488 nm and measuring emission at λ_e=500-600 nm.

pH calibration using CLSM

Samples were dissolved in a citrate (20 mM)/phosphate (100 mM) buffer, whose pH was adjusted to the desired value by dissolving the proper amounts of each basic or acid species of the salts in MiliQ water. When necessary, pH was adjusted by addition of solid NaOH.

Soluble sYFP: 2 mg sYFP/mL was diluted 1:2 in calibration buffer of required pH and 200 µL of this solution was transferred into a µ-Slide. Imaging was performed at room temperature in a thermostated chamber (Cell Observer-Zeiss) as described above.

sYFP immobilizates: For immobilized sYFP as well as sYFP-PGA coimmobilizates (both containing around 10 mg sYFP/g of carrier) immobilizates were washed with MiliQ water. A 1:10 (w/v) preparation in MiliQ water was further diluted 1:20 in each calibration buffer and 200 µL of this suspension was analyzed as described for soluble sYFP.

pH of all preparations was controlled using a standard pH meter before microscopy analysis.

pH time course measurements

Soluble sYFP: Soluble sYFP (2 mg/mL) was diluted 1:2 in 10 mM or 100 mM SPB, pH 9. From this solution 180 µL were transferred to a µ-Slide well and imaging was started. 10 µL of soluble PGA were added followed by the start of the reaction by addition of 10 µL 200 mM PenG suspended in 50 mM SPB, pH 9.

sYFP immobilizates: Immobilized sYFP was washed with either 10 mM or 100 mM SPB and 10 µL of a 1:100 (w/v) suspension was transferred to a µ-slide well containing 170 µL of the same buffer. Reactions were performed as described for soluble sYFP.

sYFP-PGA coimmobilizates were washed with SPB buffer at the pH and concentration specified in the specific experiment. 10 µL of a 1:100 (w/v) suspension together with 10 µL of a 1:100 (w/v) suspension of control particles (see above) were transferred to a µ-slide well containing 170 µL of the same buffer. Reactions were started with addition of 10 µL of a 400 mM PenG solution in 50 mM SPB, pH 9.

It was controlled that addition of PenG without PGA present in the reaction mixture will not lead to any unspecific decrease of pH. For soluble and (co-)immobilized sYFP photobleaching was controlled by imaging sample over the duration of an average measurement. Since particles might move upon addition of liquid to the µ-slide well, it was controlled that this effect does not lead to a misinterpretation of particle movement as unspecific pH changes by addition of 10 µL of the corresponding buffer.

2.11 ANALYSIS OF pH RESPONSE

For each pH value different regions of interest (ROIs) were defined in each processed image. Mean intensity of selected area was used to calculate fluorescence intensity ratio (R) of the two

wavelength couples chosen for excitation (F(488, 500-600)/F(458, 500-600)) and emission (F(458, 515-600)/F(458, 475-515)) ratiometric setup respectively.

Dependence between R and pH can be described by the two-side model of chromophore protonation suggested by [46, 53] according to following equation:

$$R = R_0 \cdot \left(\frac{R_f + 10^{(pK' - pH)}}{1 + 10^{(pK' - pH)}} \right) \qquad (4)$$

R_0 (ratiometric offset) represents the lower asymptote in a plot of R against pH. R_f (dynamic range) depict the amplitude and pK' (ratiometric pK') the mid-point. R_0, R_f and pK' were acquired from a fit of experimental R measured upon pH using equation 4. Ratiometric nature of all parameters in Eq. 4 makes R independent on fluorescence variations originating from differences in fluorophore concentration, photobleaching or the optical system. pK' and R_f only depend on the photophysical and thermodynamic properties of the fluorescent protein as well as on selected wavelength couples. R_0 is influenced by instrumental characteristics such as excitation intensity and detector efficiency as it represents a fluorescence ratio taken with two distinct excitation/emission setups [46].

The fluorescent molecule only behaves as a ratiometric probe when $R_f \neq 1$, i.e. fluorescence probe undergoes a different variation in optical signal between the two chosen wavelength couples. R is not a function of the actual pK of the protein but of the apparent pK'. The maximal sensitivity of the ratiometric sensor is displayed in the range pK'±1, where R versus pH shows an almost linear dependence [46].

2.12 pH CALCULATION AND ERROR PROPAGATION ANALYSIS

pH was calculated according to equation 5 following the dependency onto R derived from Eq. 4.

$$pH = pK - log_{10}\left(\frac{\frac{R}{R_0} - R_f}{1 - \frac{R}{R_0}} \right) \qquad (5)$$

The calculation of pH is affected by different sources of uncertainties. Among those the main error is related to the precision in the measurement of R. Precision was estimated from multiple determination of R from different ROIs in each image of a specific pH value and was expressed

in the form of a standard deviation (SD). This error was used for the quantification or error propagation associated with the measurement of pH according to equation 6 [71–73].

$$\Delta pH = \sqrt{\sum_{i=1}^{n} s_i^2 \cdot e_i^2} \qquad (6)$$

Where n is the number of independent variables affected by the error e and s is the sensitivity coefficient of each independent variable presented in Eq. 5. The sensitivity quantifies the effect of small changes in R onto pH and is calculated according to equation 7 as the partial derivative of the pH function (see Eq. 5) with respect to each variable x [71, 72].

$$s_i = \frac{\partial pH}{\partial x} \qquad (7)$$

Taking only the uncertainty of determination of R and the error associated to the calculation of pK', the equation for the calculation of the error propagation is:

$$\Delta pH = \sqrt{\left(\frac{1 - \frac{R}{R_0}}{\frac{R}{R_0} - R_f} \cdot \frac{1}{ln10} \cdot \frac{\frac{1}{R_0} \cdot \left(1 - \frac{R}{R_0}\right) + \frac{1}{R_0} \cdot \left(\frac{R}{R_0} - R_f\right)}{\left(1 - \frac{R}{R_0}\right)^2} \right)^2 \cdot (\Delta R)^2 + (\Delta pK)^2} \qquad (8)$$

The value of ΔR is the average SD for all analyzed ROIs and pH values (includes pH values far above and below the dynamic range of sYFP). The result is the calculation of the maximum possible error since the value of R precision decreases with decreasing R and when pH lies in the dynamic range or below. Equivalently, the sensitivity of R to pH changes for each measurement setting can be calculated according to the first derivative of R with respect to pH.

$$\frac{\Delta R}{\Delta pH} = \frac{\partial R}{\partial pH} = R_0 \cdot \frac{-10^{pK-pH} \cdot ln10(1 + 10^{pK-pH}) + 10^{pK-pH} \cdot ln10\left(R_f + 10^{pK-pH}\right)}{(1 + 10^{pK-pH})^2} \qquad (9)$$

Eq. 9 can be used for the interpretation of the change of R expected for a defined acidification rate and compared with the signal-to-noise ratio from the measurements. When the needed change in R calculated for a pH value and desired precision in pH determination approaches the value of precision of R, the use of the sensor is not advisable.

3 RESULTS AND DISCUSSION

3.1 EVALUATION OF sYFP AS AN EXCITATION AND EMISSION RATIOMETRIC pH SENSOR

3.1.1 pH response of soluble sYFP

Suitability of sYFP as a ratiometric pH indicator in excitation and in emission was evaluated. For all wavelength ratiometric methods the measureable fluorescence ratio and therefore the apparent pK' are very sensitive on the choice of emission/excitation couples. A thorough study of E^2GFP was published by Bizarri et al. [53]. Settings of an emission ratiometric and of an excitation ratiometric setup were adapted from there and tested for studying the pH response. For excitation ratiometric setup, excitation is switched between two suitable wavelengths of the indicator, emission range is kept constant. We decided to set the emission window to λ_e=500-600 nm and as excitation wavelengths λ_{x1}=458 nm and λ_{x2}=488 nm were chosen, because published data suggested a good dynamic range (R_f=8.3) and an apparent pK' around 6.91 [53]. In general response sensitivity of optical pH sensors is highest at pK'± 1 [19], hence, a pH range from 8.0-6.0 should be optimally resolved. Most of enzymes are stable and active at a pH range from 5.0-8.5. Hence, pK' of sYFP analyzed with excitation ratiometric method would fit well to the pH range relevant for enzyme catalyzed reactions [15, 17]. Moreover, both excitation wavelengths are emission lines of the widely available Argon laser.

In the emission ratiometric setup, excitation wavelength of the indicator is kept constant, whereas range of emission is changed. We decided to fix excitation at λ_x=458 nm and emission was measured in two windows at λ_{e1}=475-515 nm and λ_{e2}=515-600 nm, providing a good compromise between dynamic range (R_f=6.4) and apparent pK' (7.50). With these settings again the Argon laser can be used as light source and pK' correspond well to the required pH range.

Dependence of fluorescence ratio upon pH was analyzed with both methods for a suspension containing 2 mg/mL of soluble sYFP in buffer. pH response curves are shown in Figure 1. For each pH condition three different regions of interest (ROI) were analyzed in each image. A sigmoidal dependency is observed for both methods where no significant deviation in the measured fluorescence intensity ratio was detectable between different regions chosen for analysis. Differences remain lower than 1% even for high pH values where the expected sensor response is significantly lower. Result shows that a reliable signal can be obtained for the

analyzed pH range independent on the ratiometric method used under the applied settings. These settings were successively kept constant for further studies of the sensor.

Differences of pH response on specific configuration of each method can be observed. Emission ratiometric settings lead to a curve more shifted to basic pH compared to the ones chosen for the excitation ratiometric option, following the expected trend derived from the data published by Bizarri et al. [53].

From the graph it can be observed that the change of fluorescence ratio with pH is highest from pH 9.0 to 6.5 for emission and from pH 5.0 to 8.5 for excitation ratiometric method, suggesting an optimal resolvable pH window in these areas. In the latter method it is not completely sure how much from the acidic pH area can be resolved since range of pH chosen for analysis does not explore completely the acidic area.

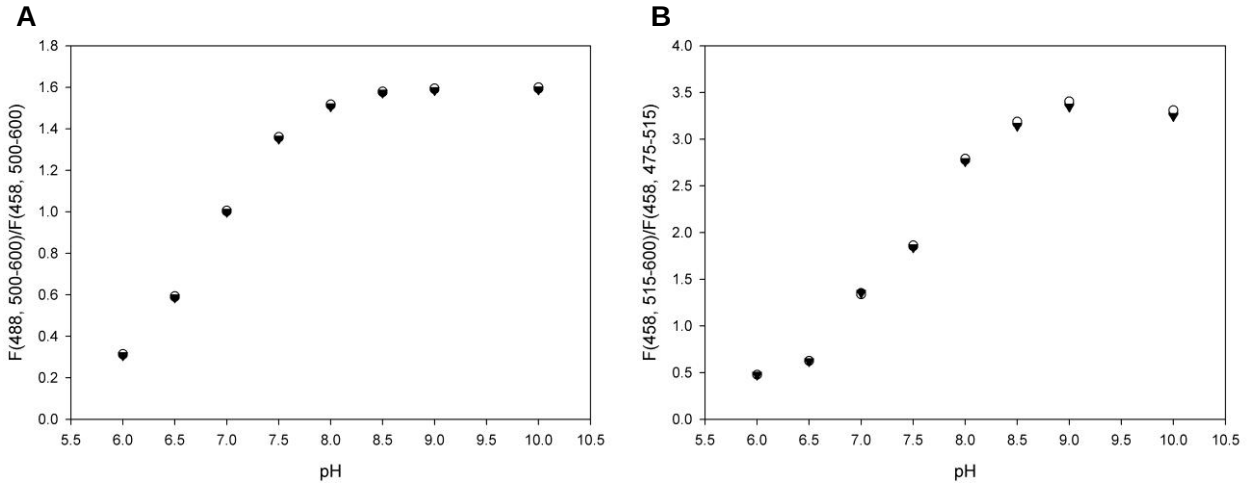

Figure 1. Dependence of fluorescence ratio onto pH. **A** Excitation and **B** emission ratiometric calibration of soluble sYFP. For each calibration three different ROIs were analyzed.

Fluorescence ratio was averaged for each pH and sigmoidal dependence quantified according to Eq. 4. Result of fitting is shown in Figure 2 and summarized in Table 2.

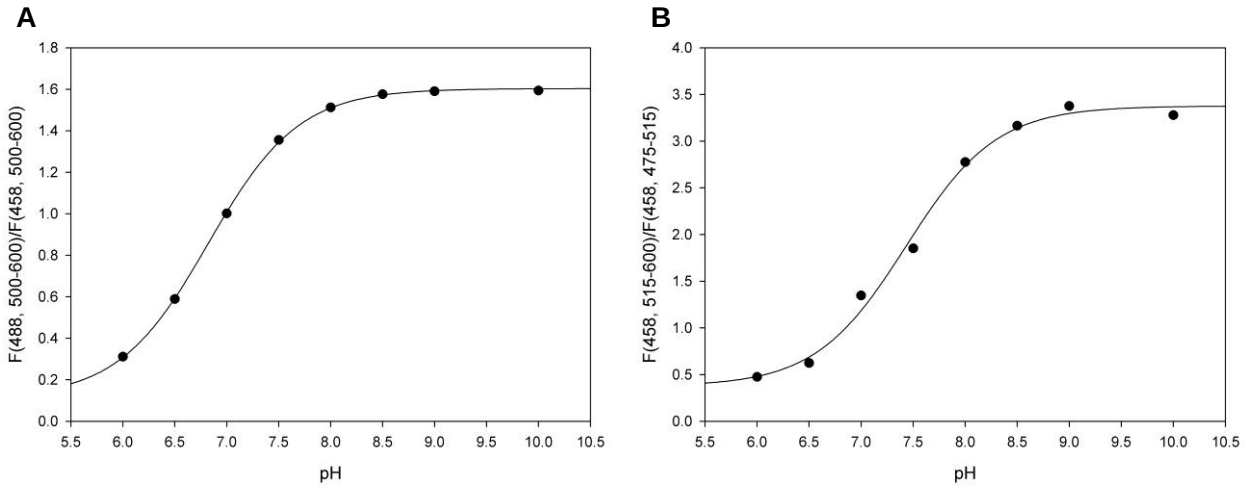

Figure 2. Dependence of fluorescence ratio onto pH. **A** Excitation and **B** emission ratiometric calibration of soluble sYFP. Each point represents an average of three different ROIs. pH response curve was fitted to Eq. 4.

For excitation ratiometric method apparent pK' was determined to be 6.82, for emission ratiometric settings pK' is 7.43. Dynamic range (R_f) is about 5 points higher for excitation compared to emission ratiometric method, providing a better capability of pH resolution in principle.

Standard error for excitation ratiometric method is noticeable lower for all three fitting parameters. This might be due to the brighter fluorescence measured by this setting due to a wider emission window. Generally, standard deviation is very low for pK' and R_0 but significantly higher confidence limits were found for R_f in case of both methods. Accurate determination of R_f might turn problematic, especially for excitation ratiometric method. Calibration performed in emission ratiometric manner covers the whole area of sigmoidal dependence on pH, whereas for excitation ratiometric method dynamic range might be a bit overestimated attributed to a lack of values in a more acidic pH range. The availability of more points in the acidic range might permit more accurate quantification of R_0 and therefore affect to the value of dynamic range. This observation does not offer a limitation in the context of this analysis, since the aim was a location of the measurable pH range by application of sYFP as pH sensor under the chosen settings. According to pH sensing by means of fluorescence methods [19], sYFP seems to be suitable to be used as ratiometric pH sensor in excitation (pH 6.82±0.75) and emission (pH 7.43±0.75).

It should be emphasized that the wavelength couples chosen for this work are not the only possible. Observable pH range might be slightly shifted to basic or acidic area by the proper election of other wavelength couples. Other couples and their influence onto pK' and dynamic

range were investigated by Bizarri et al. [53] and might be adoptable as the once chosen for this work since generally results show a good agreement with the data published. Hence, depending on the microscope or read-out system used resolve-able pH range might be suited to some extend by a simple change of the wavelength couples without the need to change the fluorescent probe.

Table 2. Parameters obtained through fitting of soluble sYFP pH response curves to Eq. 4.

Ratiometric method	Excitation			Emission		
Parameter	R_0	pK'	R_f	R_0	pK'	R_f
Coefficient	0.11	6.82	14.12	0.37	7.43	9.03
Standard Error	0.01	0.01	1.49	0.10	0.07	2.45

3.1.2 Photostability of soluble sYFP

Photostability is a very important parameter for all optical probes. A suspension of 2 mg/mL sYFP in buffer pH 9 was investigated under illumination conditions for emission and excitation ratiometric settings and for the the timespan of the enzyme reactions analysed. Figure 3 shows that fluorescence intensity is very stable. Nevertheless, a small intensity increase can be observed for the two methods which in both cases is higher for the corresponding brighter channel, i.e. F(458, 515-600) for emission and F(488, 500-600) for excitation ratiometric setup, respectively. This intensity increase might be attributed to a change of the focus due to particle movement in the z-plane. However, as expected taking the ratio of both intensity emission windows a constant signal was obtained.

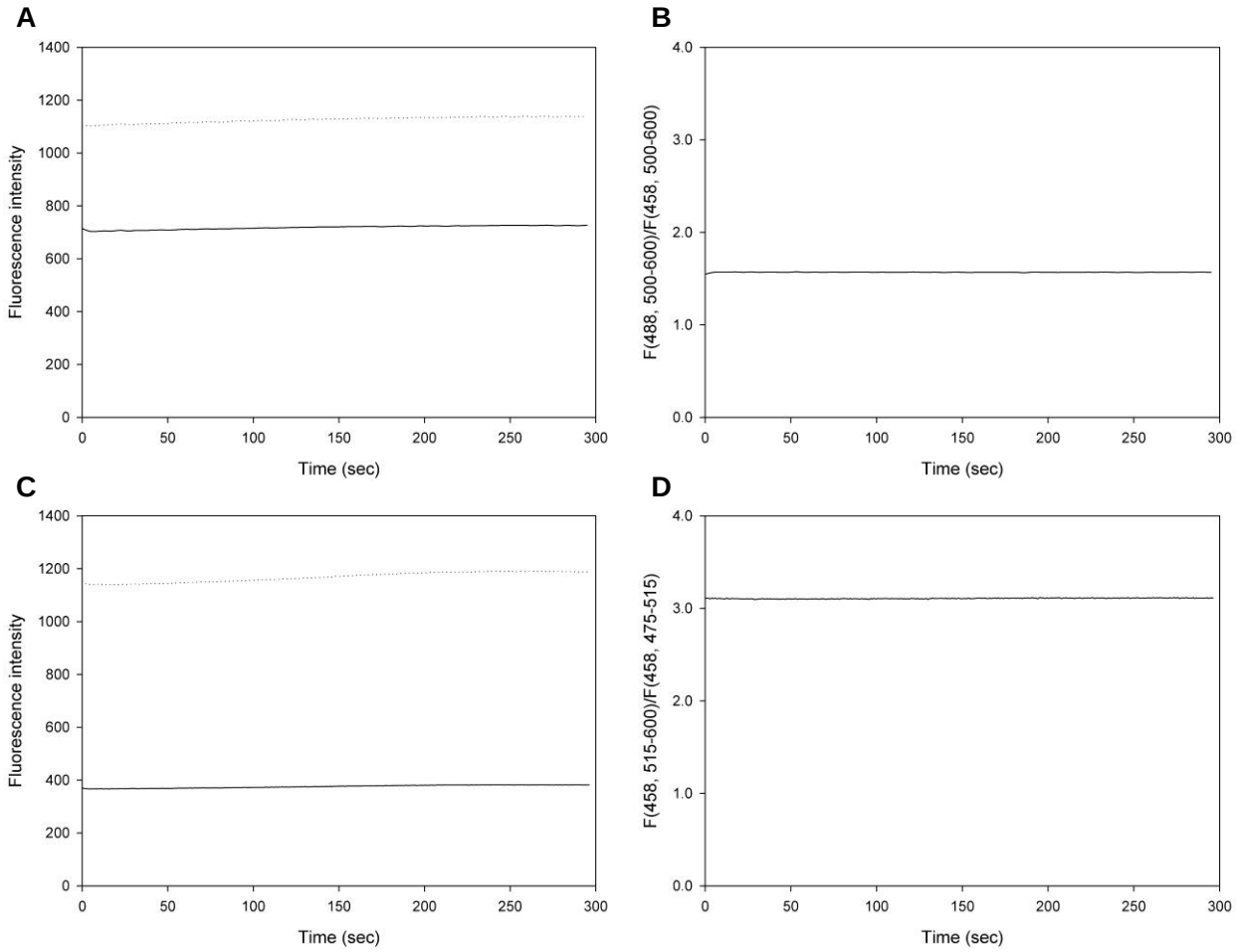

Figure 3. Photobleaching analysis of soluble sYFP during the timespan of an enzyme catalyzed reaction observed in this work. Fluorescence intensity measured with **A** excitation ratiometric setup, F(458, 500-600) (solid line), F(488, 500-600) (dotted line) and **C** emission ratiometric setup, F(458, 515-600) (dotted line), F(458, 475-515) (solid line). Corresponding ratiometric fluorescence signal obtained with **B** excitation and **D** emission ratiometric method.

3.1.3 Dynamic pH response

sYFP dynamic response was studied to test suitability of sensor for monitoring enzyme catalyzed pH changes taking place in homogeneous liquid phase. An enzyme catalyzed acidification reaction was chosen; PGA catalyzing the hydrolysis of PenG to 6APA and PAA. The acidification of a liquid phase by a homogeneous enzyme catalyzed reaction could provide two sort of relevant information; first the range where pH can be analyzed and the adequate response velocity of each applied microscope setting.

To choose a window of hydrolysis rates and buffering capacity interesting for our study, pH decrease catalyzed by soluble PGA was monitored in a stirred suspension by a standard pH-meter. Figure 4 A displays time course data for three different enzyme activities, Figure 4 B shows hydrolysis rates measured at different buffer concentrations. pH 9 was chosen to localize the initial pH that can be reliable measured, even if we are aware that this pH value might be the upper borderline of the dynamic range of sYFP. A clear dependence of hydrolysis rate on enzyme activity and buffer concentration was obtained. An activity of 30 IU_{PenG}/mL under a low buffered system displays a fast initial acidification rate of 0.3 pH units/sec which quickly drops to 0.1 pH units/sec after 5 seconds of reaction. In total a pH drop of 2 units is observed after 30 seconds of reaction with a final pH slightly lower than 6.5. The use of this high volumetric activity and low 10 mM substrate concentration leaves to the situation where reaction terminates due to nearly total substrate consumption. This activity should be high enough to challenge the monitoring of pH depletion under static conditions applied in the microscopy setup. A volumetric activity of 3 IU_{PenG}/mL, depicts an initial rate of pH decrease in solution of 0.05 pH units/sec, decreasing to 0.02 units after 10 seconds. Decrease is about one pH unit after 60 seconds of reaction. An activity of 0.06 IU_{PenG}/mL, provides a pH decrease of 0.04 pH units/min. This low activity was tested in order to be able to elucidate the sensitivity of the sYFP to very small pH changes.

Additionally a suitable range of buffering capacity was studied for application in the further characterization of the sensor protein. Chosen activity was 14.6 IU_{PenG}/mL and buffer concentration was varied between 10-200 mM. The lowest concentration displays an initial pH decrease rate of 0.1 pH units/sec, dropping to 0.02 pH units/sec; a decrease of 2.5 pH units is observed after 120 sec of reaction. The increase of the buffering capacity to 100 mM decreases the initial rate to 0.03 pH units/sec and after 30 sec further to 0.01 pH units/sec. A total decrease of 1.3 pH units is observed after 120 seconds of reaction. Increase of buffer concentration to 200 mM only leads to a minor further decrease of the rates and pH drop.

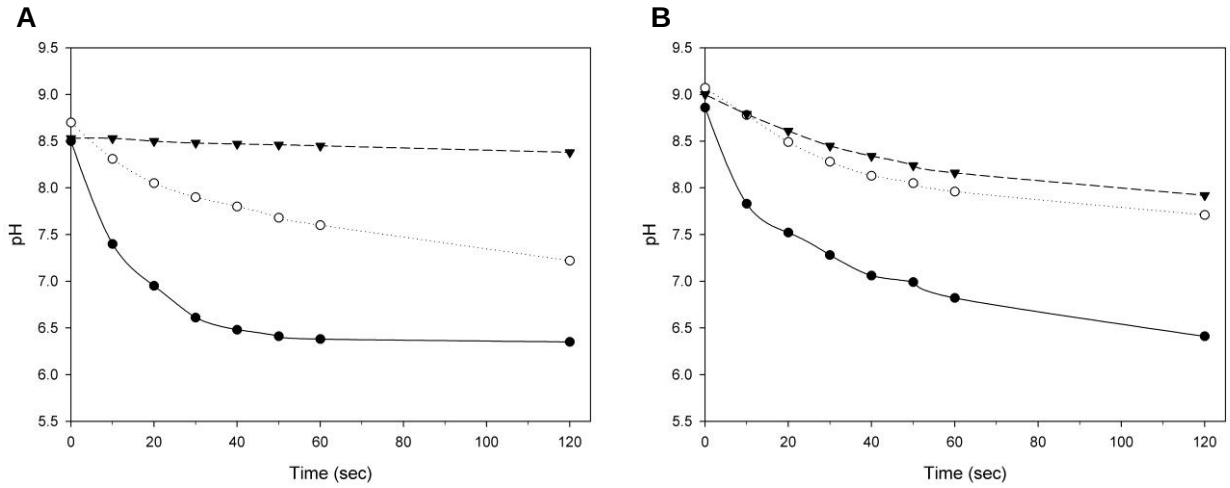

Figure 4. pH time courses for the hydrolysis of 10 mM PenG catalyzed by soluble PGA at pH 9 and RT. **A** Time courses measured at 10 mM SPB with 30 IUPenG/mL (●), 3 IUPenG/mL (○) and 0.06 IUPenG/mL (▼). **B** Times courses measured with a volumetric activity of 14.6 IUPenG/mL in 10 mM SPB (●), 100 mM SPB (○) and 200 mM SPB (▼).

Decrease of pH promoted by PGA catalyzed hydrolysis of PenG in a stagnant solution containing soluble sYFP was analyzed microscopically with excitation and emission ratiometric method. From the former results two enzymatic activities were chosen, i.e. 30 IU_{PenG}/mL and 3 IU_{PenG}/mL. Lowest activity was increased to 0.3 IU_{PenG}/mL to try to resolve a pH change of 0.004 pH units/sec. In addition, highest activity was studied at two buffer ionic strength, 10 mM and 100 mM SPB. All reactions were set to pH 9.

Figure 5 A displays time course data for three different enzymatic activities, Figure 5 B shows hydrolysis rates measured at two different buffer capacities. First PGA was added to reaction mixture, second PenG in order to start reaction. When analyzing acidification reactions two drops of pH can be observed, first a small decline just after the start of the measurement and once signal is stable again a second more steep decrease. The first can be attributed to the addition of soluble PGA. When enzyme was used without previous dialysis, addition of enzyme to reaction mixture led to an unspecific pH decrease. Second pH drop depicts acidification corresponding to hydrolysis rate of PenG by the previously added soluble PGA. This second and significant decrease was used for the calculation of initial acidification rates and compared with the ones expected from calculations using corresponding initial pH. Addition of PenG to reaction mixture without enzyme present did not lead to a decrease of pH in solution.

Another feature that can be observed is a deviation in initial pH between reactions and pH set in the buffer. Reactions measured with emission ratiometric method start all around pH 8.5. Only by increasing the salt concentration to 100 mM initial pH value was slightly shifted to a more

basic value but still lower than the one initially set. Aberration is significantly higher for excitation (initial pH between 8.2 and 9.2) compared to emission ratiometric method. We are attributing this deviation of initial pH to two effects, first influences to the initial pH like spontaneous acidification or addition of soluble enzyme and second the reliable dynamic range that can be resolved with each method.

A spontaneous acidification maybe due to dissolution of gaseous CO_2 was observed for 10 mM SPB at pH 9. Between buffer preparation and use pH was controlled and changes around 0.2 to 0.5 pH units were observed. This instability of SPB at pH 9 was not detected for higher ionic strengths and is explained by their higher buffer capacity. Therefore, reactions performed at higher salt concentration usually start clearly at a higher initial pH in case of both methods.

Certainly, some inaccuracy might also be attributed to resolvable dynamic range. A general observed trend is that emission ratiometric method is able to resolve basic area more reliable than excitation ratiometric method. This is explained by a shift of the dynamic range to a higher pH area due to the increase of the apparent pK' (see Table 2). However, since variation of initial pH is observable for both methods an initial pH of 9 is beyond the pH that can be trustable resolved using soluble sYFP as pH indicator under chosen settings.

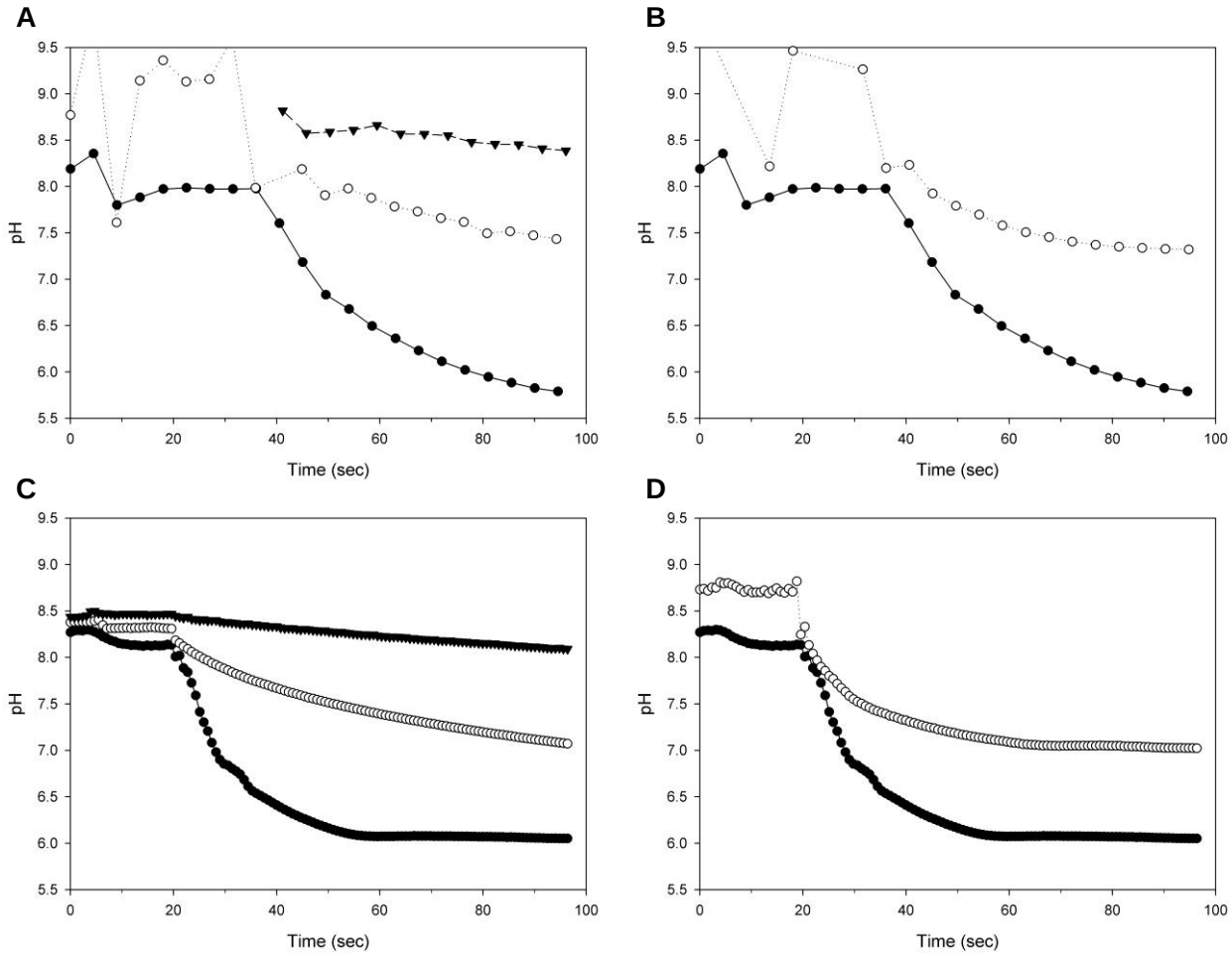

Figure 5. pH time courses obtained using soluble sYFP as fluorescent pH sensor. The hydrolysis of 10 mM PenG was catalyzed by soluble PGA at pH 9 and RT. Time courses were measured with **A** excitation and **C** emission ratiometric setup at 10 mM SPB and 30 IUPenG/mL (●), 3 IUPenG/mL (○) and 0.3 IUPenG/mL (▼). Times courses were measured with **B** excitation and **D** emission ratiometric setup with a volumetric activity of 30 IUPenG/mL in 10 mM SPB (●) and 100 mM SPB (○).

The experiments of monitoring homogeneous hydrolysis of PenG showed that both methods are able to resolve a difference in hydrolysis rate in dependence on enzyme and salt concentration. A volumetric activity of 30 IU_{PenG}/mL provides an initial acidification rate of 0.1 pH units/sec averaged over the first 10 seconds of enzyme reaction. Both methods are able to resolve this quick acidification rate, but initial pH drop is better resolved using emission setup due to faster collection of data points (0.8 seconds versus 4.2 sec for specific settings). pH decrease slows down and reaches a pH around 6.0 after 80 sec for both methods, corresponding well to the expected end of the reaction observed previously (see Figure 4 above). An earlier saturation is observed for emission ratiometric reaction, probably due to the end of dynamic range at acidic

values since pH decreases around 1.5 pH units below pK'. For the two lower volumetric activities tested, both methods are able to detect similar acidification rates. An initial hydrolysis rate of 0.02 to 0.03 pH units/sec was determined for 3 IU_{PenG}/mL and an expected final pH of 7.0 was reached after 1.5 minutes of reaction. Lowest activity of 0.3 IU_{PenG}/mL a rate between 0.003 to 0.004 pH units/sec was measured and a final pH of 8.0 was reached after the same time.

The increase of buffering capacity reduces acidification rate three times, however attenuation is less pronounced than expected, probably due to the lack of dynamic range at chosen start of reaction in the basic pH area.

An analysis of error propagation associated with the precision of the signal measurement was calculated for each pH value measured during hydrolysis reaction with emission and excitation ratiometric settings and result is depicted in Figure 6. Error is high at basic area for both methods but is significantly decreasing when measured pH reaches values inside the effective dynamic range of sYFP for each setup. Therefore, we suggest an optimal area of resolution lower than pH 8.00±0.05 for excitation ratiometric and pH 8.40±0.08 for emission ratiometric method. Around pK' error is around 0.03 for excitation and around 0.03 for emission ratiometric settings permitting reliable pH quantification and monitoring. When pH is far below pK' error starts to increase again suggesting the progressive end of the dynamic range. This is more clearly identified for emission settings, where a plateau at acidic values is observed. Based on precision of determination, the lowest pH which can be advisably resolved is pH 6.00±0.02 with excitation ratiometric method and pH 6.60±.0.08 for emission ratiometric option. Note that at acidic values, the lowest values for intensity ratios are measured and the values of R variation are easily compromised by the intrinsic noise of the signal.

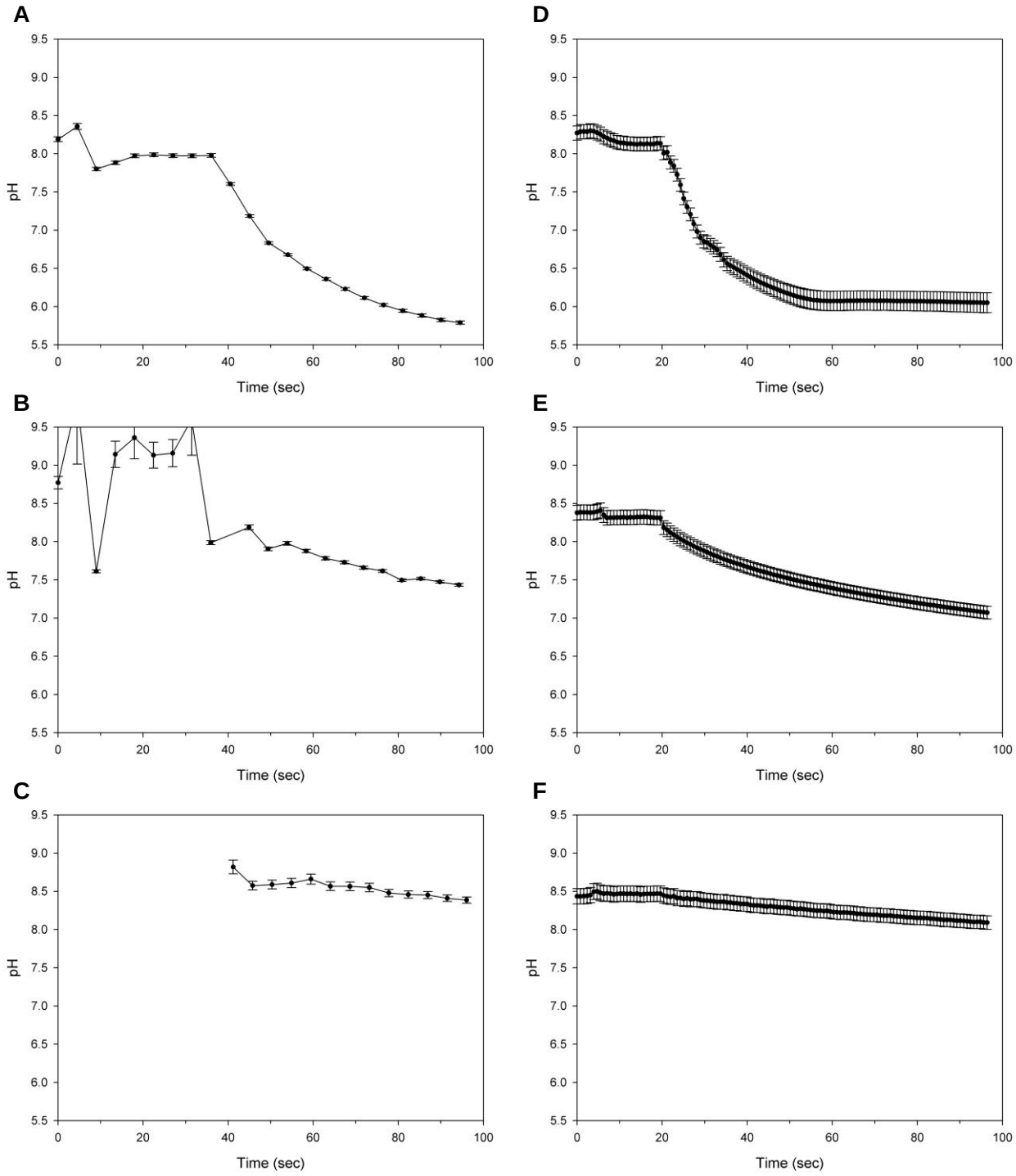

Figure 6. pH time courses obtained using soluble sYFP as fluorescent pH sensor. Uncertainties of pH determination calculated according to Eq. 8 are shown. Reactions were performed at RT in 10 mM SPB, pH 9, using 10 mM PenG as substrate. **A**, **D** 30 IU_{PenG}/mL; **B**, **E** 3 IU_{PenG}/mL; and **C**, **F** 0.3 IU_{PenG}/mL measured with excitation and emission ratiometric setup respectively.

3.2 DEVELOPMENT OF INTERNAL pH RESPONSIVE ENZYME CARRIERS: EVALUATION OF SOLID SUPPORTED sYFP AS AN EXCITATION AND EMISSION RATIOMETRIC pH INDICATOR

3.2.1 Development of sYFP general immobilization strategy on Agarose for internal pH measurements

The development of a heterogeneous sensor requires the incorporation of sYFP into a solid support. Cross-linked Agarose (Agarose BCL) was chosen as model carrier. This support is a widely used commercial enzyme carrier in biocatalysis and permit flexible immobilization of proteins with a wide range of different strategies [2, 12]. Moreover, well known protocols for attachment of PGA as pH dependent catalyst are available [2, 12, 59–61, 66]. Using 6 BCL Agarose about 60 mg of PGA can be immobilized per gram of carrier [2]. An initial amount of 10 mg sYFP per gram of carrier is aimed to be attached (equivalent to 0.4 µmol/g of carrier), expecting that this loading will permit a good and reliable internal pH resolution. This loading was tested since given the similar density of agarose suspension and water, an effective concentration of 10 mg sYFP/mL would be reached, what results theoretically in an excellent resolved pH by soluble sYFP with previous settings. Also, with this amount of sensor protein loading capacity of the carrier for the target catalyst will not be significantly reduced.

However, whenever trying to reach only a minor loading of a protein per mass of support the localization pattern of this protein inside the carrier matrix might be heterogeneous [39, 40, 74][39, 40]. A homogeneous distribution of a small amount of protein requires the smart control of the rate of immobilization; the ratio between specific velocities of surface-protein attachment reaction and protein diffusion into the pores determines the final protein distribution. There are several strategies available for the modulation of immobilization rate [74] by controlling (i) nature of physico-chemical interaction between protein and surface (reactive groups), (ii) reactive group density and/or (iii) addition of competitors of chemical reaction.

Regarding the strategy of physico-chemical incorporation onto the carrier, the goal of the present work is the design of a heterogeneous sensor via coimmobilization with the target enzyme even without minimal disturbances towards the original catalyst. The sensor design should be generally applicable irrespective of material and target enzyme immobilization. On the other hand the preservation of the pH response should be ensured or minimally affected by the immobilization of the sensor protein. So, a high degree of compatibility between carrier material, sensor protein and target enzyme attachment is aimed to be reached.

For this reason a strategy based on the immobilization of poly-His-tagged sYFP to Ag-Ni was chosen. The oriented immobilization via the poly-His-Tag is carried out at very mild immobilization conditions. Moreover, interaction between carrier surface and protein will occur presumably only via the Tag leading to a major amount of immobilized protein with the same orientation [75]. This is favorable since harsh conditions or direct attachment via reactive amino acid side chains exposed to the solvent might lead to changes of protein tertiary structure by the immobilization [12]. In this context conformational changes could be especially problematic. Small influences onto the local environment of the sYFP fluorochrome, e.g. amino acids in the surrounding, might have a big influence onto pH response capacity and spectral behavior, further leading to a heterogeneous population of fluorescent sensor protein which might differ in their pH response characteristics [42].

sYFP distribution was visualized by confocal microscopy. As shown in Figure 7 A immobilization of 10 mg sYFP per gram of carrier under standard binding conditions [65, 76] lead to an inhomogeneous distribution of sYFP. As reported previously [74, 77] rate of immobilization can be modulated by addition of imidazole as competitor. When immobilization was performed in the presence of high imidazole concentrations a homogeneous distribution of sYFP throughout the carrier matrix could be reached (Figure 7 B and C). However, a dependence of protein loading onto amount of competitor can be observed as difference in the fluorescence signal.

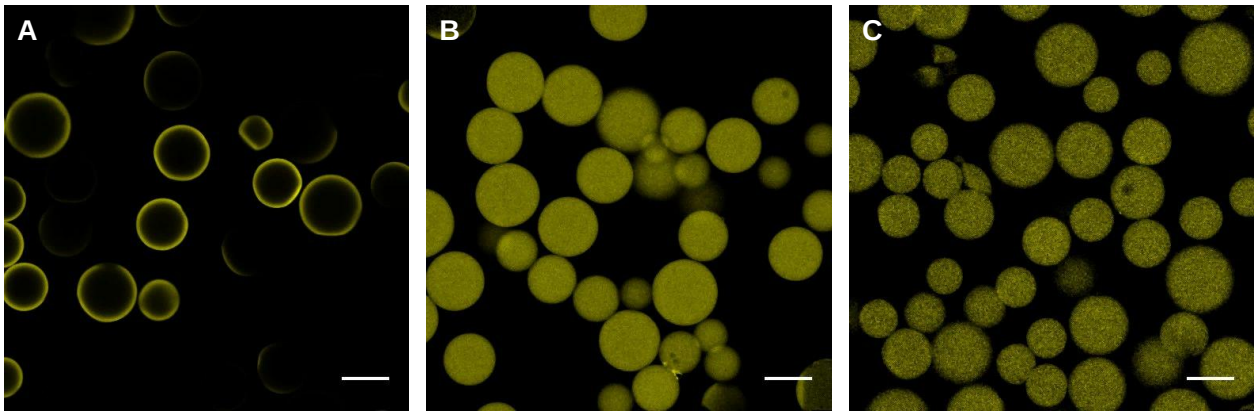

Figure 7. Confocal images of sYFP distribution onto Ag-Ni. Immobilization was conducted **A** in absence of imidazole, **B** in presence of 50 mM imidazole and **C** 100 mM imidazole. Scale bar: 100 µm.

The lower fluorescence signal can be compensated by a time consuming optimization of imidazole concentration (required protein loading vs. imidazole concentration) or adjustment of microscopy settings (e.g., detector sensitivity, laser intensity), which might lead to increased probability of photobleaching or amplification of background noise.

Therefore a gradual decrease of imidazole concentration during immobilization process was tested. This strategy starts with a high concentration of imidazole allowing the protein to diffuse inside the porous network of the carrier and finish with such a low amount of competitor permitting a complete attachment of all offered sYFP. Figure 8 shows the decrease of protein concentration in supernatant during immobilization on Ag-Ni and protein distribution obtained with this approach.

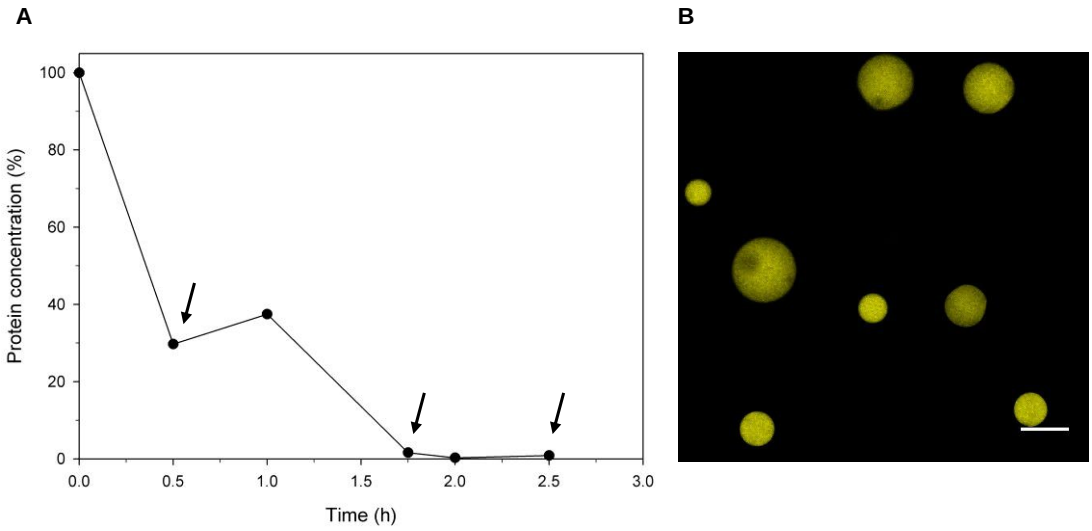

Figure 8. Immobilization course and resulting sYFP distribution on Ag-Ni. **A** Decrease of protein concentration in supernatant during immobilization of sYFP conducted at an initial imidazole concentration of 300 mM. 1:2 dilutions of imidazole concentration by addition of fresh buffer are indicated by arrows. Immobilizate was left to incubate overnight at 37.5 mM imidazole. **B** Confocal image of sYFP distribution after overnight incubation. Scale bar: 100 µm.

IMAC-chemistry is widely used in protein chromatography for purification of poly-His-tagged proteins from crude cell extract [65, 76, 78–80]. Former strategy was applied to test suitability as one-step immobilization/purification approach by selectively immobilizing overexpressed poly-His-tagged sYFP out of crude *E. coli* cell extract homogeneously into Ag-Ni. Purity of attached protein was confirmed with an SDS-Gel, shown in Figure 9. An almost pure attachment of sYFP onto Agarose particles was obtained. Residual impurities were removed by a washing step in the presence of a low imidazole concentration. Distribution of attached sYFP was completely homogeneous depicting the success of this method as a one-step immobilization purification strategy from the sensor protein out of a crude cell extract.

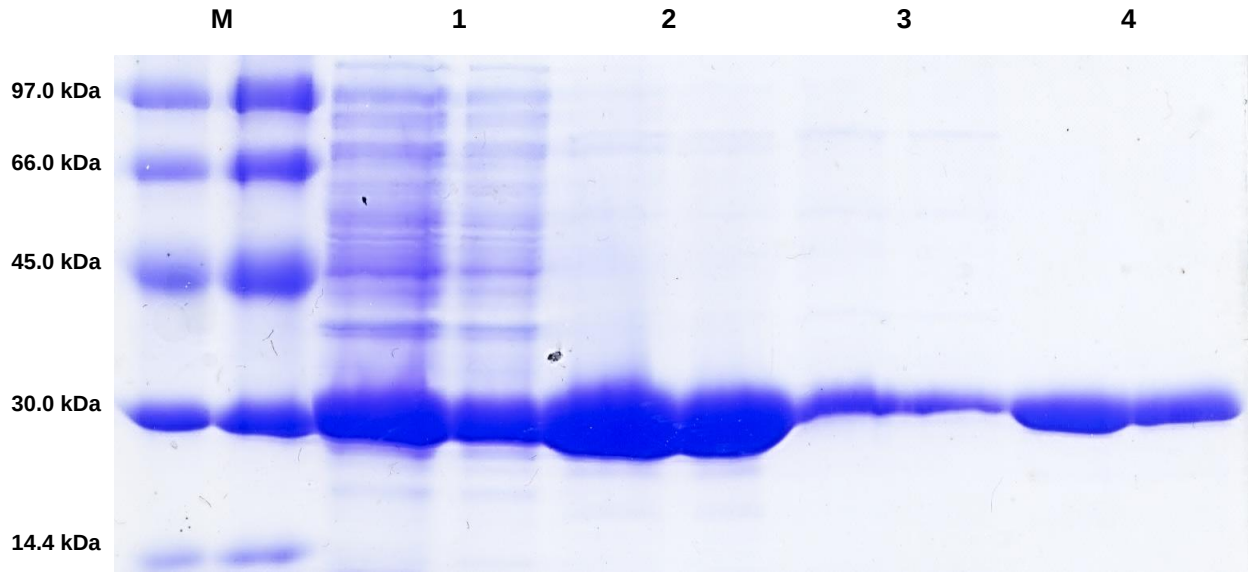

Figure 9. SDS-PAGE of different steps in the purification-immobilization of sYFP out of cell lysate onto Ag-Ni. Molecular weight of sYFP is about 27 kDa [56]. Molecular weight marker (M), E. coli crude extract (1), sYFP attached to Ag-Ni by application of previously explained immobilization approach (2), protein remaining attached after washing with 25 mM imidazole (3), protein desorbed from Ag-Ni (4);

3.2.2 Characterization of pH response and dynamics of sYFP immobilized onto Ag-Ni

sYFP incorporated into Ag-Ni was characterized to reveal suitability of heterogeneous sensor as tool for resolution of pH.

pH response was evaluated with emission and excitation ratiometric method for an immobilizate containing 10 mg sYFP per gram of Ag-Ni. Dependence of fluorescence ratio upon pH is shown in Figure 10. For each pH condition five different particles were analyzed in each image. pH response shows clearly a sigmoidal behavior. Deviation in fluorescence ratio between different particles was found for both methods with the variation again higher for the basic pH area (see Figure 10 A and B). Discrepancy for emission ratiometric method remains lower than 3%, while for excitation setup variation is below 2%. Same trend in the shift of resolvable pH range can be observed between the two settings. Excitation ratiometric method might be used for a more acidic pH area than emission ratiometric method.

These results show that configurations established for soluble sYFP can be adopted without modifications for analysis of heterogeneous sensor protein, indicating that attachment approach does not affect significantly to reliability of signal for analyzed pH range or pH response

properties of sYFP. Result of fitting for averaged fluorescence ratios is shown in Figure 10 C and D, quantification in Table 3.

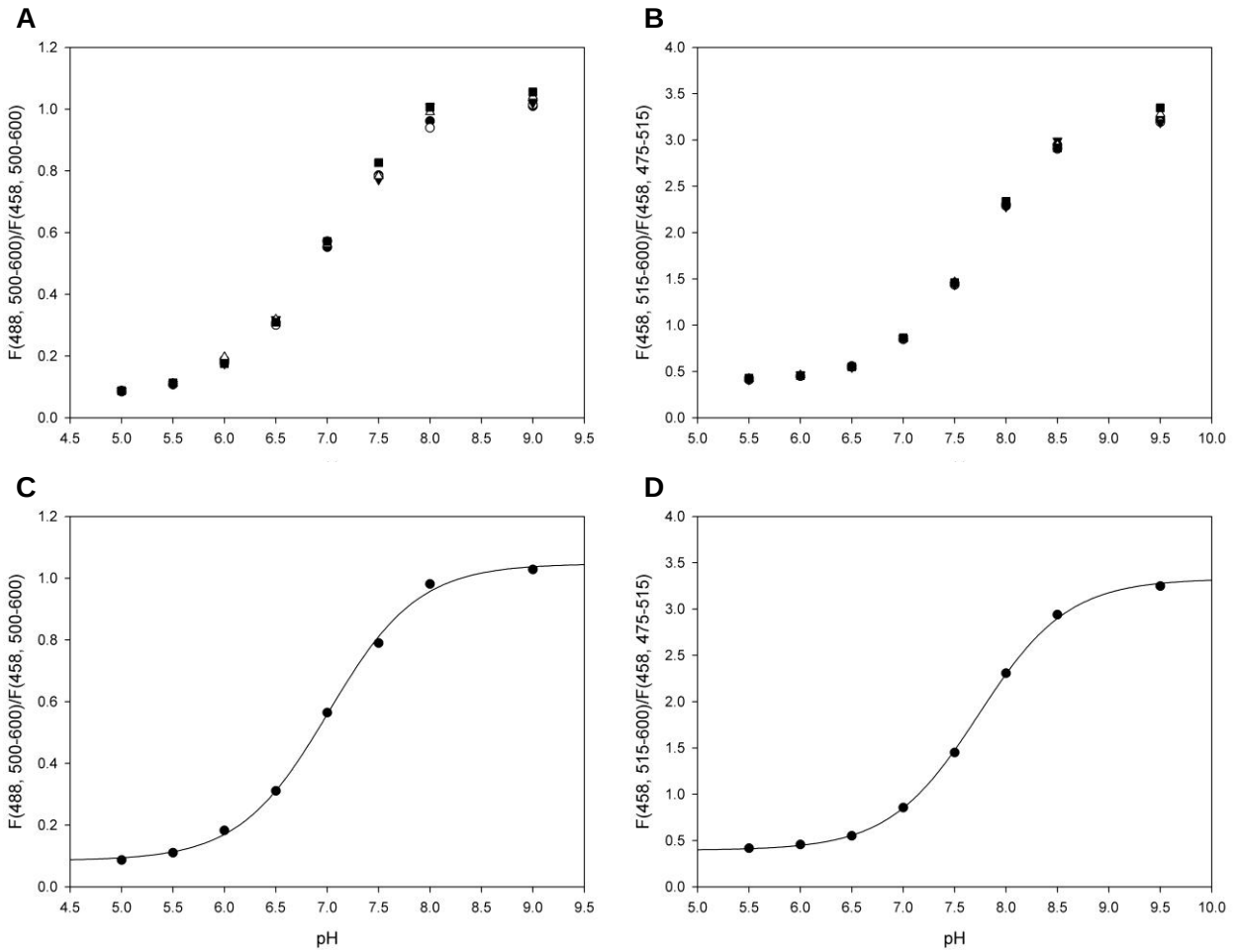

Figure 10. pH response curves obtained for sYFP-Ag-Ni. **A** Excitation and **B** emission ratiometric calibration. For each calibration five different ROIs were analyzed. **C** Excitation and **D** emission ratiometric calibration fitted to Eq. 4. Each point represents an average of five different ROIs.

An apparent pK' of 7.01 was determined for excitation and a pK' of 7.73 for emission ratiometric method. Dynamic range (R_f) is about 4 points higher for excitation setup. Apparent pK' of immobilized sYFP is higher compared to soluble counterpart under the same conditions and measurement settings. This deviation might be caused by the surface topology and composition of the material used for protein immobilization. Ag-Ni contains two carboxylic groups per IDA-group, that theoretically should be blocked with metal to give a neutral surface. However, in some form they might participate in hydrogen binding and therefore affect to the overall pK' value obtained for the immobilizate, emphasizing the importance of a thorough characterization of immobilized sYFP when attached to a new carrier or by a different strategy.

Dynamic range is slightly smaller for solid supported sYFP in comparison to soluble protein. Decrease of R_f was found to be more severe for excitation ratiometric option. Some of this difference might be attributed to an overestimation of dynamic response capacity due to a lack of points in the acidic pH range for excitation ratiometric method especially for analysis of soluble sYFP.

Previously a dependence of pH calibration onto scanning depth was found [27]. When this effect was further studied main cause of distortion was attributed to wavelength dependent Rayleigh scattering and pH-dependent re-absorption of emitted fluorescence [21]. For our study, a big influence of light scattering onto fluorescence ratio is not expected since Agarose BCL is a transparent material in contrast to others previously analyzed [25, 27]. In addition the size of the particles used here (around 150 µm) is lower than the range analyzed by Heinnemann (300-1000 µm) [21]; hence findings cannot be directly related. Signal distortion by pH dependent re-absorption for sYFP would theoretically be more probable at lower wavelengths (closer to absorption range) and at high pH. However, considering the low amount of fluorescence protein used (0.4 µmol/g of carrier) influence onto fluorescence ratio should also be small.

Even though, in the context of this studied, signal distortion should be minimal, the absence of possible sources of errors by the use of wavelength ratiometric method should not be generalized quickly at large and a study relating fluorescence intensity ratio with particle diameter, especially for macroscopic or non-transparent particles, should be performed.

Table 3. Parameters obtained through fitting of sYFP-Ag-Ni pH response curves to Eq. 4.

Ratiometric method	Excitation			Emission		
Parameter	R_0	pK'	R_f	R_0	pK'	R_f
Coefficient	0.08	7.01	12.3	0.39	7.73	8.43
Std Error	0.01	0.03	1.56	0.02	0.02	0.33

As for soluble sYFP dynamic response of immobilized sYFP was analyzed by an acidification reaction catalyzed by soluble PGA. Figure 11 A depicts hydrolysis reaction for three different enzyme activities, Figure 11 B for two different buffer capacities.

Reactions were set to start at pH 9. Soluble PGA was added and hydrolysis started by addition of PenG to the mixture. A small first unspecific drop of pH due to enzyme addition was only detectable for highest enzyme concentration at 10 mM SPB.

Again a variation in initial pH was found for both microscopy settings due to spontaneous acidification. Reactions start between pH 8.0 to 8.2 for both methods, except for higher buffering capacity where the pH approaches 9.0.

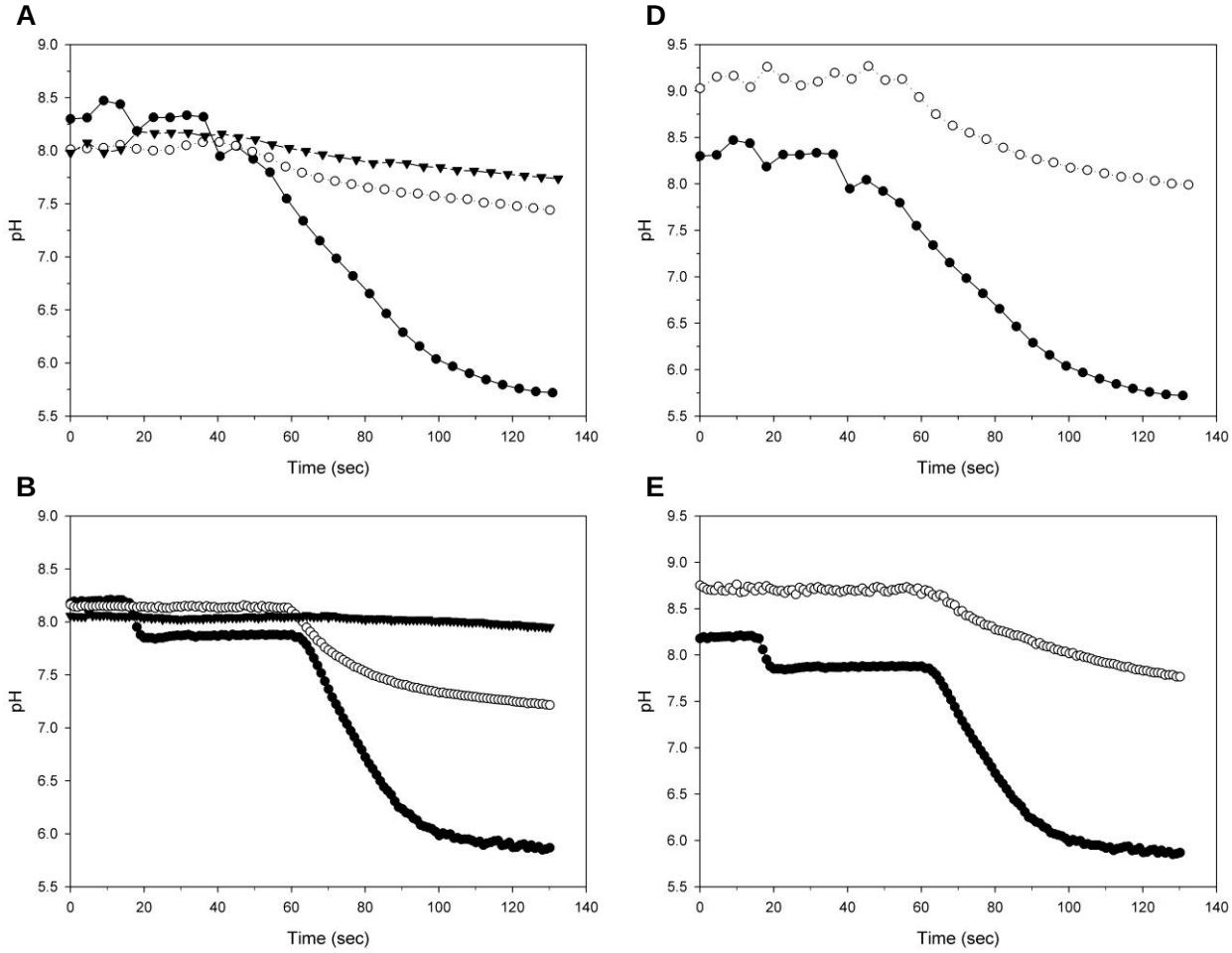

Figure 11. pH time courses obtained using sYFP-Ag-Ni as fluorescent pH sensor. The hydrolysis of 10 mM PenG was catalyzed by soluble PGA at pH 9 and RT. Time courses were measured with **A** excitation and **C** emission ratiometric setup at 10 mM SPB and 30 IUPenG/mL (●), 3 IUPenG/mL (○) and 0.3 IUPenG/mL (▼). Times courses were measured with **B** excitation and **D** emission ratiometric setup with a volumetric activity of 30 IUPenG/mL in 10 mM SPB (●) and 100 mM SPB (○).

Differences between reaction rates and buffer concentrations can be quantified with both methods. For a volumetric activity of 30 IU_{PenG}/mL, a rate of 0.1 pH units/sec was measured. Both methods resolve a decrease of pH until the expected value of around 5.8-6.0, where the reaction is almost completed. An initial hydrolysis rate of 0.02 pH units/sec was observed for 3 IU_{PenG}/mL, decreasing pH to 7.20-7.30 after two minutes of reaction.

Lowest volumetric activity applied (0.3 IU_{PenG}/mL) could also be resolved by immobilized sYFP but some observation should be pointed out. With respect to analysis for soluble sYFP this low activity corresponds to a rate of 0.003 to 0.004 pH units/sec. However, for emission ratiometric method a roughly measureable rate of 0.002 pH units/sec was determined, whereas with excitation setup an expected decrease of 0.004 pH units/sec was nicely resolved. Since initial pH might be beyond dynamic range for both methods and applied volumetric activity is very low, reaction rate might be underestimated and should be interpreted with caution. Increasing buffer capacity reduces pH decrease about three times. This is the same magnitude determined for soluble sYFP and the also same final values are reached.

Results follow the trend observed for soluble sYFP. An analysis of precision of each measured pH value is shown in Figure 12. Errors for emission measurement remain lower than 0.05 and increases when pH is pK'±0.6, for excitation ratiometric method error remains lower than 0.04 until pH distances pK'±0.8. Based on precision of signal determination, pH can be optimally resolved below pH 8.50±0.05 and above 7.30±0.06 for emission ratiometric settings. Excitation ratiometric method resolves optimally below pH 8.30±0.05 and above pH 6.40±0.05.

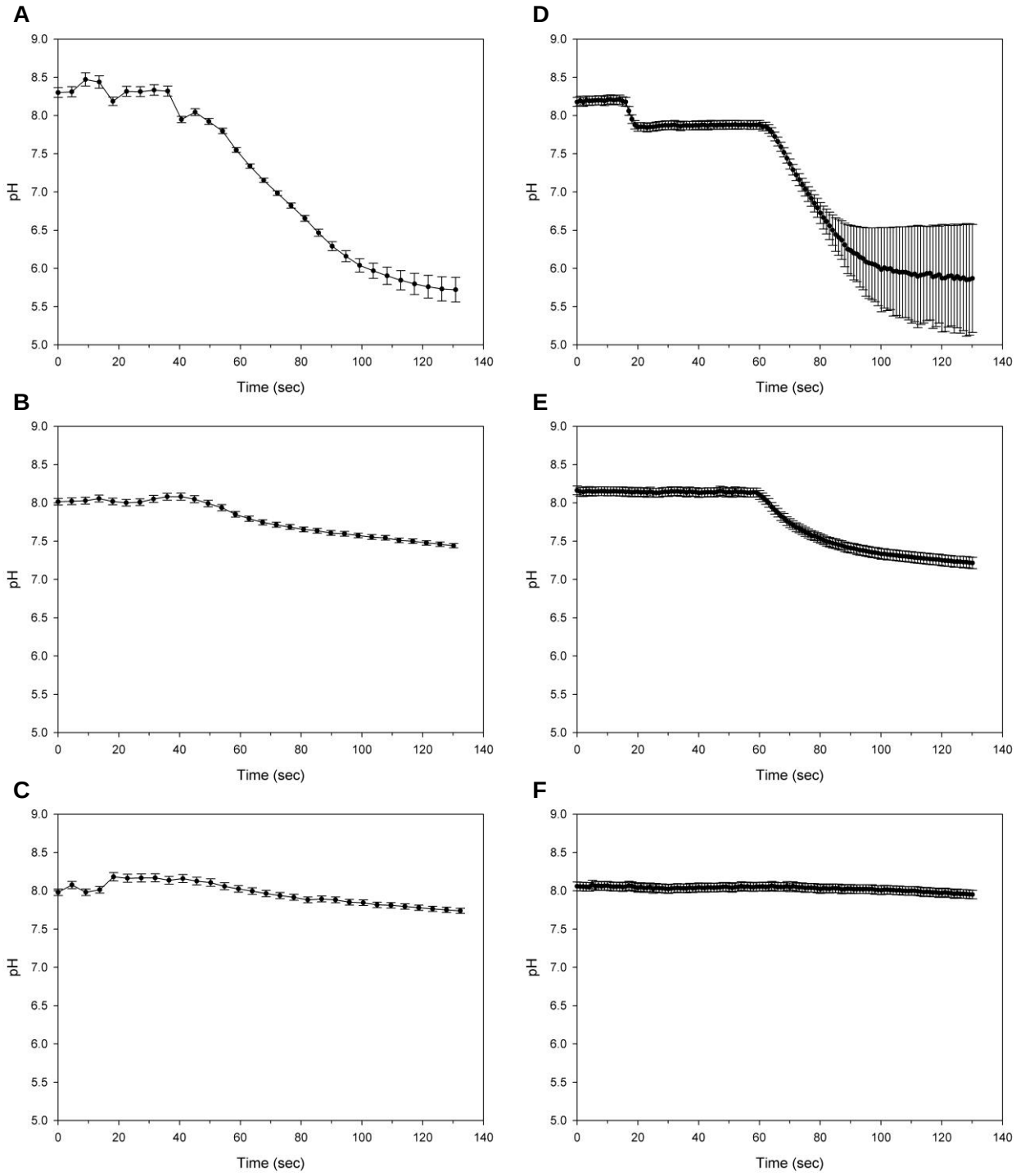

Figure 12. pH time courses obtained using sYFP-Ag-Ni as fluorescent pH sensor. Uncertainties of pH determination calculated according to Eq. 8 are shown. Reactions were performed at RT in 10 mM SPB, pH 9, using 10 mM PenG as substrate. **A**, **D** 30 IU_{PenG}/mL; **B**, **E** 3 IU_{PenG}/mL; and **C**, **F** 0.3 IU_{PenG}/mL measured with excitation and emission ratiometric setup respectively

3.3 STUDY OF THE FLEXIBILITY OF PREPARATION OF INTERNAL pH RESPONSIVE MATERIALS BASED ON SOLID-SUPPORTED sYFP

In this work a general and widely applicable method for quantification of internal pH in immobilized pH dependent biocatalysts by means of coimmobilized sYFP should be developed. pH response, dynamic range and response velocity of immobilized sYFP into Agarose BCL have been shown to be suitable for potential use as pH sensor. Another immobilization principle and enzyme carriers will be tested to study the feasibility of generalization of internal pH sensing based on immobilized sYFP.

3.3.1 Extension to other immobilization strategy: Covalently attached sYFP

The former strategy of oriented sYFP attachment is a straight forward method of controllable immobilization of sYFP via His-Tag. In addition, another conventional strategy of immobilization was performed. This immobilization strategy is based on a multipoint covalent attachment of sYFP onto Ag-glyoxyl via exposed Lysine residues of the protein to glyoxyl groups of the carrier [63, 81, 82]. Attachment occurs at harsh conditions, coupling to the carrier surface is formed directly via the protein. Therefore, conformational changes of the protein tertiary structure due to immobilization are frequent and a high rate of inactivation can be found for many enzymes [12, 63, 81, 82]. However, immobilization via glyoxyl groups lead to a rigidification of the protein structure and to an altered stability, useful if sYFP need to be re-used or target catalyst works best at harsh conditions or unconventional media. Moreover, after attachment a completely inert carrier surface can be obtained.

Feasibility of florescence labeling based on a covalent attachment strategy and the properties of attached sYFP as ratiometric sensor will be studied. When trying to immobilize the previous amount of sYFP (10 mg sYFP per gram of carrier) an inhomogeneous protein distribution was found. To reach a homogeneous distribution pattern immobilization rate was reduced by three different strategies, a temperature decrease to 4°C, and addition of ethanolamine or Tris-Base. The latters are small molecules containing an amino group capable to compete with the protein for the glyoxyl groups on the carrier surface.

Figure 13 depicts the resulting sYFP distribution following the former mentioned strategies. Decrease of immobilization temperature slowed down immobilization rate but led to a heterogeneous distribution (Figure 13 A). Immobilization in presence of competitors was performed again by a gradual decrease of competitor concentration. In case of ethanolamine a

homogeneous distribution of sYFP inside Agarose beads was obtained (Figure 13 B), whereas Tris-Base did not have any effect onto immobilization rate (Figure 13 C). For further studies immobilizates prepared in presence of ethanolamine were used.

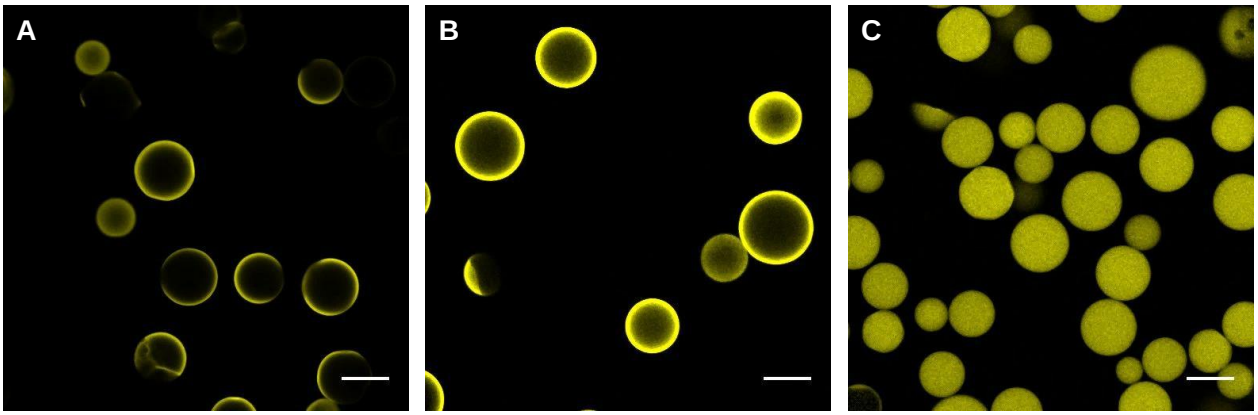

Figure 13. Confocal images of sYFP distribution onto Ag-glyoxyl. Immobilization was conducted **A** at 4°C, **B** in presence of 1 M Tris-Base and **C** 1 M ethanolamine. Scale bar: 100 µm.

pH response characteristics of 10 mg sYFP attached to 1 g Ag-glyoxyl was studied. When analyzing response curves obtained for excitation and emission ratiometric settings (see Figure 14) expected sigmoidal dependence on pH was obtained with excitation ratiometric method more shifted to acidic pH range. Discrepancy between fluorescence ratios calculated for five different particles at each pH value is again higher at basic area but remain lower than 2% for both setups.

Table 4 shows results of fit of pH response. An apparent pK' of 6.61 was obtained for excitation ratiometric method and 7.31 for emission ratiometric method. This pK' is slightly lower than the one calculated for soluble sYFP or sYFP immobilized onto Ag-Ni. In this case dynamic range was found to be higher for emission ratiometric method. We attribute this finding to a lack of points in the acidic range for excitation ratiometric settings.

Table 4. Parameters obtained through fitting of sYFP-glyoxyl pH response curves to Eq. 4.

Ratiometric method	Excitation			Emission		
Parameter	R_0	pK'	R_f	R_0	pK'	R_f
Coefficient	0.22	6.61	4.96	0.45	7.31	8.01
Std Error	0.03	0.05	0.78	0.05	0.03	0.92

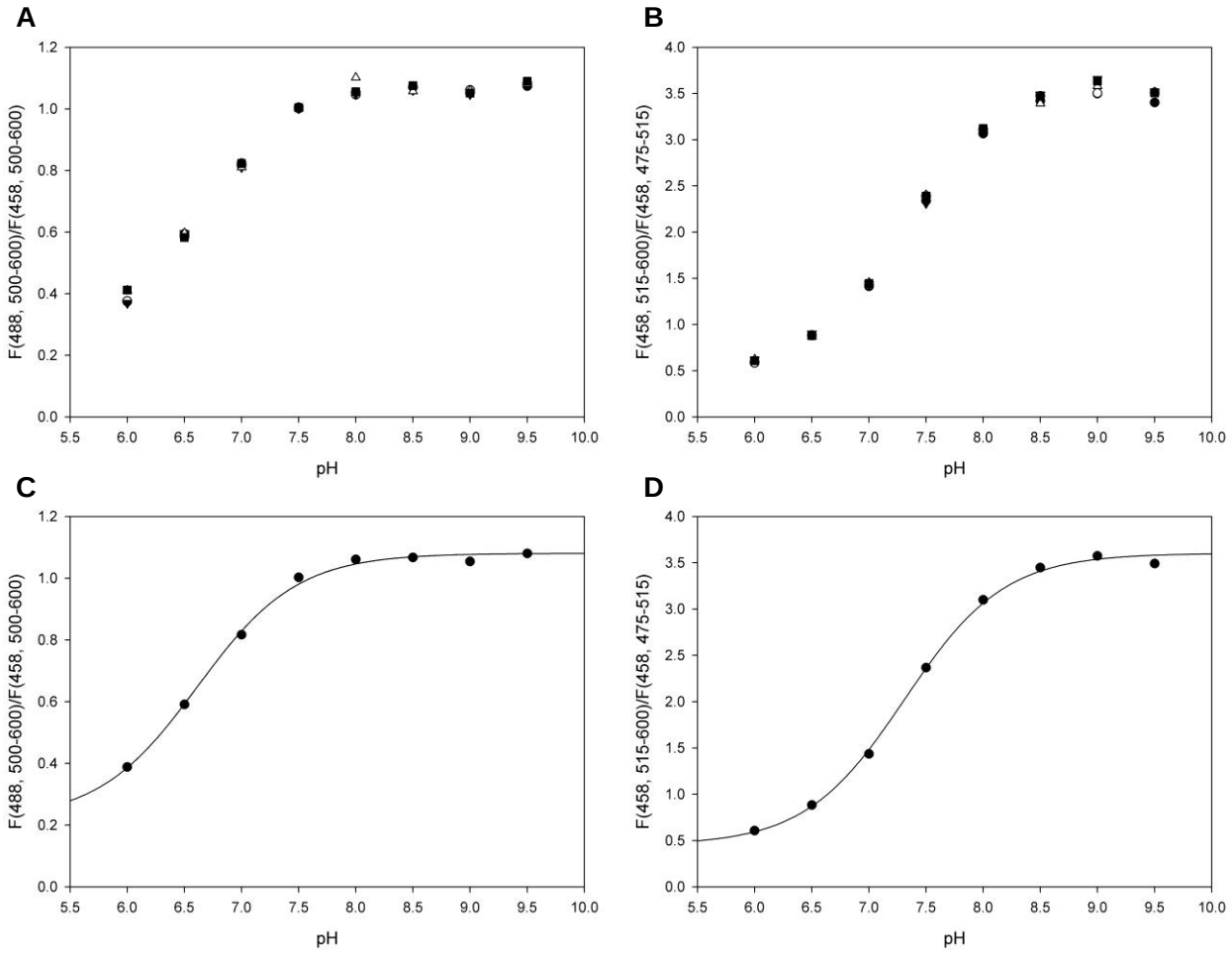

Figure 14. pH response curves obtained for sYFP-glyoxyl. **A** Excitation and **B** emission ratiometric calibration. For each calibration five different ROIs were analyzed. **C** Excitation and **D** emission ratiometric calibration fitted to Eq. 4. Each point represents an average of five different ROIs.

To evaluate dynamic response of sYFP-Ag-glyoxyl previous characterization was applied. It was possible to follow acidification rates between 0.2 and 0.004 pH units/sec corresponding well to those measured for soluble sYFP and sYFP-Ag-Ni with the same enzyme volumetric activities and buffer concentrations (see appendix Figure S1). Values of associated error are between 0.05-0.06 for pH in the dynamic range. For this heterogeneous pH probe reliable range for resolution is lower than pH 7.20±0.07 for excitation and pH 8.10±0.07 for emission ratiometric method, with lowest resolvable pH of 6.10±0.07 for excitation and 6.60±0.07 for emission ratiometric option.

Multipoint covalent attachment of sYFP onto Ag-glyoxyl did not lead to a major change in pH response characteristics or dynamic response behavior. Settings can be applied without modifications; however, excitation ratiometric calibration should be performed in a slightly more

acidic pH area to explore the complete pH response range and obtain more reliable results with a lower error.

3.3.2 Extension to other enzyme carriers: sYFP immobilization onto CPG-Ni and Sep-Ni

The principle of controllable sYFP immobilization was extended to other commercial enzyme carriers of high relevance in the scientific community. Beside Agarose BCL, which constitutes one representation of natural organic polymer based materials, TRISOPERL® controlled pore glass (CPG) were chosen as representative of inorganic enzyme carriers based on silica material, Sepabeads® (Sep) as representative of synthetic organic materials.

Homogeneous sYFP incorporation was performed by the previously established strategy of oriented immobilization via the His-Tag of the protein. Protein loading of 10 mg sYFP per gram of carrier was adopted due to the good signal obtained for Agarose BCL. Figure 15 shows the distribution of sYFP inside CPG-Ni (Figure 15 A) and Sep-Ni (Figure 15 B) after immobilization. For both carriers a homogeneous distribution could be obtained. The more obscure particle middle of Sepabeads is attributed to the opaqueness of the material. Emission intensity decreases with increasing particle thickness/diameter for which reason particle middle seem to contain less protein. Agarose BCL and CPG are transparent materials.

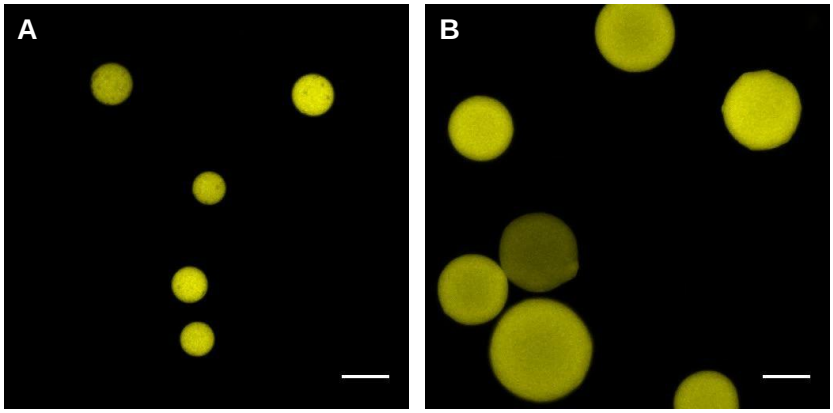

Figure 15. Confocal images of sYFP distribution onto **A** CPG-Ni and **B** Sep-Ni. Immobilization was conducted in presence of 300 mM Imidazole. Scale bar: 100 µm.

pH response characteristics and dynamic behavior was studied for immobilizates of 10 mg sYFP attached to either 1 g of CPG-Ni or Sep-Ni.

When analyzing sYFP-CPG-Ni (see Figure 16 A and B) a sigmoidal dependence upon pH was obtained. Again pH response curve for excitation ratiometric setup is slightly shifted to a more acidic pH range. Analysis of deviation of fluorescence ratio for five different particles at each pH

for both methods depicted a significantly lower error for emission (2%) compared to excitation ratiometric setting (4%), especially at basic values. Averaged fluorescence ratios were fitted and results are shown in Figure 16 C and D and summarized in Table 5.

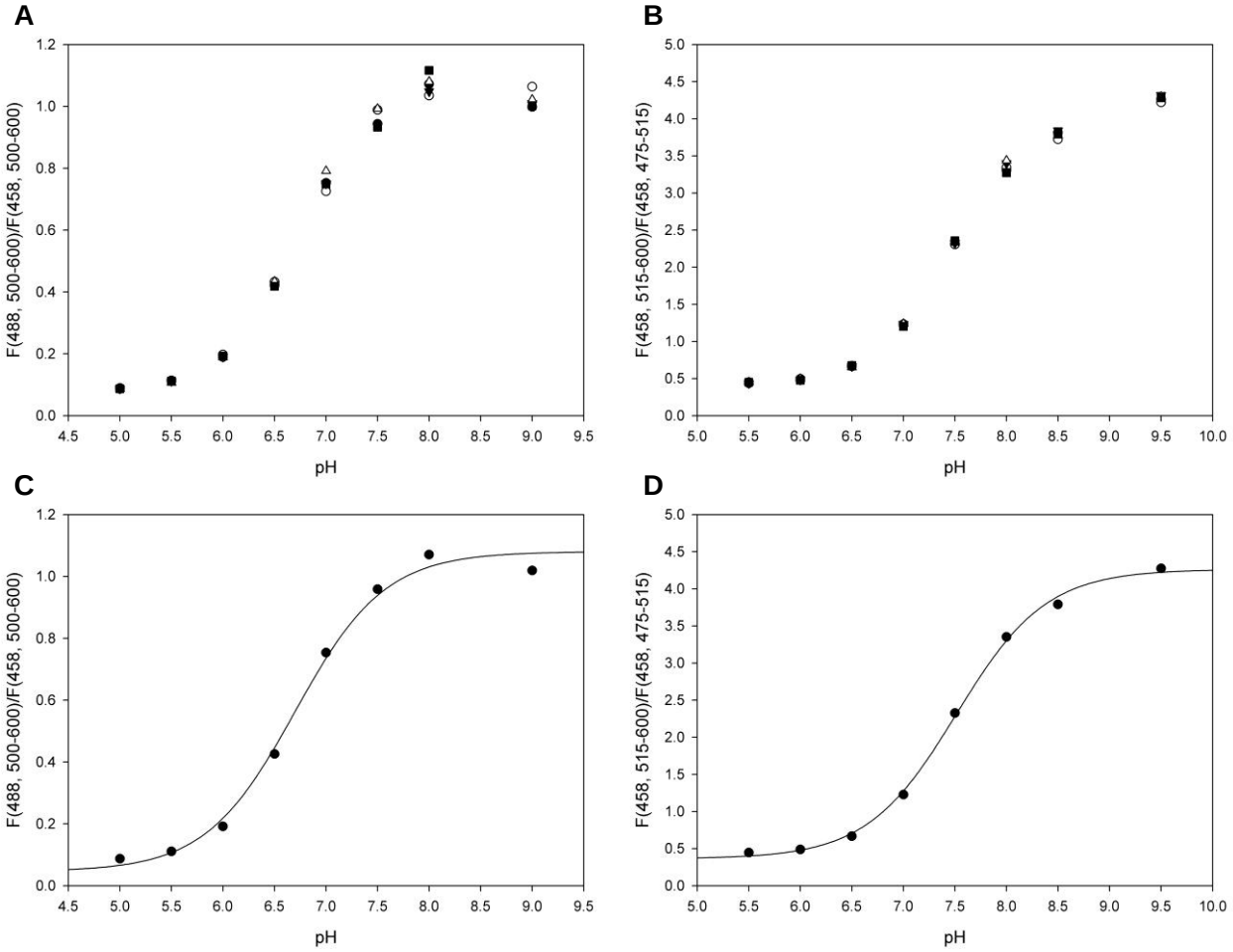

Figure 16. pH response curves obtained for sYFP-CPG-Ni. **A** Excitation and **B** emission ratiometric calibration. For each calibration five different ROIs were analyzed. **C** Excitation and **D** emission ratiometric calibration fitted to Eq. 4. Each point represents an average of five different ROIs.

Apparent pK' is determined to be 6.70 for excitation and 7.51 for emission ratiometric method. Dynamic range is higher for excitation setup. The high R_f for excitation ratiometric option is associated with an increased standard error and might be attributed to the higher deviation of fluorescence ratio between different particles at the same basic pH and the low values of R measured at acidic pH. Compared with another immobilized sYFP, the values are slightly shifted to acidic pH. Even if the material was previously chemically modified for the introduction of IDA-Ni^{2+} groups via silanisation, a lower isoelectric point of the surface due to the residual presence of silanol groups could be possible. Dynamic response evaluation revealed acidification rates

between 0.2-0.002 pH units/sec corresponding to different volumetric activities and buffer concentrations (see appendix Figure S2). Uncertainty remained lower than 0.07 for all pH values in the dynamic range, decreasing to 0.05 around the pK'. The advisable highest pH that can be resolved is pH 7.70±0.06 for excitation and pH 8.00±0.06 for emission ratiometric setups. Lowest measureable pH is 6.20±0.06 for excitation and 6.70±0.06 for emission ratiometric method.

Table 5. Parameters obtained through fitting of sYFP-CPG-Ni pH response curves to Eq. 4.

Ratiometric method	Excitation			Emission		
Parameter	R_0	pK'	R_f	R_0	pK'	R_f
Coefficient	0.05	6.70	23.52	0.36	7.51	11.72
Std Error	0.03	0.07	14.49	0.05	0.03	1.49

For sYFP attached to Sep-Ni pH response also shows a sigmoidal behavior (see Figure 17 A and B). Deviations of fluorescence ratio for five different particles at each studied pH value were higher than for the other heterogeneous sYFP and soluble sYFP. Difference is around 4% for both methods and especially high at basic pH. According to this analysis, use of sYFP-Sep-Ni as heterogeneous sensor will result in more noisy measurements at basic values or equivalently a lower reliable dynamic range is obtained. Averaged fluorescence ratios were fitted, results are shown in Figure 17 C and D and are summarized in Table 6.

Table 6. Parameters obtained through fitting of sYFP-Sep-Ni pH response curves to Eq. 4.

Ratiometric method	Excitation			Emission		
Parameter	R_0	pK'	R_f	R_0	pK'	R_f
Coefficient	0.07	6.99	17.20	0.38	7.69	9.41
Std Error	0.02	0.04	5.24	0.04	0.04	1.03

The apparent pK' for sYFP-Sep-Ni is calculated to be 6.99 for excitation and 7.69 for emission ratiometric method. Dynamic range of excitation setup is almost the double than R_f obtained for emission ratiometric settings.

Analyzing dynamic response, acidification rates of 0.2 to 0.005 pH units/sec could be observed corresponding to the volumetric activities and buffer concentrations tested (see appendix Figure S3). The error for pH values in the dynamic range remains below 0.07, but R_f seem to be smaller than for the other heterogeneous sensors. The optimal resolvable range of pH is 7.50±0.07 for excitation and pH 8.20±0.07 for emission ratiometric method. For excitation setup lowest resolvable pH is 6.30±0.07, for emission 7.00±0.07.

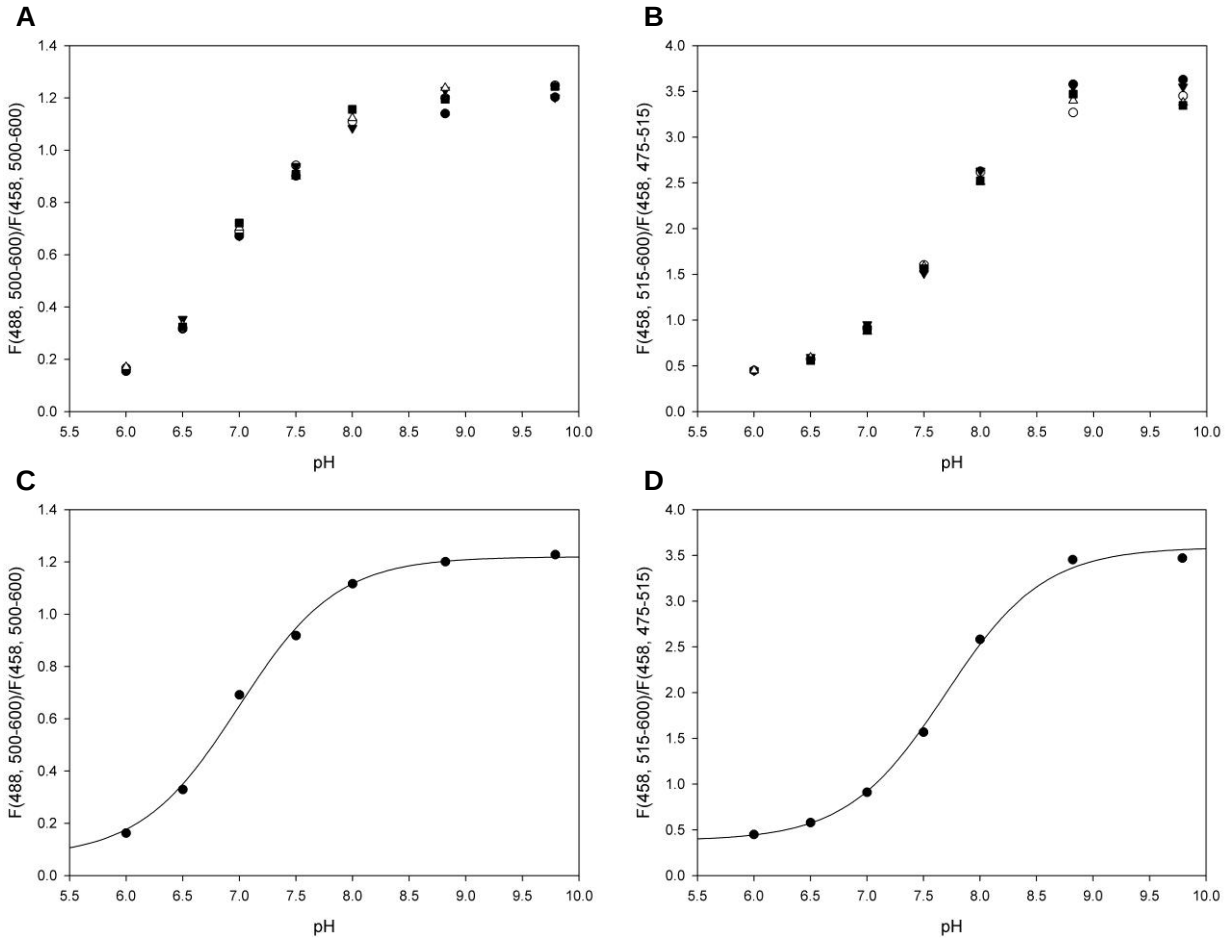

Figure 17. pH response curves obtained for sYFP-CPG-Ni. **A** Excitation and **B** emission ratiometric calibration. For each calibration five different ROIs were analyzed. **C** Excitation and **D** emission ratiometric calibration fitted to Eq. 4. Each point represents an average of five different ROIs.

Incorporation of sYFP by two different routes, i.e. oriented attachment of sYFP via the His-Tag to different materials activated with IDA-Ni^{2+} groups as well as a multi-point covalent attachment onto Ag-glyoxyl, retained pH response characteristics of soluble fluorescent protein. All heterogeneous sensors offer a good signal-to-noise ratio even when only a small amount of sensor protein is attached (10 mg/g of carrier). pH response shows expected sigmoidal

dependence. However, a dependency of pK' and R_f onto specific material and attachment strategy was observed. Nevertheless, dynamic response for all tested sensors was shown to be suitable for the measurement of pH time courses promoted by the hydrolysis of PenG by soluble PGA under stagnant conditions. Analysis of pH time course and associated error provided an advisable range of resolvable pH for each immobilized sYFP well in the range of interest for enzyme catalyzed reactions.

Indeed, only a small variety of available enzyme immobilization protocols and carriers was tested in the context of this thesis, however, obtained results indicate the flexibility and robustness of sYFP as heterogeneous pH sensor for enzyme catalyzed reactions. Solid-supported sYFP clearly presents the possibility to be suited to meet specific requirements without losing its optical properties and hence, might be an outstanding option to be applied in any other study where a pH dependent process needs to be analyzed by means of fluorescence based pH sensing.

3.4 COIMMOBILIZATION OF sYFP AND PGA ONTO Ag-Ni-Glyoxyl: DEVELOPMENT OF INTERNAL pH RESPONSIVE IMMOBILIZED BIOCATALYSTS

The developed heterogeneous sensor should be used as tool for the resolution of internal pH gradients originated by a solid supported enzyme catalyzed hydrolytic reaction. This implies the co-attachment of target enzyme and sensor protein into the same defined porous material. The target enzyme chosen, PGA, has been widely studied immobilized on glyoxyl activated carriers and resulting catalyst is a presumed candidate to be controlled by diffusional restrictions and internal pH gradients [59–61, 66, 83]. Between the two former established sYFP immobilization approaches, oriented immobilization via His-Tag and multipoint covalent attachment on glyoxyl supports, first strategy would be advantageous for combination with PGA attachment since the use of different reactive groups could permit an easy control of immobilization of each protein independently.

For this reason a strategy based on a hetero-functional surface activation was developed following well established carrier preparation protocols [2, 62]. The enzyme carrier was prepared to contain some concentration of IDA groups where the sensor protein will be incorporated with an oriented immobilization and some concentration of glyoxyl groups for the multipoint covalent attachment of the target enzyme. As model carrier, Agarose BCL was chosen.

3.4.1 Adaptation of PGA immobilization protocol

As first step PGA was tried to be immobilized onto the new hetero-functional Ag-IDA-glyoxyl using a previously reported immobilization protocol to control the immobilization towards glyoxyl groups [63, 81, 82]. Figure 18 depicts immobilization courses for Ag-IDA-glyoxyl, offering an activity of 130 U PGA per gram of support. Surprisingly, no attachment of the enzyme was observable after a timespan where immobilization was reported for mono-functional support [66]. The reasons of this unexpected behavior must be found in the singular character of the PGA as ionic exchanger. Is it known that PGA is adsorbed neither onto cationic or anionic exchangers [84–86]. The carrier used offers the character of a cationic exchanger due to the presence of deprotonated carboxylic groups of IDA at the pH of immobilization, what opens the scenario of a repulsion of PGA from the surface.

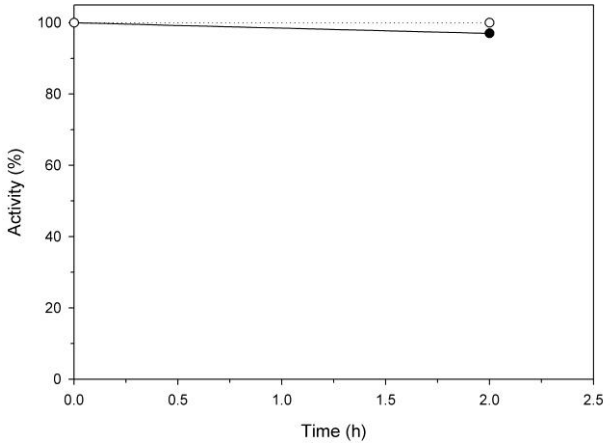

Figure 18. Immobilization of 130 IU_{NiPAB}/g on Ag-IDA-glyoxyl conducted in 0.1 M SBB supplemented with 25% glycerol and 0.1 M PAA at pH 10.05 and RT. Activity was measured using NiPAB as substrate. Suspension (●), supernatant (○).

An analysis of the surface residues distribution might help to support this hypothesis. Scheme 3 shows the distribution of charges onto the surface of a PGA molecule. Positively charged surface residues are shown in red, negatively charged ones in blue. A homogeneous distribution of residues over the enzyme surface can be seen. Close proximity of oppositely charged residues probably favor formation of a network of salt bridges.

The nature of immobilization on glyoxyl groups is a reversible reaction where equilibrium is shifted to dissociation. Covalent attachment is only possible if enzyme is in close proximity to carrier surface and if it interacts with the glyoxyl groups in a multipoint manner. Enzyme attachment on hetero-functional carrier is therefore of special difficulty and a new immobilization

strategy is required which implies the dissolution of repulsive forces in order to permit attachment.

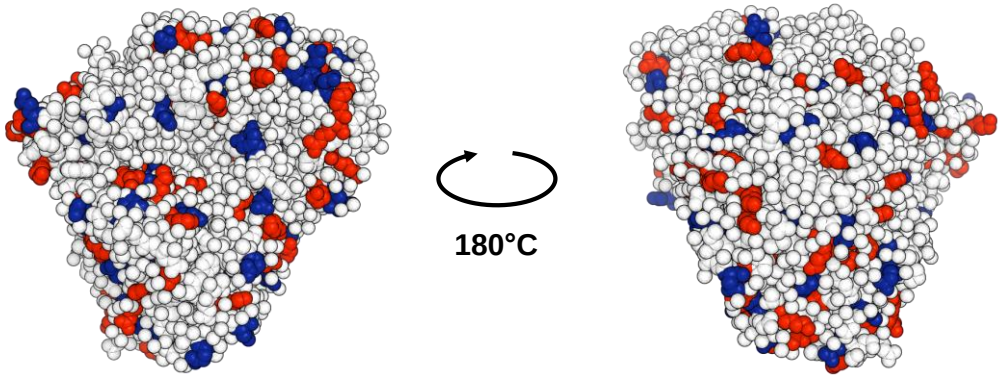

Scheme 3. Surface charge distribution of PGA from E.coli (PDB ID. 1EMA). Positively charged residues (Arg, Lys) are shown in red, negatively charged ones (Glu, Asp) in blue.

One strategy to overcome repulsion forces is supplementation with some concentration of sodium chloride. A high salt concentration might shield negative charges on the carrier permitting the enzyme to diffuse close to the surface. Figure 19 shows immobilization courses of PGA on Ag-IDA-glyoxyl in presence of three different salt concentrations, 250 mM, 500 mM and 1 M.

At all tested salt concentrations, a clear effect onto immobilization pattern is observed: activity is gradually decreasing in the supernatant maybe indicating a progressive enzyme immobilization but also a decrease of activity in the enzyme suspension is observable, depicting a loss of activity during immobilization. These effects are increasing with increase of the salt concentration. At highest salt concentration, the activity preserved after the immobilization is extremely low, what might be explained by PGA inactivation in the presence of salt. However, when immobilization is performed at a decreased temperature of 4°C soluble enzyme can be stabilized (see Figure 19 C). Immobilization rate was not compromised by decrease of temperature but final measureable activity in suspension is still only around 70% of activity offered. This might be attributed to structural distortion of PGA by immobilization caused by a different surface topology of the material due to the introduction of a new negatively charged group on the hetero-functional carrier. IDA-groups which are longer in size than glyoxyl groups might stick up over the surface of the carrier like mountain peaks. Upon enzyme immobilization these mountain peaks might drill inside the protein molecule distorting its structure when it interacts with subjacent glyoxyl groups to undergo reaction.

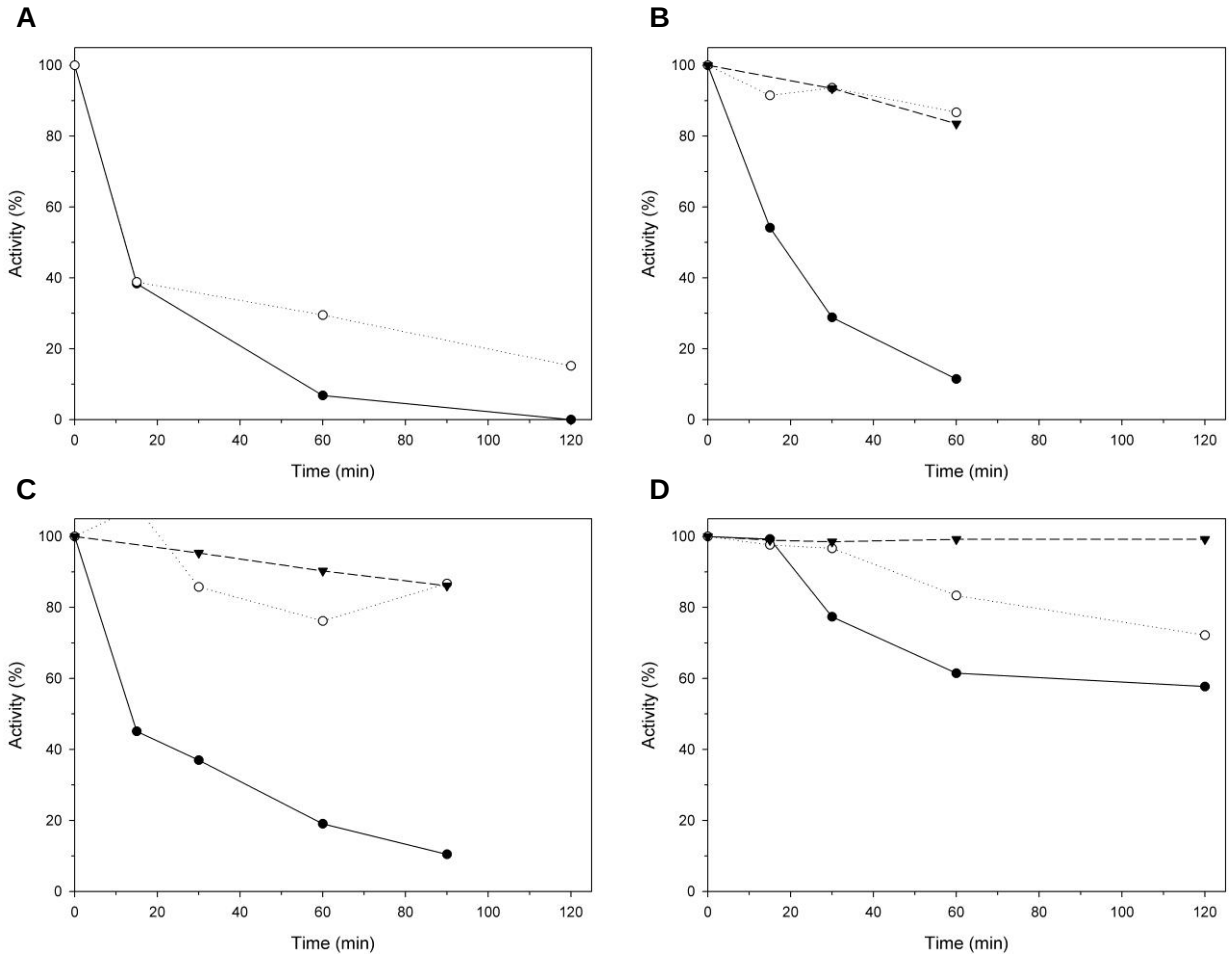

Figure 19. Immobilization of 130 IU_{NiPAB}/g on Ag-IDA-glyoxyl conducted in 0.1 M SBB supplemented with 25% glycerol and 0.1 M PAA at pH 10.05 and RT. Immobilization was in presence of **A** 1 M NaCl, **B** 500 mM NaCl, **C** 250 mM NaCl and **D** 1 M NaCl at 4°C. Activity was measured using NiPAB as substrate. Suspension (●), supernatant (○) and soluble PGA (▼).

Another approach tested was the attachment of PGA after blocking carboxylic groups with a positively charged metal, such as Ni^{2+}. In this case carboxylic groups are interacting with metal leaving the surface neutral. Figure 20 depicts immobilization course of 130 U PGA per gram of Ag-Ni-glyoxyl. Also by this strategy surface repulsive forces were surmounted. As advantage the fast immobilization velocity should be underlined; in comparison to former strategy after only 15 min all offered enzyme activity is immobilized. Moreover, soluble PGA is stable under immobilization conditions.

The final activity measureable for suspension of around 80% of the activity offered is in the same range than the one obtained with the two lower salt concentrations (250 mM and 500 mM NaCl)

and immobilization at 4°C, supporting the idea of enzyme inactivation due to immobilization of catalyst.

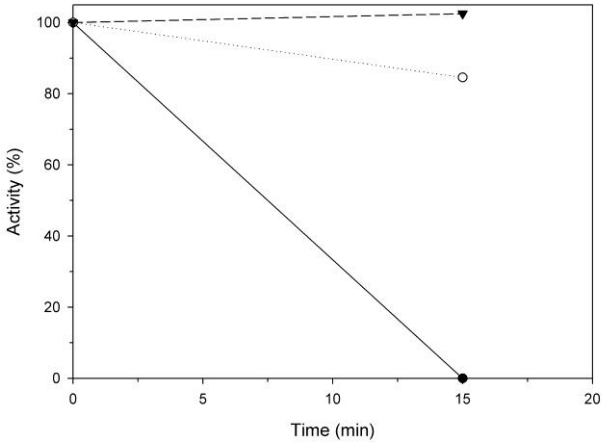

Figure 20. Immobilization of 130 IU_{NiPAB}/g on Ag-Ni-glyoxyl conducted in 0.1 M SBB supplemented with 25% glycerol and 0.1 M PAA at pH 10.05 and RT. Activity was measured using NiPAB as substrate. Suspension (●), supernatant (○) and soluble PGA (▼).

Both immobilization strategies permit immobilization of PGA at high yield and with a high expressed activity. An overview about all tested conditions is shown in Figure 21.

Immobilization yield was found to be between 40% and 100% where the highest yield was obtained for immobilization on Ag-IDA-glyoxyl in presence of a salt concentration of 1 M and for Ag-Ni-glyoxyl where surface is blocked with metal. This result is attributed to the more neutral surface obtained by these two conditions compared to the others tested. Expressed activity is lowest for immobilization in presence of 1 M salt probably due to a high instability of soluble enzyme under high sodium chloride concentrations. Reducing temperature or amount of salt is increasing stability of soluble enzyme and therefore measureable activity, however, accompanied by a decrease of immobilization yield to around 40%.

From these results we decided to choose the immobilization on Ag-Ni-glyoxyl as immobilization approach for PGA. With this strategy a high yield with an acceptable expressed activity can be obtained. All later used PGA immobilizates were prepared using this protocol.

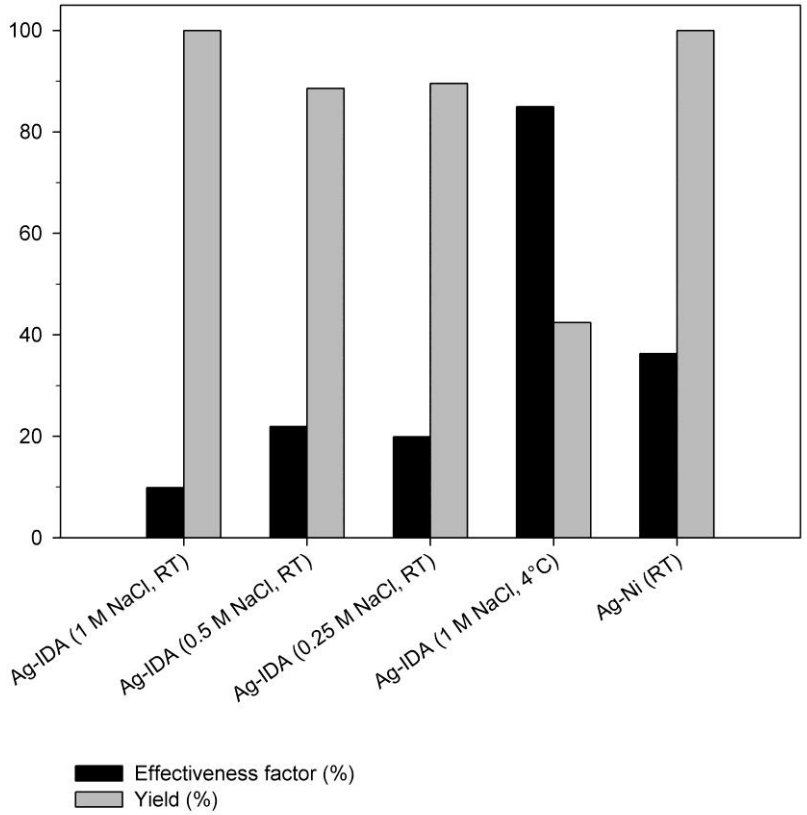

Figure 21. Immobilization yield and effectiveness factor of PGA immobilized under different conditions.

3.4.2 Characterization of immobilized PGA

Performance of PGA immobilized covalently onto Ag-Ni-glyoxyl was analyzed by studying the relation between effectiveness factor, expressed activity and enzyme loading. Figure 22 A shows catalytic properties obtained for NiPAB as substrate, Figure 22 B those determined for PenG. When increasing the enzyme loading onto the carrier measurable activity is also raising. However, even at low enzyme loadings increase is not linear, hence, effectiveness factor decreases for both substrates with increasing immobilized activity.

The observed decrease of catalytic efficiency in dependency on enzyme loading is more pronounced for NiPAB. A theoretical loading of 2 IU_{NiPAB} per gram of carrier only shows a measureable activity of almost 90% and decrease to 40% when the loading is increased to only 18 IU_{NiPAB} per gram of carrier. For PenG a steep dependency is not observable since small enzyme loadings were difficult to quantify using the titration based measurement applied in this

thesis. However, all measureable loadings showed a clear decrease in catalytic efficiency. In which extent this loss of activity is clearly attributed to biochemical or physical effects is hardly explainable based on this macroscopic analysis.

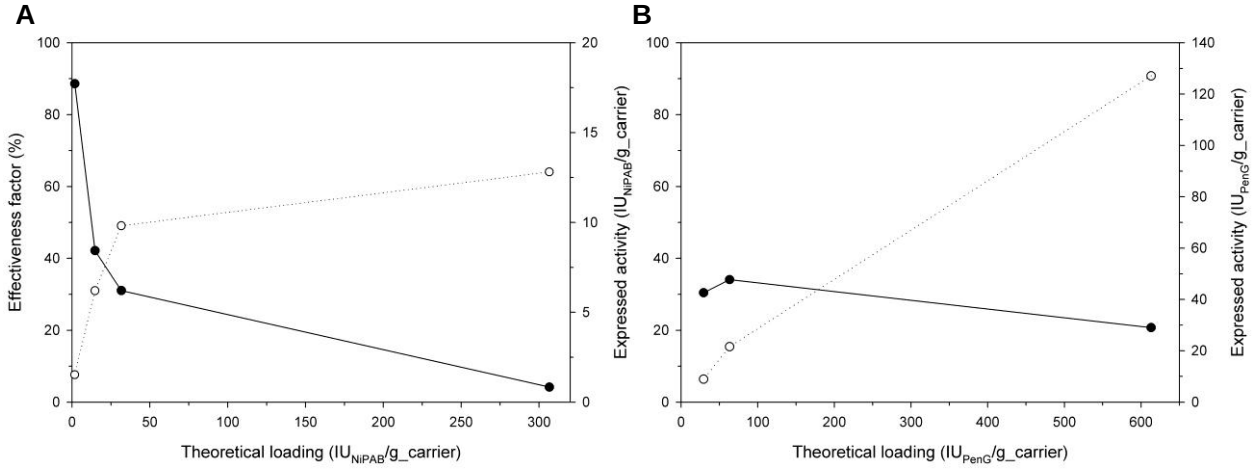

Figure 22. Dependence of effectiveness factor (●) and expressed activity (○) onto theoretical immobilized activity for PGA immobilized onto Ag-Ni-glyoxyl determined with **A** NiPAB or **B** PenG as substrate. The effectiveness factor is the ratio of observed and theoretical immobilized enzyme activity. Theoretical activity is determined from a balance of activity measureable in the supernatant before and at the end of immobilization.

A decrease of expressed activity for an immobilized enzyme compared to its soluble counterpart is usually found when enzymes are attached to solid supports [5, 12, 14, 82]. Lower activity might be attributed to two main effects, the inactivation of the enzyme by conformational distortions when attached to the carrier or diffusional restrictions for substrate and product due to a high enzyme loading.

An apparent loss of enzyme activity in dependency onto enzyme loading usually is a hint for diffusional hindrances of substrate and products. The performance of PGA immobilized onto Ag-glyoxyl has been widely studied and the influence of diffusional limitations on the activity and catalyst productivity was recently analyzed. The hydrolysis reaction is highly diffusional controlled. Depletion of PenG, accumulation of inhibiting PAA or a shift of internal pH due to acidification reaction is held to be responsible [59, 60].

Among these factors, the internal pH might determine a crucial influence not only on activity but also on selectivity and operational stability of the enzyme [15, 66]. Depending on the volumetric activity, pH might suffer a significant drop into the carrier that could be subject to variations depending on catalytic features or reaction conditions (buffering capacity). A comprehensive

characterization of PGA catalyst would require the quantification of internal conditions during catalyzed reaction.

Another biocatalyst characterization that has not received very much attention traditionally is the enzyme distribution into the enzyme carrier; however, distribution might have a clear influence onto final biocatalytic properties governed by mass transfer.

Distribution of PGA onto Ag-IDA-glyoxyl was verified by fluorescence microscopy after labeling of immobilized enzyme with c-PtTFPP. NHS activated dye was attached covalently via formation of an amide linkage between luminophore and amine groups of enzyme. Unbound dye was removed; however, some amount of luminophores remained unspecific adsorbed onto the carrier material. Distribution of three different PGA loadings on Ag-IDA-glyoxyl is shown in Figure 23. Luminescence signal was corrected for weak background noise originated from unspecific bound c-PtTFPP.

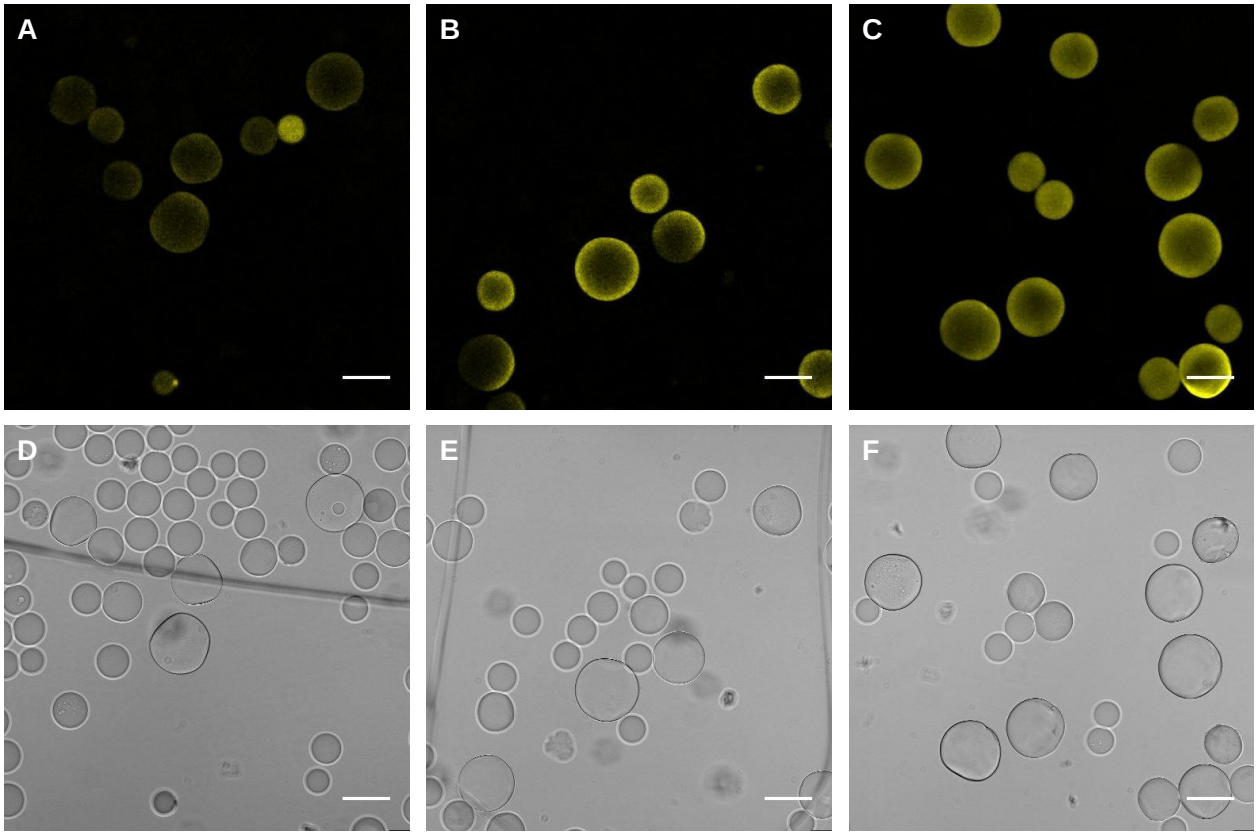

Figure 23. Confocal images of PGA distribution immobilized onto Ag-IDA-glyoxyl. PGA was labeled with carboxylted PtTFPP according to the conditions described in the materials and methods section. Fluorescence and brightfield images of **A, D** 27 IU_{PenG}/g of carrier, **B, E** 135 IU_{PenG}/g of carrier and **C, F** 805 IU_{PenG}/g of carrier.

Distribution of PGA was heterogeneous for all tested loadings. A deeper penetration of PGA into the particles was observable with increasing PGA loading. Heterogeneous distribution of commercial PGA biocatalyst has already been observed by Van Roon [87–91] and the importance of enzyme distribution onto biocatalytic properties is discussed. The application of techniques for the visualization of protein distribution together with techniques for the intraparticle measurement of analytes would constitute a step-forward in the comprehensive characterization and design of immobilized biocatalysts controlled by mass transfer [92]

3.4.3 sYFP labeled immobilized PGA biocatalyst: Preparation and analysis

Two independent incorporation routes of YFP and PGA have been developed. By using a heterofunctional activated enzyme carrier proteins were coimmobilized using a sequential immobilization approach. First PGA is immobilized via covalent attachment; second sYFP is incorporated mediated by the His-tag. After the PGA immobilization, the carrier is reloaded with $NiSO_4$ to guarantee the success of sYFP immobilization. Unbound $NiSO_4$ was removed and activity of immobilized PGA was controlled. No loss of activity was found. Before attachment of sYFP catalysts were equilibrated with SPB containing 300 mM imidazole in order to avoid dilution of initial imidazole concentration by residual water inside the pores. Immobilization of sYFP was performed applying the protocol prescribed in the previous chapter. Immobilization of PGA does not compromise the fluorescence labeling.

Three loadings were prepared containing an immobilized PGA activity of 805 IU_{PenG}, 135 IU_{PenG} and 27 IU_{PenG} per gram of Ag-Ni support and a sYFP loading of 8 mg per gram of carrier. For highest PGA loading only 7.5 mg sYFP could be attached per gram of carrier.

Optical properties of sYFP-PGA-coimmobilizates were analyzed. pH response curves for both methods and all loadings are shown in Figure 24. Irrespective of the catalyst pH response is very similar. Fluorescence ratio shows a sigmoidal behavior upon pH. Resolvable pH range is shifted to more acidic values for excitation ratiometric method.

When different ROIs were analyzed differences are merely found for highest loading at basic values when intensity ratios are exceeding the dynamic response of the sensor. Error remains lower than 2% for both methods. Highest PGA loading follows the trend observable for all catalysts with a slightly lower dynamic range. This difference in pH response is not necessary attributed to the presence of more PGA in the close surrounding of the sensor protein but might be due to the use of different microscopy settings for this loading in case of both methods due to a slightly lower sYFP loading.

The same analysis was performed for control particles which do not contain PGA but the same loading of sYFP. These particles will be used to quantify pH in bulk solution. The unique difference is that control particles differ in diameter from Ag-IDA-glyoxyl used for coimmobilization in order to facilitate differentiation during microscopic measurement. Calibration was performed simultaneously under the specific microscopy settings optimal for the corresponding catalyst. There was no noticeable difference found between catalyst and bulk particles.

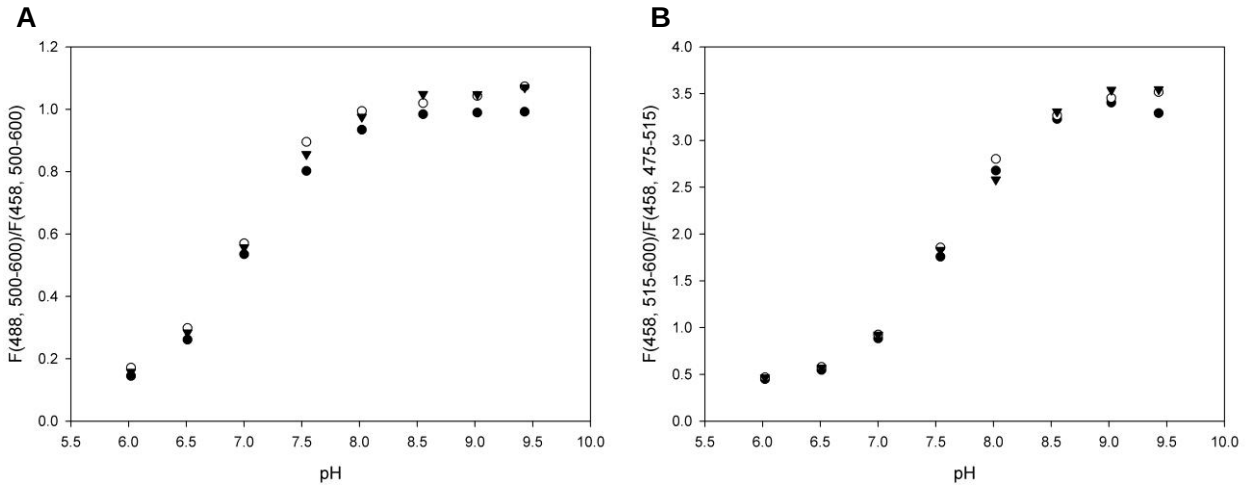

Figure 24. Dependence of fluorescence ratio onto pH. **A** Excitation ratiometric and **B** emission ratiometric calibration of sYFP-PGA coimmobilizate onto Ag-Ni-glyoxyl. For each calibration three loadings were analyzed, 805 IU_{PenG}/g of carrier (●), 135 IU_{PenG}/g of carrier (○) and 27 IU_{PenG}/g of carrier (▼).

Response curves were obtained and quantified results are shown in Table 7 for catalyst and control particles. Apparent pK' for excitation ratiometric method was around 7.00±0.05, for emission ratiometric option 7.60±0.05. Values for apparent pK' lie in the range of sYFP-Ag-Ni characterized previously. Excitation setup shows a higher dynamic range than emission ratiometric option. Compared to sYFP-Ag-Ni an increase in R_f could be observed for both methods, however, also associated with a higher standard deviation. Especially for excitation ratiometric method increase in R_f might be explained by a lack of points in the acidic range of the calibration.

pH response curves are completely overlapping for emission ratiometric method below 8.5 and for excitation ratiometric method below 8.0. An optimal range for pH resolution between 8.50±0.06 to 7.00±0.05 for emission and 8.00±0.06 to 6.30±0.05 for excitation ratiometric method is suggested. This estimation correlates well with the resolvable pH range for sYFP-Ag-Ni previously studied by pH time course measurements.

All calibrations shown up to now were performed with an cross section of 60 µm. For sYFP-PGA coimmobilizate pH response was also analyzed for a smaller volume, i.e.10 µm z-axis. Similar pK' values and dynamic range were obtained.

By the use of standard carrier activation protocols and established immobilization techniques compatibility between sYFP attachment and enzyme immobilization could be accomplished. Sequential approach based on the activation of a carrier with two distinct chemical groups offers the advantage of the control of each immobilization and protein distribution independently from each other. Final obtained coimmobilizate reveals enzyme activity and optical properties unaltered by the presence of the other protein and attachment approach. These results have shown that developed co-attachment approach is suitable for the study of internal pH in sYFP-PGA-coimmobilizates.

Table 7. Parameters obtained through fitting of pH response curves of sYFP-PGA coimmobilizate on Ag-Ni-glyxoyl to Eq. 4.

Ratiometric method		Excitation						Emission					
Sample		Enzyme particle			Control particle			Enzyme particle			Control particle		
Enzymatic Loading	Parameter	R_0	pK'	R_f	R_0	pK'	R_f	R_0	pK'	R_f	R_0	pK'	R_f
805 IU_{PenG}/g	Coefficient	0.04	6.98	26.93	0.04	7.02	28.89	0.31	7.59	11.17	0.31	7.62	11.55
	Std Error	0.02	0.03	12.77	0.04	0.07	32.03	0.07	0.05	2.55	0.08	0.05	2.72
135 IU_{PenG}/g	Coefficient	0.05	6.95	21.42	0.05	6.96	21.16	0.33	7.58	10.92	0.31	7.59	11.99
	Std Error	0.03	0.06	14.82	0.05	0.08	20.26	0.05	0.03	1.61	0.07	0.05	2.78
27 IU_{PenG}/g	Coefficient	0.05	7.00	20.49	0.05	7.02	22.44	0.37	7.66	9.82	0.33	7.61	11.59
	Std Error	0.02	0.03	6.44	0.03	0.04	11.01	0.04	0.03	1.03	0.07	0.05	2.49

3.5 MEASUREMENTS OF INTERNAL pH DURING REACTIONS CATALYZED BY COIMMOBILIZED PGA

3.5.1 Study of dynamic response of sYFP-PGA-coimmobilizate in presence of a heterogeneous acidification reaction

The developed method and pH responsive biocatalysts were applied for the resolution of internal conditions during an immobilized enzyme catalyzed reaction. Previously, we focused on the time response of the immobilized and soluble sYFP to monitor changes of pH promoted by a homogenous enzyme-catalyzed reaction. When the enzyme is immobilized enzyme-catalyzed acidification reaction takes place only exclusively inside the porous carrier structure. Under this scenario any mechanism of mass transfer (substrate, protons) is driven by molecular diffusion. Depending on the relative velocities of proton generation (enzyme activity) and proton transfer, the characteristic time of diffusion might exceed the characteristic time of reaction. A fast local depletion of pH would occur inside the catalyst leading to an intraparticle pH significantly lower than in bulk. A slower acidification would take place, following the apparent reaction rate of the catalyst.

A high loaded catalyst was studied for presence of diffusional hindrances during PenG hydrolysis in a stagnant solution. Reaction was measured suiting analyzed pH range to the optimal resolution capacity corresponding to each ratiometric method. In our experimental set-up reaction takes place in a stagnant 10 mM buffer solution. Particles containing 805 IU_{PenG} per gram of carrier remain static during the complete experiment. pH decrease in bulk solution is analyzed by addition of control particles. For the given amount of catalyst present in the whole suspension (0.5 mg particles/mL) a maximal acidification rate of 0.4 mM/min would be expected in the whole suspension, equivalent to 0.005 pH units/sec.

Figure 25 shows pH maps of a pH time course obtained with excitation ratiometric setup. Reaction was set to start at pH 8.0 according to the optimal range of resolution for this method. Exemplary two catalyst and two control particles were analyzed. After addition of substrate pH starts to decrease inside catalyst (ROI 1 and ROI 2) whereas any acidification is observable in bulk (ROI 3 and ROI 4). After 13 seconds a gradient of pH of 7.5 to 8.0 can be observed in control particles close to catalyst, according to the velocity of diffusion of generated protons from catalyst into bulk. After 22 seconds of reaction pH drops about 1 unit inside catalyst, control particle close to catalyst depict a pH of 7.5. In distance pH in bulk still remains at pH 8.0 as initially set for the reaction. During the time course of the reaction pH drops further until

approximately a pH of 6.5 is reached at the end of reaction. At that point also a gradient of pH is observable in the catalyst. Bulk surrounding catalyst is decreased to around pH 7.0, whereas pH more distant was slowly decreasing slightly below pH 8.0.

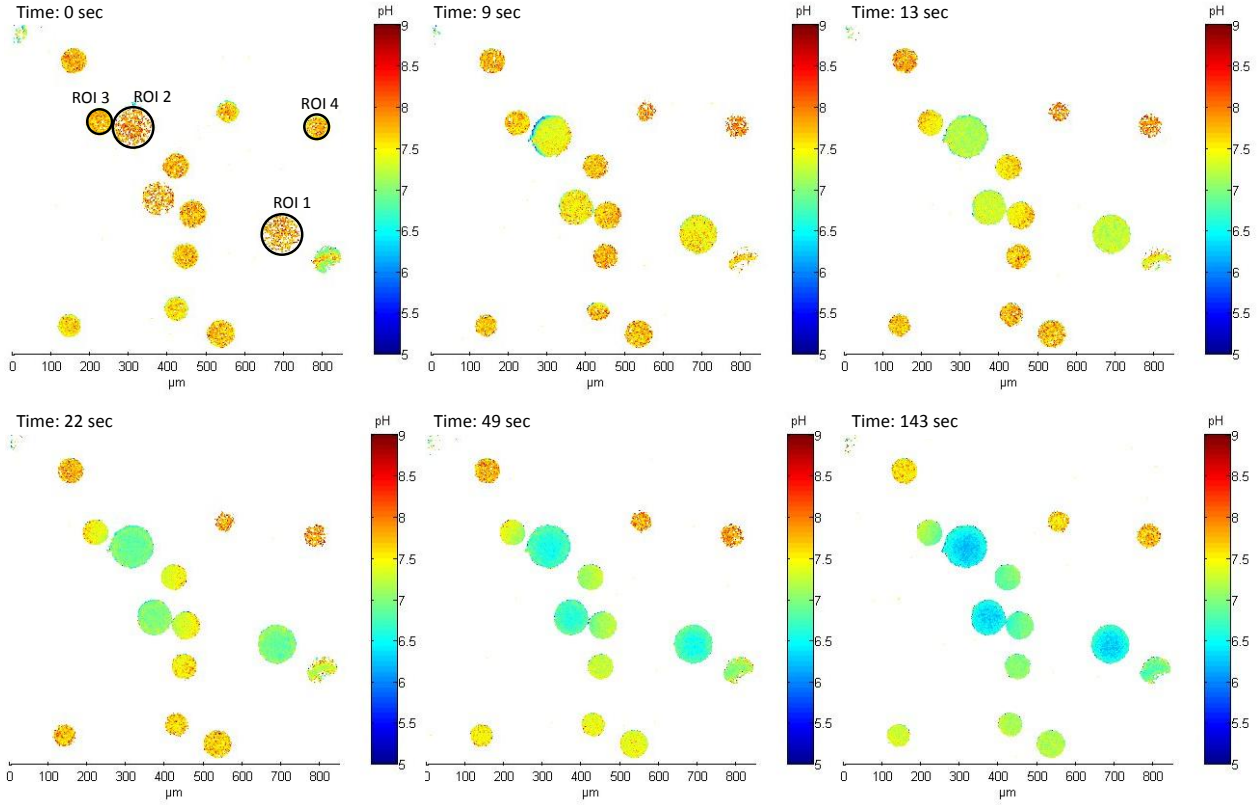

Figure 25. pH maps obtained with excitation ratiometric setup for the PenG hydrolysis catalyzed by a sYFP-PGA-coimmobilizate on Ag-Ni-glyoxyl. Reaction was performed with a PGA loading of 805 IU_{PenG}/g of carrier at RT in 10 mM SBP, pH 8.0 using 20 mM PenG as substrate. ROI 1 and 2 mark catalysts, ROI 3 and 4 control particles.

Figure 26 shows pH maps obtained when emission ratiometric settings were adopted. Reaction starts at a pH around 8.2, even though the reaction mixture was prepared at 8.5, due to pronounced acidification at this initial pH. A similar trend as for previous acidification reaction can be observed. After addition of PenG again pH starts to decrease inside catalyst whereas bulk remains at initial pH. After 20 seconds of reaction pH drops to 7.0 and bulk solution decreases half a pH unit in close proximity to catalyst. More distant only a small change of pH is observable. At the end of reaction, pH decreases until around 6.5 in catalyst, where again a slightly heterogeneous proton distribution is observable. For bulk solution close to catalyst pH is around 7.0, more distant around pH 8.0.

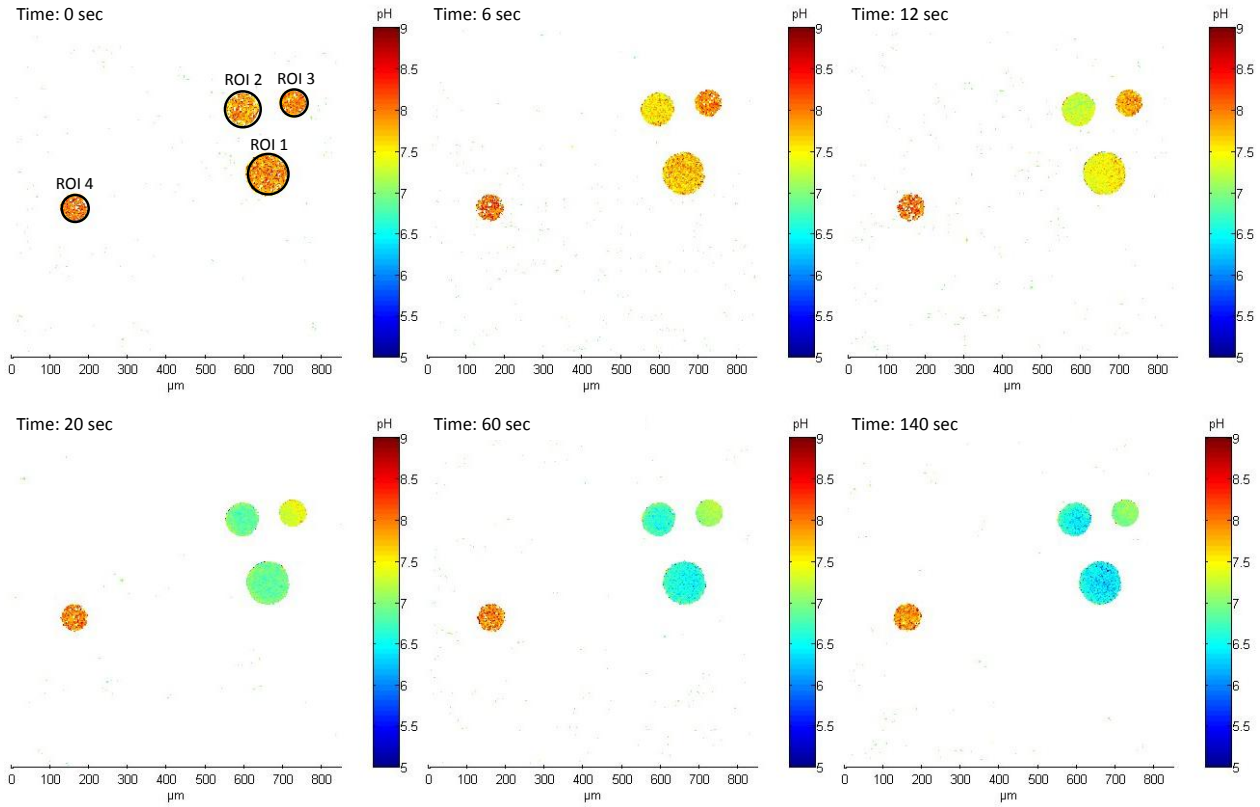

Figure 26. pH maps obtained with emission ratiometric setup for an acidification reaction catalyzed by a sYFP-PGA-coimmobilizate on Ag-Ni-glyoxyl. Reaction was performed with a PGA loading of 805 IU_{PenG}/g of carrier at RT in 10 mM SBP, pH 8.5 using 20 mM PenG as substrate. ROI 1 and 2 mark catalysts, ROI 3 and 4 control particles.

In contrast to convective mass transfer existing in a stirred particle suspension of enzyme reactors, the mass transfer in the stagnant suspension is driven purely by molecular diffusion. Control particles near catalyst particles are also affected by the pH gradient due to the excess of acidification rate over proton diffusion in the analyzed volume (case of ROI 3 for both methods). However, the scenario at the intraparticle level would not be essentially different to a stirred suspension since inside the catalyst particle internal proton diffusion would remain the solely transport mechanism. Internal acidification would only depend on biocatalyst and carrier features. This is the reason because we believe that this platform of analysis is suitable for the study and characterization of biocatalysts with respect to mass transport phenomena, obviously avoiding an overpopulation of particles and mutual incidence of catalyst particles in the suspension as requirements for a trustable analysis.

Time courses corresponding to the two above shown reactions are depicted in Figure 27. The observation of internal pH courses in high loaded immobilized PGA preparations shows a quick

instantaneous pH decrease inside the particles exceeding the acidification in bulk solution according to the volumetric activity used in suspension (0.005 pH units/sec). For both a fast initial drop of about 1 pH unit is observable after only 10 seconds of reaction, followed by a slower constant decrease. Bulk pH decreases depending on the velocity of diffusion of generated protons and the distance where pH was measured in bulk. The immense drop of pH inside catalyst just after addition of substrate compared to pH in bulk clearly indicates the huge diffusional limitation under tested conditions. Intraparticle pH sensing based on heterogeneous coimmobilized sYFP is able to deliver the evidence of this extreme diffusional control of the catalytic reaction with a very much faster internal proton accumulation than external diffusion or buffering capacity.

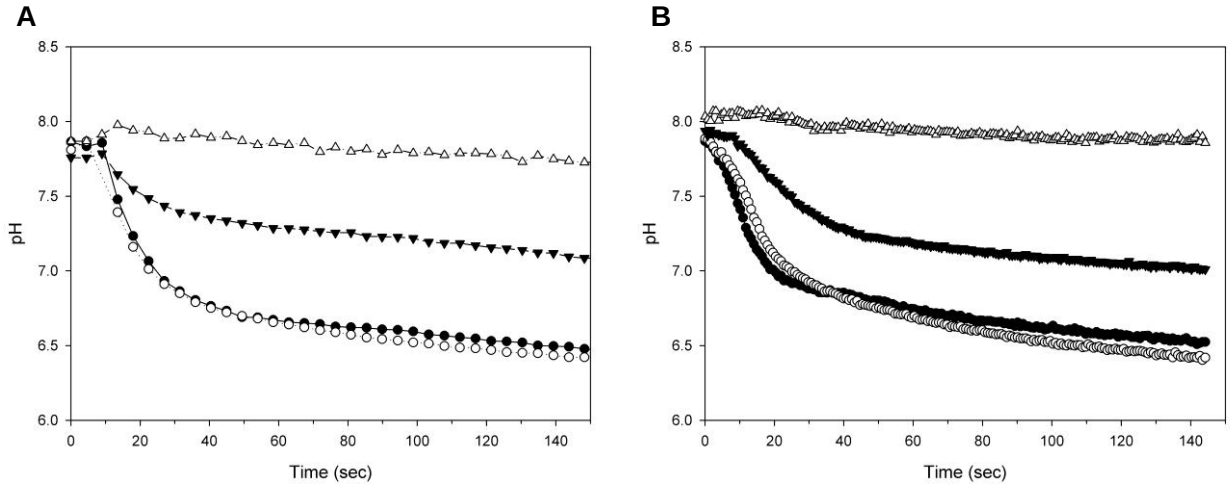

Figure 27. pH time courses catalyzed by a sYFP-PGA-coimmobilizate on Ag-Ni-glyoxyl measured with **A** excitation and **B** emission ratiometric setup. PGA loading was 805 IU_{PenG}/g of carrier. Reactions were performed at RT using 20 mM PenG as substrate in 10 mM SBP, set to pH 8.0 for excitation and pH 8.5 for emission ratiometric method; ROI 1 (●), ROI 2 (○), ROI 3 (▼) and ROI 4 (△).

3.5.2 Time-resolved internal pH analysis at conditions modulating the internal pH gradient

Internal conditions during PenG hydrolysis are highly dependent onto different parameters set for reaction and catalyst features. In unbuffered or slightly buffered systems, even small amounts of generated acids (or bases) may give a pH in the carrier that differs significantly from the external pH. Accumulated protons generated within the pores of a catalyst cause the formation of a proton gradient, to an extent that predominantly is a function of the proton-formation rate, and therefore dependent on the immobilized enzyme activity, the transport of

protons to the outside of the catalyst particles driven by mass-transfer and the buffer used to neutralize them.

In the following dynamic pH change was analyzed in response to a change of catalyst loading or a variation in buffer concentration. Figure 28 depicts time courses of a reaction carried out with a catalyst containing 805 IU_{PenG} per gram of Agarose BCL at three different buffer concentrations. Reaction mixture was prepared to start at pH 8.0 for excitation and pH 8.5 for emission ratiometric method. However, reactions carried out at 10 mM SPB start for both methods slightly lower than the pH set due to spontaneous acidification of buffer solution at this initial pH.

The same previously observed abrupt initial drop of pH can be seen for lowest tested buffer concentration. pH decreases 1 unit after 10 seconds of reaction, followed by a further slower gradual decrease until pH 6.0 for excitation ratiometric method and pH 6.5 for emission ratiometric option during monitored time range. Emission ratiometric method is able to resolve a first acidification drop of 0.2 pH units/sec whereas excitation ratiometric is resolving 0.1-0.15 pH units/sec. This difference in acidification rate is explained by the faster time response capability of emission ratiometric method. Also, decrease seems slightly less abrupt in case of excitation ratiometric method due to the lower initial pH.

An increase of buffer concentration to 100 mM leads to a decrease of the rate and initial pH drop. For the reaction monitored with emission ratiometric method (starting at pH 8.5) the initial reaction rate is slowed down slightly (0.1 pH units/sec) and first drop is about half a pH unit smaller. A clear effect is observed once pH reaches the area of highest buffering capacity (pK_a=7.2±0.75) where acidification slows down significantly. Obviously for excitation method (starting at pH 8), buffering effect is more pronounced. Reaction depicts a substantially lower initial acidification rate (0.025 pH units/sec) and around 7.5 a minor progressive pH decrease follows. When buffer concentration was increased further to 200 mM first instantaneous depletion of pH inside catalyst was dramatically slowed down in case of both methods indicating clearly the effect of buffer concentration onto internal acidification rate. When the reaction starts at pH 8, first drop is hardly observed but a gradual slow decrease follows.

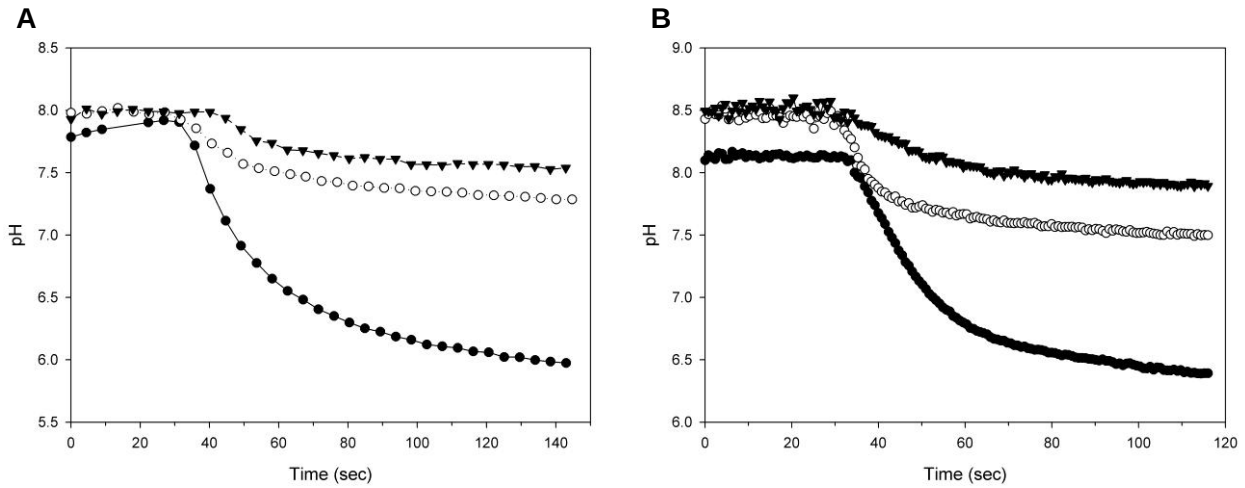

Figure 28. pH time courses catalyzed by a sYFP-PGA-coimmobilizate on Ag-Ni-glyoxyl measured with **A** excitation and **B** emission ratiometric setup. PGA loading was 805 IU_{PenG}/g of carrier. Reactions were performed at RT using 20 mM PenG as substrate in a SBP concentration of 10 mM (●), 100 mM (○) and 200 mM (▼) set to pH 8.0 for excitation and pH 8.5 for emission ratiometric method.

Deviating catalyst loading depicts a similar trend in the modulation of first initial pH drop and second acidification phase. Reactions measured at three different PGA loadings are shown in **Figure 29**. Buffer concentration was 10 mM SPB and reactions were set to start at pH 8.0 for excitation and pH 8.5 for emission ratiometric settings.

Highest immobilized activity of 805 IU_{PenG} per gram of carrier depicts again the expected instantaneous pH decrease. For the reaction measured with emission ratiometric method, a steep initial drop of 0.4 pH units/sec is resolved and a pH of 1.3 units reached after 10 seconds of reaction followed by a further slower gradual decrease. Excitation ratiometric method reveals a slower initial acidification rate of 0.15 pH units/sec, probably due to lower initial pH and lower time resolution velocity for this method. After 15 seconds pH decreases about 1 pH unit and further 1.5 units during the second gradual pH decrease. Intermediate enzyme loading of 135 IU_{PenG} per gram of carrier still promotes an initial drop of 0.6 pH units after substrate addition. Acidification rate is very similar for both methods (0.15 pH units/sec). Again a slower second phase follows in which it seems that diffusion velocity and buffering capacity are able to compensate velocity of reaction. pH decreases until a pH of 7.2 for excitation and pH 7.5 for emission ratiometric method is reached at the end of reaction. When a volumetric activity of 27 IU_{PenG} per gram of carrier was tested only a gradual pH decrease of 0.0013 pH units/sec and 0.0015 pH units/sec was observable for excitation and emission ratiometric method respectively. The velocity of internal proton generation due to hydrolysis reaction seems to be balanced by

diffusion and buffering. The slight progressive decrease is typical for the presence of a low volumetric activity in solution.

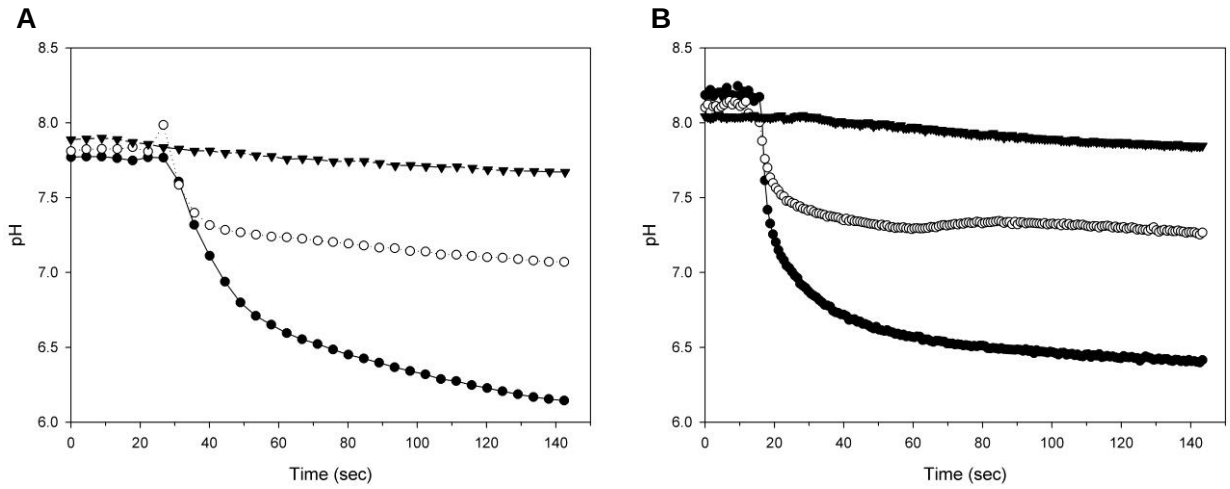

Figure 29. pH time courses catalyzed by a sYFP-PGA-coimmobilizate on Ag-Ni-glyoxyl measured with **A** excitation and **B** emission ratiometric setup. Reactions were performed at RT using 20 mM PenG as substrate in 10 mM SBP set to pH 8.0 for excitation and pH 8.5 for emission ratiometric method. PGA loading was 805 IU_{PenG}/g of carrier (●), 135 IU_{PenG}/g of carrier (○) and 27 IU_{PenG}/g of carrier (▼).

Intraparticle pH sensing show expected results for modulation of internal pH gradients in immobilized pH dependent biocatalysts. Internal conditions are affected according to enzymatic loading or buffering capacity. Decrease of immobilized activity or increase of buffer concentration depicts a progressive reduction of pH gradient and internal acidification rate. Initial instantaneous change of internal microenvironment is a common perseverative observation in the analysis of biocatalysts controlled by diffusional limitations. Abrupt first decrease is followed by a further second phase where internal rate of substrate consumption or product generation is equivalent to rate measureable in bulk solution by external observations. The first drop might be interpreted like a transition state during which high initial reaction rate is being balanced with the mass transfer given by molecular diffusion through the catalyst particles.

In case of a simple substrate limitation as for immobilized oxidases interpretation is immediate, internal oxygen concentration decreases until enzyme activity and diffusion rate are balanced. For proton consuming reactions situation is more complex. Acidification of internal microenvironment is not only dependent onto enzyme activity but also on the chosen reaction conditions (buffer concentration). Furthermore, kinetic of the enzyme might be affected by substrate limitation and inhibition phenomena.

However, in any case microenvironment governs the real performance of the catalyst. Observation at a microscale allready offered valuable information for a better biocatalyst

understanding and bioprocess design [15, 25, 27, 30, 31]. The consistency between apparent catalytic properties, modeling of enzyme kinetics and internal measurement was shown as a useful tool for comprehensive design.

Regarding to the specific work with immobilized PGA in this thesis, Illanes and Valencia carried out a comprehensive study of the effect of diffusional limitations onto performance of PGA immobilized on Ag-glyoxyl in hydrolysis and synthesis reactions [59–61]. Hydrolysis reaction of PenG is controlled by mass transfer due to substrate limitation and accumulation of phenyl acetic acid inhibiting the reaction. Reverse reaction is also dramatically controlled by diffusion since the accumulation of the product would favor the hydrolytic reaction decreasing synthesis yield.

Van Roon and coworkers have performed an exhaustive study of the efficiency of Assemblase®, an industrial immobilized catalyst of PGA, applied in the synthesis of Cephalexin [87, 91]. Authors claim that because of diffusional limitation enzyme catalyzes synthesis at sub-optimal conditions.

Models and assumption work under the principle that a high enough buffering capacity hinder the creation of pH gradients. The studies are focused on substrate and product diffusional limitations working with buffer concentration higher than 50 mM. However, depending on the used enzyme loading, we show that even with 100 mM still a clear internal pH gradient can be observed, especially under conditions where the buffering capacity of phosphate is diminishing. The combination of internal pH measurements together with a comprehensive reaction-diffusion model could be advantageous to bring forward the understanding of the complex process involved in heterogeneous catalysis.

The group of Guisán has studied biotransformations catalyzed by immobilized PGA trying to tune the internal pH gradient based on macroscopic observations. They state that generation of gradients inside the particle could be a profitable tool to improve biocatalyst performance. In this way two distinct pH values were established to obtain an optimal combination of operational stability and activity; an external pH of 8.0 and an internal pH estimated to be around pH 5.5. Values of internal pH were not measured but are based on macroscopic assumptions [83]. We show for similar catalysts and enzyme loadings “only” a pH gradient of about 1.5 pH units inside the carrier. This result again emphasizes that a systematic and synergetic use of internal pH sensing together with macroscopic observations would lead to an enhanced understanding of biotransformations offering new design opportunities.

4 GENERAL CONCLUSIONS

- The suitability of soluble sYFP as intensity ratiometric pH sensor has been studied. sYFP depict a adequate dynamic pH response in the range of pH 6.0-8.0 for excitation and 6.5-8.5 for emission ratiometric setup.
- A general strategy for the preparation of internal pH responsive porous enzyme carriers has been developed based on the oriented controlled immobilization of His-tagged sYFP. The methodology has enabled a homogeneous incorporation into agarose beads and could be extended to other relevant enzyme carriers, controlled pore glass particles and Sepabeads. Additionally, sYFP has been immobilized via a multipoint covalent attachment strategy on glyoxyl activated agarose depicting the flexibility of sYFP as heterogeneous sensor.
- The suitable pH range and dynamic response of immobilized sYFP has been studied. A range of pH 6.0-8.5 and reaction rates (0.3-30 mM/min equivalent to acidification rates of 0.005-0.2 pH units/sec.) could be conveniently resolved.
- The preparation of internal pH responsive immobilized biocatalysts has been shown exemplary by the coimmobilization of sYFP and PGA. Via simple tuning of immobilization conditions and by suiting well-established techniques of hetero-functional carrier activation, coimmobilizates have been prepared without alteration of biocatalyst properties or optical pH response.
- The coimmobilized pH responsive biocatalysts have been applied to study the feasibility of real time ratiometric internal pH imaging in immobilized PGA via analysis of stagnant catalyst suspensions in CLSM.
- The methodology has enabled the real time monitoring and quantification of internal pH under the presence of heterogeneous enzyme-catalyzed hydrolysis of PGA. Internal gradient has been quantified and the effects of different modulators studied, i.e. buffering capacity or internal catalytic activity.
- The resolution and quantification of internal pH gradients during heterogeneous catalysis of PGA has offered new insight into analysis and understanding of immobilized PGA.
- The methodology described seems to be a valuable opportunity for analysis and characterization of pH-dependent immobilized biocatalysts. Spatial resolution providing high-

detailed local pH depletion might be explored in conjunction with enzyme distribution into catalytic particles.

- Adaption to other optical read-out systems and experimental set-ups would give opportunities for high-throughput screening or real-time biotransformation monitoring: Microplate reader, Fiber optics, stirred particle suspensions and flow chambers containing fixed biocatalytic particles.
- Modulation of pH response range to the areas of interest for specific applications might be explored by protein engineering and/or tuning of applied settings (wavelength couples).

5 REFERENCES

1. Bucholz K. KV. 2005. Biocatalysts and enzyme technology. Weinheim: Wiley-VCH.
2. Guisán JM. 2010. Immobilization of enzymes and cells. Totowa, New Jersey: Humana Press.Illanes A. 2008. Enzyme biocatalysis principles and applications. Springer.
3. Illanes A. 2008. Enzyme biocatalysis principles and applications. Springer.
4. Liese A, Hilterhaus L. 2013. Evaluation of immobilized enzymes for industrial applications. Chem. Soc. Rev. 42:6236.
5. Garcia-Galan, C., Berenguer-Murcia, A., Fernandez-Lafuente, R., & Rodrigues, RC. 2011. Potential of different enzyme immobilization strategies to improve enzyme performance. Adv. Synth. Catal. 353:2885–2904.
6. Rodrigues RC, Ortiz C, Berenguer-Murcia Á, Torres R, Fernández-Lafuente R. 2013. Modifying enzyme activity and selectivity by immobilization. Chem. Soc. Rev. 42:6290.
7. Sheldon RA, van Pelt S. 2013. Enzyme immobilisation in biocatalysis: why, what and how. Chem. Soc. Rev. 42:6223.
8. Cantone S, Ferrario V, Corici L, Ebert C, Fattor D, Spizzo P, Gardossi L. 2013. Efficient immobilisation of industrial biocatalysts: criteria and constraints for the selection of organic polymeric carriers and immobilisation methods. Chem. Soc. Rev. 42:6262-6276
9. Sheldon RA. 2007. Enzyme Immobilization: The Quest for Optimum Performance. Adv. Synth. Catal. 349:1289–1307.
10. Bommarius AS, Paye MF. 2013. Stabilizing biocatalysts. Chem. Soc. Rev. 42:6534.
11. Hanefeld U, Gardossi L, Magner E. 2009. Understanding enzyme immobilisation. Chem. Soc. Rev. 38:453–468.
12. Mateo C, Palomo JM, Fernandez-Lorente G, Guisan JM, Fernandez-Lafuente R. 2007. Improvement of enzyme activity, stability and selectivity via immobilization techniques. Enzyme Microb. Technol. 40:1451–1463.
13. Secundo F. 2013. Conformational changes of enzymes upon immobilisation. Chem. Soc. Rev. 42:6250.
14. Talbert JN, Goddard JM. 2012. Enzymes on material surfaces. Colloids Surf. B Biointerfaces 93:8–19.
15. Tischer W, Kasche V. 1999. Immobilized enzymes: Crystals or carriers? Trends Biotechnol. 17:326–335.
16. Doran PM. 2013. Bioprocess engineering principles 2nd ed. Waltham, MA: Focal Press.
17. Tischer W. and Wedekind F. Immobilized Enzymes: Methods and Applications in Biocatalysis - From Discovery to Application Topics in Current Chemistry Volume 200, 1999, pp 95-126 Heidelberg: Springer Berlin Heidelberg

18. Bolivar JM, Consolati T, Mayr T, Nidetzky B. 2013. Shine a light on immobilized enzymes: real-time sensing in solid supported biocatalysts. Trends Biotechnol. 31:194–203.

19. Wencel D, Abel T, McDonagh C. 2014. Optical Chemical pH Sensors. Anal. Chem. 86:15–29.

20. Boniello C, Mayr T, Bolivar JM, Nidetzky B. 2012. Dual-lifetime referencing (DLR): a powerful method for on-line measurement of internal pH in carrier-bound immobilized biocatalysts. BMC Biotechnol. 12:11.

21. Heinemann M, Limper U, Büchs J. 2004. New insights in the spatially resolved dynamic pH measurement in macroscopic large absorbent particles by confocal laser scanning microscopy. J. Chromatogr. A 1024:45–53.

22. Huang HY, Shaw J, Yip C, Wu XY. 2008. Microdomain pH gradient and kinetics inside composite polymeric membranes of pH and glucose sensitivity. Pharm. Res. 25:1150–1157.

23. Kuwana E, Liang F, Sevick-Muraca EM. 2004. Fluorescence lifetime spectroscopy of a pH-sensitive dye encapsulated in hydrogel beads. Biotechnol. Prog. 20:1561–1566.

24. Schwendt T, Michalik C, Zavrel M, Dennig A, Spiess AC, Poprawe R, Janzen C. 2010. Determination of temporal and spatial concentration gradients in hydrogel beads using multiphoton microscopy techniques. Appl. Spectrosc. 64:720–726.

25. Spiess A, Schlothauer R, Hinrichs J, Scheidat B, Kasche V. 1999. pH gradients in immobilized amidases and their influence on rates and yields of beta-lactam hydrolysis. Biotechnol. Bioeng. 62:267–277.

26. Spiess AC, Zavrel M, Ansorge-Schumacher MB, Janzen C, Michalik C, Schmidt TW, Schwendt T, Büchs J, Poprawe R, Marquardt W. 2008. Model discrimination for the propionic acid diffusion into hydrogel beads using lifetime confocal laser scanning microscopy. Chem. Eng. Sci. 63:3457–3465.

27. Spiess AC, Kasche V. 2001. Direct measurement of pH profiles in immobilized enzyme carriers during kinetically controlled synthesis using CLSM. Biotechnol. Prog. 17:294–303.

28. Thörn C, Carlsson N, Gustafsson H, Holmberg K, Åkerman B, Olsson L. 2013b. A method to measure pH inside mesoporous particles using protein-bound SNARF1 fluorescent probe. Microporous Mesoporous Mater. 165:240–246.

29. Yamaguchi A, Namekawa M, Kamijo T, Itoh T, Teramae N. 2011. Acid-base equilibria inside amine-functionalized mesoporous silica. Anal. Chem. 83:2939–2946.

30. Zahel T, Boniello C, Nidetzky B. 2013. Real-time measurement and modeling of intraparticle pH gradient formation in immobilized cephalosporin C amidase. Process Biochem. 48:593–604.

31. Boniello C, Mayr T, Klimant I, Koenig B, Riethorst W, Nidetzky B. 2010. Intraparticle concentration gradients for substrate and acidic product in immobilized cephalosporin C

amidase and their dependencies on carrier characteristics and reaction parameters. Biotechnol. Bioeng. 106:528–540.

32. Lakowicz JR. 2006. Principles of fluorescence spectroscopy 1 p. Principles of Fluorescence Spectroscopy.

33. Kuwana E. 2003. Sensing of pH in multiply scattering media with fluorescence lifetime. In: SPIE, Vol. 4958, pp. 32–42.

34. Day RN, Davidson MW. 2009. The fluorescent protein palette: tools for cellular imaging. Chem. Soc. Rev. 38:2887.

35. Dedecker P, De Schryver FC, Hofkens J. 2013. Fluorescent Proteins: Shine on, You Crazy Diamond. J. Am. Chem. Soc. 135:2387–2402.

36. Frommer WB, Davidson MW, Campbell RE. 2009. Genetically encoded biosensors based on engineered fluorescent proteins. Chem. Soc. Rev. 38:2833.

37. Nienhaus K, Nienhaus GU. 2014. Fluorescent proteins for live-cell imaging with super-resolution. Chem. Soc. Rev. 43:1088–1106.

38. Lippincott-Schwartz J, Patterson GH. 2003. Development and Use of Fluorescent Protein Markers in Living Cells. Science 300:87–91.

39. Barondeau DP, Kassmann CJ, Tainer JA, Getzoff ED. 2005. Understanding GFP Chromophore Biosynthesis: Controlling Backbone Cyclization and Modifying Post-translational Chemistry†,‡. Biochemistry (Mosc.) 44:1960–1970.

40. Wachter RM. 2007. Chromogenic cross-link formation in green fluorescent protein. Acc. Chem. Res. 40:120–127.

41. Brejc K, Sixma TK, Kitts PA, Kain SR, Tsien RY, Ormö M, Remington SJ. 1997. Structural basis for dual excitation and photoisomerization of the Aequorea victoria green fluorescent protein. Proc. Natl. Acad. Sci. 94:2306–2311.

42. Sample V, Newman RH, Zhang J. 2009. The structure and function of fluorescent proteins. Chem. Soc. Rev. 38:2852.

43. Kneen M, Farinas J, Li Y, Verkman AS. 1998. Green fluorescent protein as a noninvasive intracellular pH indicator. Biophys. J. 74:1591–1599.

44. Patterson GH, Knobel SM, Sharif WD, Kain SR, Piston DW. 1997. Use of the green fluorescent protein and its mutants in quantitative fluorescence microscopy. Biophys. J. 73:2782–2790.

45. Bizzarri R, Nifosì R, Abbruzzetti S, Rocchia W, Guidi S, Arosio D, Garau G, Campanini B, Grandi E, Ricci F, Viappiani C, Beltram F. 2007. Green Fluorescent Protein Ground States: The Influence of a Second Protonation Site near the Chromophore†,‡. Biochemistry (Mosc.) 46:5494–5504.

46. Bizzarri R, Serresi M, Luin S, Beltram F. 2009. Green fluorescent protein based pH indicators for in vivo use: a review. Anal. Bioanal. Chem. 393:1107–1122.

47. Seward HE, Bagshaw CR. 2009. The photochemistry of fluorescent proteins: implications for their biological applications. Chem. Soc. Rev. 38:2842.

48. Bell, AF., He, X., Wachter, RM., & Tonge, PJ. 2000. Probing the Ground State Structure of the Green Fluorescent Protein Chromophore Using Raman Spectroscopy. Biochemistry-US, 39:4423–4431.

49. Elsliger, M-A., Wachter, RM., Hanson, GT., Kallio, K., & Remington, SJ. 1999. Structural and Spectral Response of Green Fluorescent Protein Variants to Changes in pH. Biochemistry-US, 38:5296–5301.

50. Chattoraj M, King BA, Bublitz GU, Boxer SG. 1996. Ultra-fast excited state dynamics in green fluorescent protein: multiple states and proton transfer. Proc. Natl. Acad. Sci. 93:8362–8367.

51. Lossau H, Kummer A, Heinecke R, Pöllinger-Dammer F, Kompa C, Bieser G, Jonsson T, Silva CM, Yang MM, Youvan DC, Michel-Beyerle ME. 1996. Time-resolved spectroscopy of wild-type and mutant Green Fluorescent Proteins reveals excited state deprotonation consistent with fluorophore-protein interactions. Chem. Phys. 213:1–16.

52. Bencina M. 2013. Illumination of the Spatial Order of Intracellular pH by Genetically Encoded pH-Sensitive Sensors. Sensors 13:16736–16758.

53. Bizzarri R, Arcangeli C, Arosio D, Ricci F, Faraci P, Cardarelli F, Beltram F. 2006. Development of a Novel GFP-based Ratiometric Excitation and Emission pH Indicator for Intracellular Studies. Biophys. J. 90:3300–3314.

54. Serresi M, Bizzarri R, Cardarelli F, Beltram F. 2009. Real-time measurement of endosomal acidification by a novel genetically encoded biosensor. Anal. Bioanal. Chem. 393:1123–1133.

55. Wachter RM, Elsliger M-A, Kallio K, Hanson GT, Remington SJ. 1998. Structural basis of spectral shifts in the yellow-emission variants of green fluorescent protein. Structure 6:1267–1277.

56. Al-ramahi González, Y. 2013. PhD Thesis: Ingeniería de proteínas fluorescentes y aplicaciones de localización celular en microorganismos termófilos. Universidad Autónoma de Madrid, Facultad de Ciencias, Departamento de Biología Molecular.

57. Bradford MM. 1976. A rapid and sensitive method for the quantitation of microgram quantities of protein utilizing the principle of protein-dye binding. Anal. Biochem. 72:248–254.

58. Kheirolomoom A, Ardjmand M, Fazelinia H, Zakeri A. 2001. Clarification of penicillin G acylase reaction mechanism. Process Biochem. 36:1095–1101.

59. Illanes A, González JM, Gómez JM, Valencia P, Wilson L. 2010. Diffusional restrictions in glyoxyl-agarose immobilized penicillin G acylase of different particle size and protein loading. Electron. J. Biotechnol. 13:15.

60. Valencia P, Wilson L, Aguirre C, Illanes A. 2010. Evaluation of the incidence of diffusional restrictions on the enzymatic reactions of hydrolysis of penicillin G and synthesis of cephalexin. Enzyme Microb. Technol. 47:268–276.

61. Valencia P, Flores S, Wilson L, Illanes A. 2011. Effect of internal diffusional restrictions on the hydrolysis of penicillin G: reactor performance and specific productivity of 6-APA with immobilized penicillin acylase. Appl. Biochem. Biotechnol. 165:426–441.

62. Mateo C, Bolivar JM, Godoy CA, Rocha-Martin J, Pessela BC, Curiel JA, Muñoz R, Guisan JM, Fernández-Lorente G. 2010. Improvement of Enzyme Properties with a Two-Step Immobilizaton Process on Novel Heterofunctional Supports. Biomacromolecules 11:3112–3117.

63. Guisán J. 1988. Aldehyde-agarose gels as activated supports for immobilization-stabilization of enzymes. Enzyme Microb. Technol. 10:375–382.

64. Bernal C, Sierra L, Mesa M. 2012. Improvement of thermal stability of β-galactosidase from Bacillus circulans by multipoint covalent immobilization in hierarchical macro-mesoporous silica. J. Mol. Catal. B Enzym. 84:166–172.

65. Armisén P, Mateo C, Cortés E, Barredo JL, Salto F, Diez B, Rodés L, García JL, Fernández-Lafuente R, Guisán JM. 1999. Selective adsorption of poly-His tagged glutaryl acylase on tailor-made metal chelate supports. J. Chromatogr. A 848:61–70.

66. Alvaro G, Fernandez-Lafuente R, Blanco RM, Guisán JM. 1990. Immobilization-stabilization of Penicillin G acylase fromEscherichia coli. Appl. Biochem. Biotechnol. 26:181–195.

67. Neuhoff V, Arold N, Taube D, Ehrhardt W. 1988. Improved staining of proteins in polyacrylamide gels including isoelectric focusing gels with clear background at nanogram sensitivity using Coomassie Brilliant Blue G-250 and R-250. Electrophoresis 9:255–262.

68. Laemmli UK. 1970. Cleavage of structural proteins during the assembly of the head of bacteriophage T4. Nature 227:680–685.

69. Hermanson GT. 2013. Bioconjugate Techniques Elsevier Inc.

70. Schindelin J, Arganda-Carreras I, Frise E, Kaynig V, Longair M, Pietzsch T, Preibisch S, Rueden C, Saalfeld S, Schmid B, Tinevez J-Y, White DJ, Hartenstein V, Eliceiri K, Tomancak P, Cardona A. 2012. Fiji: an open-source platform for biological-image analysis. Nat. Methods 9:676–682.

71. e-Handbook of statiscal methods. 2012. NIST/SEMATECH http://www.itl.nist.gov/div898/handbook/.

72. Ellison SLR., Williams A. 2012. "Eurachem/CITAC guide: Quantifying Uncertainty in Analytical Measurement, Third edition, ISBN 978-0-948926-30-3.

73. Kragten J. 1994. Tutorial review. Calculating standard deviations and confidence intervals with a universally applicable spreadsheet technique. The Analyst 119:2161.

74. Bolivar JM, Hidalgo A, Sánchez-Ruiloba L, Berenguer J, Guisán JM, López-Gallego F. 2011. Modulation of the distribution of small proteins within porous matrixes by smart-control of the immobilization rate. J. Biotechnol. 155:412–420.

75. Hernandez K, Fernandez-Lafuente R. 2011. Control of protein immobilization: Coupling immobilization and site-directed mutagenesis to improve biocatalyst or biosensor performance. Enzyme Microb. Technol. 48:107–122.

76. Porath J. 1992. Immobilized metal ion affinity chromatography. Protein Expr. Purif. 3:263–281.

77. Batalla P, Bolívar JM, Lopez-Gallego F, Guisan JM. 2012. Oriented covalent immobilization of antibodies onto heterofunctional agarose supports: a highly efficient immuno-affinity chromatography platform. J. Chromatogr. A 1262:56–63.

78. Pessela BCC, Mateo C, Filho M, Carrascosa A, Fernández-Lafuente R, Guisan JM. 2007. Selective adsorption of large proteins on highly activated IMAC supports in the presence of high imidazole concentrations: Purification, reversible immobilization and stabilization of thermophilic α- and β-galactosidases. Enzyme Microb. Technol. 40:242–248.

79. Pina AS, Lowe CR, Roque ACA. 2014. Challenges and opportunities in the purification of recombinant tagged proteins. Biotechnol. Adv. 32:366–381.

80. Uhlén M. 2008. Affinity as a tool in life science. BioTechniques 44:649–654.

81. Mateo C, Abian O, Bernedo M, Cuenca E, Fuentes M, Fernandez-Lorente G, Palomo JM, Grazu V, Pessela BCC, Giacomini C, Irazoqui G, Villarino A, Ovsejevi K, Batista-Viera F, Fernandez-Lafuente R, Guisán JM. 2005. Some special features of glyoxyl supports to immobilize proteins. Enzyme Microb. Technol. 37:456–462.

82. Mateo C, Palomo JM, Fuentes M, Betancor L, Grazu V, López-Gallego F, Pessela BCC, Hidalgo A, Fernández-Lorente G, Fernández-Lafuente R, Guisán JM. 2006. Glyoxyl agarose: A fully inert and hydrophilic support for immobilization and high stabilization of proteins. Enzyme Microb. Technol. 39:274–280.

83. Guisan JM, Alvaro G, Rosell CM, Fernandez-Lafuente R. 1994. Industrial design of enzymic processes catalysed by very active immobilized derivatives: Utilization of diffusional limitations (gradients of pH) as a profitable tool in enzyme engineering. Biotechnol. Appl. Biochem. 20:357–369.

84. Fuentes M, Batalla P, Grazu V, Pessela BCC, Mateo C, Montes T, Hermoso JA, Guisan JM, Fernandez-Lafuente R. 2007. Mixed ion exchange supports as useful ion exchangers for protein purification: purification of penicillin G acylase from Escherichia coli. Biomacromolecules 8:703–707.

85. Montes T, Grazu V, López-Gallego F, Hermoso JA, Guisan JM, Fernandez-Lafuente R. 2006. Chemical modification of protein surfaces to improve their reversible enzyme immobilization on ionic exchangers. Biomacromolecules 7:3052–3058.

86. Montes T, Grazu V, Lopez-Gallego F, Hermoso JA, Garcia JL, Manso I, Galan B, Gonzalez R, Fernandez-Lafuente R, Guisan JM. 2007. Genetic Modification of the Penicillin G Acylase surface to improve its reversible immobilization on ionic Exchangers. Appl. Environ. Microbiol. 73:312–319.

87. Van Roon JL, Joerink M, Rijkers MPWM, Tramper J, Schroën CGPH, Beeftink HH. 2003. Enzyme distribution derived from macroscopic particle behavior of an industrial immobilized penicillin-G acylase. Biotechnol. Prog. 19:1510–1518.

88. Van Roon JL, van Aelst AC, Schroën CGPH, Tramper J, Beeftink HH. 2005. Field-emission scanning electron microscopy analysis of morphology and enzyme distribution within an industrial biocatalytic particle. Scanning 27:181–189.

89. Van Roon JL, Boom RM, Paasman MA, Tramper J, Schroën CGPH, Beeftink HH. 2005b. Enzyme distribution and matrix characteristics in biocatalytic particles. J. Biotechnol. 119:400–415.

90. Van Roon JL, Groenendijk E, Kieft H, Schroën CGPH, Tramper J, Beeftink HH. 2005c. Novel approach to quantify immobilized-enzyme distributions. Biotechnol. Bioeng. 89:660–669.

91. Van Roon JL, Arntz MMHD, Kallenberg AI, Paasman MA, Tramper J, Schroën CGPH, Beeftink HH. 2006. A multicomponent reaction-diffusion model of a heterogeneously distributed immobilized enzyme. Appl. Microbiol. Biotechnol. 72:263–278.

92. Van Roon J, Beeftink R, Schroën K, Tramper H. 2002. Assessment of intraparticle biocatalytic distributions as a tool in rational formulation. Curr. Opin. Biotechnol. 13:398–405.

6 FIGURES INDEX

7 INDEX OF TABLES

8 APPENDIX

8.1 BERKELEY-MADONNA CODE FOR ANALYSIS OF PenG HYDROLYSIS

```
METHOD RK4
STARTTIME = 0
STOPTIME=2
DT = 0.1
d/dt (Hr) = V/60
d/dt (PG)=-V/60
init PG=100 ;mM
init Hr=0
Hinit= 10^ (-8)
H2PO4=H2PO4init + Hr
H2PO4init=phosphate-HPO4init
HPO4init=phosphate/(1+Hinit/keq)
HPO4=HPO4init-Hr
V = vmax/(1+10^(pk-
ph))*PG/(Km*(1+PG/km+PG*PG/km/ks+H/k1+H/k2+PG*H/km/k2+H*H/k1/k2))
km=0.13
ks=821
k1=1.82
k2=48
VpH=H2PO4/HPO4/2.302585
ph= -log10(keq)+log10((HPO4/H2PO4))
VpH=h2po4/hpo4/2.302585*(V/60*h2po4+V/60*hpo4)/H2po4/h2po4
phosphate = 10 ;mM
vmax=1
h=10^(-8)*pH
keq = 6.2*10^(-8)
pK=7
```

8.2 MATLAB CODE FOR THE CALCULATION OF pH MAPS

Excitation ratiometric setup:

```
cd Channel1
data_num_1 = numel(dir('*.txt'));
data_1 = dir('*.txt');
cd ..
cd Channel2
data_num_2 = numel(dir('*.txt'));
data_2 = dir('*.txt');
cd ..

pixel_size = 1/0.602;%[µm/pixel]
time_step = 4.49264725000004;%[s/picture]

if data_num_1 ~= data_num_2
    error('Channels have differnt picture number')
else
    data_num = data_num_1;
end

data_ind = 1:data_num-1;

for k = data_ind(1):data_ind(end)+1
    disp(k)
    tmp = importdata(data_1(k).name,' ');
    tmp(tmp<2) = NaN;
    CH1(:,:,k-data_ind(1)+1) =tmp;
end

for k = data_ind(1):data_ind(end)+1
    disp(k)
    tmp = importdata(data_2(k).name,' ');
    tmp(tmp<2) = NaN;
    CH2(:,:,k-data_ind(1)+1) =tmp;
end

Ratio = CH2./CH1;
R0 = 0.0583;
pK = 7.0391;
Rf = 24.0056;

pH = pK - log10( (Ratio/R0-Rf)./(1 - Ratio/R0));
pH(logical(imag(pH))) = nan;

figure
image(flipud(pH(:,:,1)))
[X, Y]= ginput(2);
xmin=round(min(X));
xmax=round(max(X));
ymax=size(pH,2) - round(min(Y));
```

```
ymin=size(pH,2) -round(max(Y));
tmp =pH(ymin:ymax,xmin:xmax,1);
disp([num2str(nanmean(tmp(:)))])

fig1 = figure;
sh =
surf(linspace(0,size(pH,1)*pixel_size,size(pH,1)),linspace(0,size(pH,2)*pixel_
size,size(pH,2)),pH(:,:,1),'EdgeColor','none');
set(gcf, 'color', 'w');
% set(gca, 'color', 'w');

colormap (jet);
colorbar
caxis manual;
caxis([5 9])
colorbar('location','eastoutside')
title(colorbar,'pH')
axis equal
xlabel('µm')
set(gca,'XTickLabel',{'0','100', '200', '300', '400', '500', '600', '700',
'800' })
ylabel('µm')
set(gca,'box','off','YTick',[],'YColor','w')
grid off
view([0,-90])
th1 = title('Time [s]: 0');

c = round(clock);
avifilename = ['simulation on ', date, ' time ',num2str(c(4)),' uhr
',num2str(c(5:6)),'.avi'];
mkdir('Tanja_Particles/',avifilename)
avidir = ['Tanja_Particles\',avifilename,'\'];
aviobj = avifile([avidir,avifilename],'compression','None');
pause(1)

for l = 2:size(pH,3)
        set(th1,'String',['Time [s]: ',num2str(time_step*l)])
        pause(0.05)
        set(sh,'ZData',pH(:,:,l))
        tmp =pH(ymin:ymax,xmin:xmax,l);
        POI_mean(l) = nanmean(tmp(:));
        disp([num2str(POI_mean(l))])

        F = getframe(fig1);
        aviobj = addframe(aviobj,F);
end

aviobj = close(aviobj);

plot(time_step.*(1:size(pH,3)),POI_mean)
xlabel('Time [s]')
ylabel('pH')
```

Emission ratiometric setup:

```
cd Channel1
data_num_1 = numel(dir('*.txt'));
data_1 = dir('*.txt');
cd ..
cd Channel2
data_num_2 = numel(dir('*.txt'));
data_2 = dir('*.txt');
cd ..

pixel_size = 1/0.602;%[µm/pixel]
time_step = 0.783490909090914;%[s/picture]

if data_num_1 ~= data_num_2
    error('Channels have differnt picture number')
else
    data_num = data_num_1;
end

data_ind = 1:data_num-1;

for k = data_ind(1):data_ind(end)+1
    disp(k)
    tmp = importdata(data_1(k).name,' ');
    tmp(tmp<2) = NaN;
    CH1(:,:,k-data_ind(1)+1) =tmp;
end

for k = data_ind(1):data_ind(end)+1
    disp(k)
    tmp = importdata(data_2(k).name,' ');
    tmp(tmp<2) = NaN;
    CH2(:,:,k-data_ind(1)+1) =tmp;
end

Ratio = CH2./CH1;
R0 = 0.3347;
pK = 7.6928;
Rf = 11.6522;

pH = pK - log10( (Ratio/R0-Rf)./(1 - Ratio/R0));
pH(logical(imag(pH))) = nan;

figure
image(flipud(pH(:,:,1)))
[X, Y]= ginput(2);
xmin=round(min(X));
xmax=round(max(X));
ymax=size(pH,2) - round(min(Y));
ymin=size(pH,2) -round(max(Y));
tmp =pH(ymin:ymax,xmin:xmax,1);
disp([num2str(nanmean(tmp(:)))])
```

```
fig1 = figure;
sh =
surf(linspace(0,size(pH,1)*pixel_size,size(pH,1)),linspace(0,size(pH,2)*pixel_
size,size(pH,2)),pH(:,:,1),'EdgeColor','none');
set(gcf, 'color', 'w');
% set(gca, 'color', 'w');

colormap (jet);
colorbar
caxis manual;
caxis([5 9])
colorbar('location','eastoutside')
title(colorbar,'pH')
axis equal
xlabel('µm')
set(gca,'XTickLabel',{'0','100', '200', '300', '400', '500', '600', '700',
'800' })
ylabel('µm')
set(gca,'box','off','YTick',[],'YColor','w')
grid off
view([0,-90])
th1 = title('Time [s]: 0');

c = round(clock);
avifilename = ['simulation on ', date, ' time ',num2str(c(4)),' uhr
',num2str(c(5:6)),'.avi'];
mkdir('Tanja_Particles/',avifilename)
avidir = ['Tanja_Particles\',avifilename,'\'];
aviobj = avifile([avidir,avifilename],'compression','None');
pause(1)

for l = 2:size(pH,3)
        set(th1,'String',['Time [s]: ',num2str(time_step*l)])
        pause(0.05)
        set(sh,'ZData',pH(:,:,l))
        tmp =pH(ymin:ymax,xmin:xmax,l);
        POI_mean(l) = nanmean(tmp(:));
        disp([num2str(POI_mean(l))])

        F = getframe(fig1);
        aviobj = addframe(aviobj,F);
end


aviobj = close(aviobj);

plot(time_step.*(1:size(pH,3)),POI_mean)
xlabel('Time [s]')
ylabel('pH')
```

8.3 SUPPORTING FIGURES

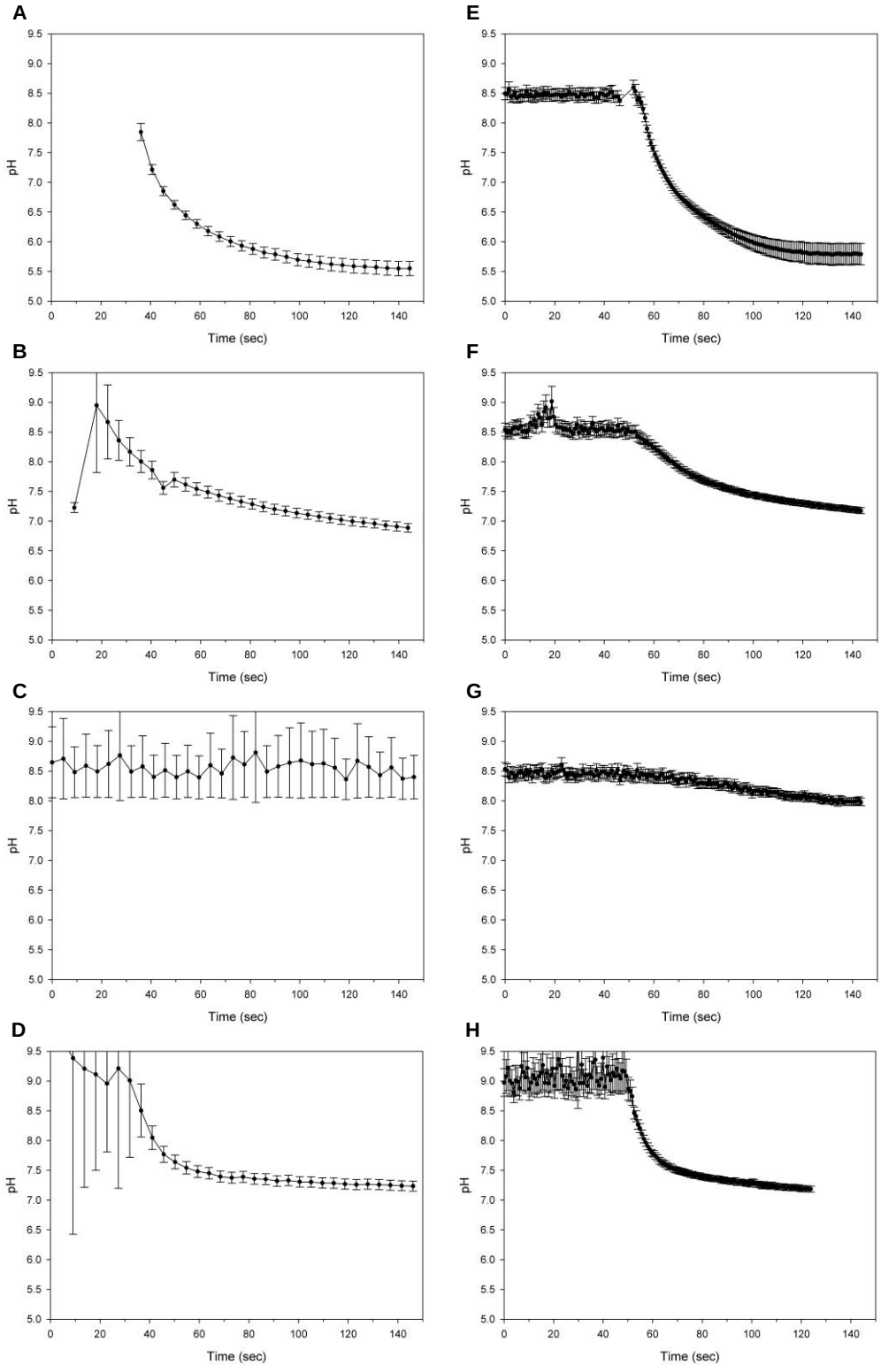

Figure S1. pH time courses obtained at RT using 10 mM PenG as substrate and sYFP-Ag-glyoxyl as fluorescent pH sensor. Uncertainties of pH determination calculated according to Eq. 8 are shown. Reactions in 10 mM SPB, pH 9, **A**, **E** 30 IU_{PenG}/mL, **B**, **F** 3 IU_{PenG}/mL, **C**, **G** 0.3 IU_{PenG}/mL and reactions in 100 mM SPB, pH 9, **D**, **H** 30 IU_{PenG}/mL were measured with excitation and emission ratiometric setup respectively.

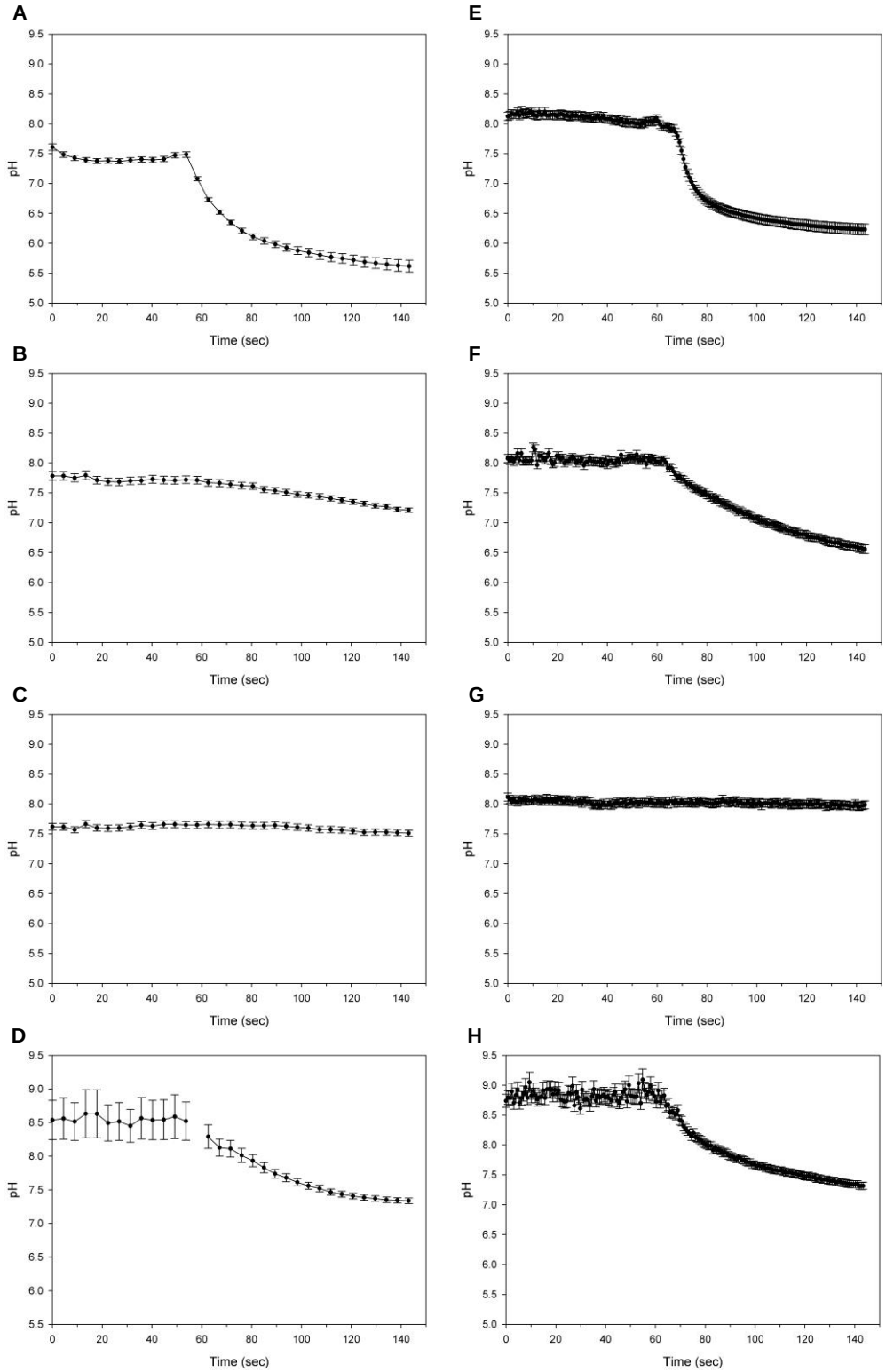

Figure S2. pH time courses obtained at RT using 10 mM PenG as substrate and sYFP-CPG-Ni as fluorescent pH sensor. Uncertainties of pH determination calculated according to Eq. 8 are shown. Reactions in 10 mM SPB, pH 9, **A**, **E** 30 IU_{PenG}/mL, **B**, **F** 3 IU_{PenG}/mL, **C**, **G** 0.3 IU_{PenG}/mL and reactions in

100 mM SPB, pH 9, **D**, **H** 30 IU_{PenG}/mL were measured with excitation and emission ratiometric setup respectively.

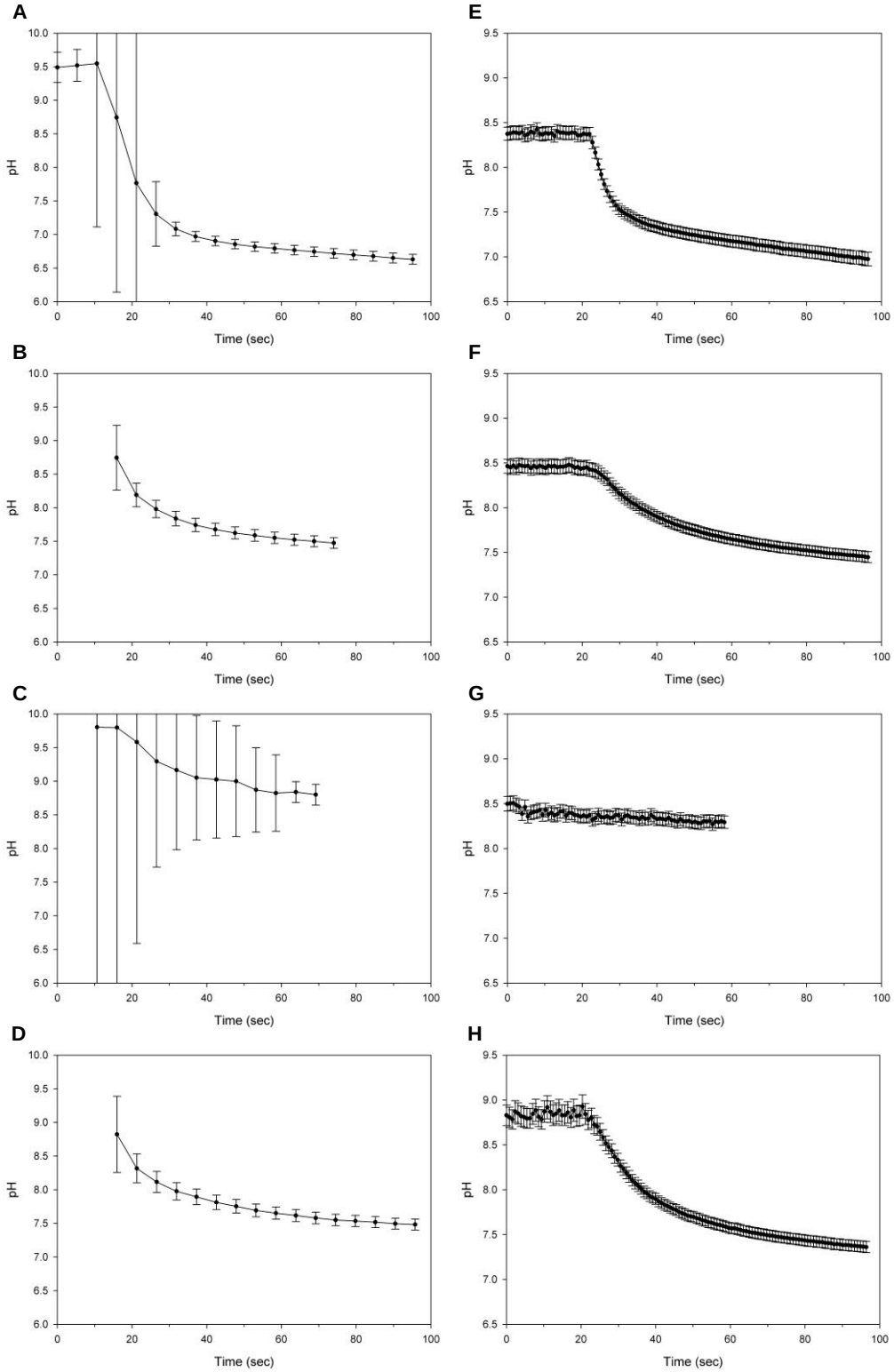

Figure S3. pH time courses obtained at RT using 10 mM PenG as substrate and sYFP-Sep-Ni as fluorescent pH sensor. Uncertainties of pH determination calculated according to Eq. 8 are shown.

Reactions in 10 mM SPB, pH 9, **A**, **E** 30 IU_{PenG}/mL, **B**, **F** 3 IU_{PenG}/mL, **C**, **G** 0.3 IU_{PenG}/mL and reactions in 100 mM SPB, pH 9, **D**, **H** 30 IU_{PenG}/mL were measured with excitation and emission ratiometric setup respectively.